ISTANBUL TECHNICAL UNIVERSITY ★ GRADUATE SCHOOL

SYNTHESIS, CHARACTERIZATION AND APPLICATIONS OF FLUORINE CONTAINING MALEIMIDE POLYMERS

M.Sc. THESIS

İpek KAYALI

Department of Chemistry

Chemistry Programme

JULY 2024

ISTANBUL TECHNICAL UNIVERSITY ★ GRADUATE SCHOOL

SYNTHESIS, CHARACTERIZATION AND APPLICATIONS OF FLUORINE CONTAINING MALEIMIDE POLYMERS

M.Sc. THESIS

İpek KAYALI
(509211263)

Department of Chemistry

Chemistry Programme

Thesis Advisor: Assoc. Prof. Dr. Tuba ÇAKIR ÇANAK

JULY 2024

İSTANBUL TEKNİK ÜNİVERSİTESİ ★ LİSANSÜSTÜ EĞİTİM ENSTİTÜSÜ

FLOR İÇEREN MALEİMİD POLİMERLERİNİN SENTEZİ, KARAKTERİZASYONU VE UYGULAMALARI

YÜKSEK LİSANS TEZİ

İpek KAYALI
(509211263)

Kimya Anabilim Dalı

Kimya Programı

Tez Danışmanı: Doç. Dr. Tuba ÇAKIR ÇANAK

TEMMUZ 2024

İpek KAYALI, a M.Sc. student of ITU Graduate School student ID 509211263, successfully defended the thesis/dissertation entitled "SYNTHESIS, CHARACTERIZATION AND APPLICATIONS OF FLUORINE CONTAINING MALEIMIDE POLYMERS", which she prepared after fulfilling the requirements specified in the associated legislations, before the jury whose signatures are below.

Thesis Advisor :	**Assoc. Prof. Dr. Tuba ÇAKIR ÇANAK** Istanbul Technical University	.....
Jury Members :	**Prof. Dr. İbrahim Ersin SERHATLI** Istanbul Technical University	.....
	Assoc. Prof. Dr. Zehra YILDIZ Marmara University	.....

Date of Submission : 20 May 2024
Date of Defense : 04 July 2024

To my family,

FOREWORD

This study has been carried out in POLMAG Laboratory (Polymeric Materials Research Group), Faculty of Science and Letters, Istanbul Technical University.

I would like to express my sincere gratitude to my advisor, Assoc. Prof. Dr. Tuba ÇAKIR ÇANAK, for her support, encouragement, expertise, motivation and patience throughout development of my thesis. I am grateful to her for always sharing her knowledge and guiding me. Her valuable ideas helped me in all the time of research and writing of this thesis.

I am profoundly grateful to Prof. Dr. İbrahim Ersin SERHATLI and Prof. Dr. Hacer Ayşen ÖNEN for their contributions to completing my research.

I would also like to thank my labmates Merve NİZAM, Şevval YILDIZ, Muhammet Ali BULUT, Zeynep Elçin SEMİZ for their help, support and friendship throughout my experiments.

I am grateful to my family for their endless love and support throughout my life. They have always been the greatest source of motivation and strength in my progress.

I would like to thank TÜBİTAK, the Scientific and Technological Research Council of Turkey, for financially supporting me during my M.Sc. studies with the BİDEB 2210/A program.

Besides, this work was supported by the Research Fund of Istanbul Technical University (Project Number: TED-2021-43192).

July 2024

İpek KAYALI
(Chemist)

TABLE OF CONTENTS

Page

ABBREVIATIONS

AIBN : 2,2'-Azobis(2-methylpropionitrile)

AM : N-aryl Maleimide

AN : Acrylonitrile

BAc : Boron Methacrylate

$CDCl_3$: Deuterated Chloroform

$CHCl_3$: Chloroform

CN : Nitrile

^{13}C-NMR : Carbon Nuclear Magnetic Resonance

CPMA : N-(4-carboxyphenyl)maleamic acid

CPMI : N-(4-carboxyphenyl)maleimide

CPMIC : N-(4-(chlorocarbonyl)phenyl)maleimide

DCM : Dichloromethane

DMF : N,N-dimethylformamide

DMSO-d_6 : Deuterated Dimethyl Sulfoxide

DPGDA : Dipropylene Glycol Diacrylate

DSC : Differential Scanning Calorimetry

DTG : Derivative Thermogravimetry

EA : Epoxy Acrylate

EG : Ethylene Glycol

ESI/MS : Electrospray Ionization/Mass Spectrometry

FMI : 3,5-bis((perfluorophenyl)methoxy)benzyl-4-(2,5-dioxo-2,5-dihydro-1H-pyrrol-1-yl)benzoate

^{19}F-NMR : Fluorine Nuclear Magnetic Resonance

FOH : 3,5-Bis(perfluorobenzyloxy)benzyl Alcohol

FRP : Free Radical Polymerization

FT-IR : Fourier Transform Infrared Spectroscopy

GPC : Gel Permeation Chromatography

^{1}H-NMR : Hydrogen Nuclear Magnetic Resonance

LOI : Limiting Oxygen Index

$MgSO_4$: Magnesium Sulfate

Na_2SO_4 **:** Sodium Sulfate

PAN **:** Polyacrylonitrile

PDI **:** Polydispersity Index

pSt **:** Polystyrene

SEM **:** Scanning Electron Microscope

St **:** Styrene

$SOCl_2$ **:** Thionyl Chloride

T_5 **:** 5% Decomposition Temperature

T_{10} **:** 10% Decomposition Temperature

T_{50} **:** 50% Decomposition Temperature

TEA **:** Triethyl Amine

Tg **:** Glass Transition Temperature

TGA **:** Thermogravimetric Analysis

THF **:** Tetrahydrofuran

TMP3POTA **:** Trimethylolpropane [3PO] Triacrylate

TPGDA **:** Tripropylene Glycol Diacrylate

UA **:** Urethane Acrylate

UV-vis **:** Ultraviolet-visible

W **:** Water

SYMBOLS

℃	**:** Degree Celsius
g	**:** Gram
h	**:** Hour
kV	**:** Kilovolt
MHz	**:** Megahertz
mg	**:** Milligram
mL	**:** Milliliter
µL	**:** Microliter
mmol	**:** Millimol
Mn	**:** Number Average Molecular Weight
Mw	**:** Weight Average Molecular Weight
m/z	**:** Mass to Charge Ratio
nm	**:** Nanometer
ppm	**:** Parts Per Million
RPM	**:** Revolutions Per Minute
wt%	**:** Weight Percentage

LIST OF TABLES

LIST OF FIGURES

SYNTHESIS, CHARACTERIZATION AND APPLICATIONS OF FLUORINE CONTAINING MALEIMIDE POLYMERS

SUMMARY

There is a high demand for the preparation of new polymers with improved mechanical and thermal properties in new materials, and the copolymerization technique is widely used to achieve this goal. Maleimides became interesting monomers to co-polymerize with other monomers in order to obtain heat-resistant materials. The five-member planar ring in the backbones of maleimide polymers ensures a high glass-transition temperature (Tg) and thermal degradation temperature. Therefore, maleimide is polymerized with vinyl monomers such as styrene (St), acrylonitrile (AN), methyl methacrylate (MMA) and vinyl acetate and is widely used in the chemical modification of polymers. Maleimide-based copolymers have versatile applications in various industries, from aerospace to medicine and microelectronics. Other applications of maleimide polymers include photo-resist with high Tg, flexibilizer for thermosetting polymers, non-linear polymer with high Tg, flame retardant etc. N-substituted maleimides, which are electron-deficient as an electron-acceptor, are copolymerized with electron-donor monomers such as styrene and vinyl ether derivatives and undergo alternative copolymerization with or without the use of radical initiators. Maleimide and vinyl monomers form copolymer by free radical polymerization (FRP).

Fluoropolymers offer a series of unique features such as outstanding thermostability, chemical resistance, low surface energy, good water and oil repellence. Due to these unique properties, fluorinated polymers can find a place in various applications such as electronics, optics, biomaterials, coatings and surfactants. Several studies demonstrated the incorporation of fluorine containing molecules into maleimide materials can effectively modify their surface properties. The presence of even a small amount of fluorinated groups or comonomers can result in a dramatic reduction of surface energy, and increase in hydrophobicity and oleophobicity.

The dominant feature of the polyacrylonitrile (PAN) molecule is the presence of strong polar nitrile groups. When acrylonitrile forms a copolymer, it contributes to hardness, strength, chemical resistance, light resistance and gas impermeability. Moreover, copolymerization of acrylonitrile with N-phenyl maleimide derivatives has shown high thermal stability and mechanical properties. Significant work has been done on polystyrene as a high-performance polymeric material. Research is being conducted on how to increase its performance and expand its application area. It is well known that N-substituted maleimide and styrene represent monomer pairs capable of forming radical copolymerization. Moreover, after copolymerization, the thermal stability of polystyrene, which is widely used as a conventional plastic, is greatly increased.

Electrospinning is a widely used technique to produce nanofibers. Characteristics of nanofibers including small diameter and extremely high surface area to volume ratio. These nanosized fibers are good candidates for many application areas such as separators, electrodes, filtration, tissue engineering, wound dressing, etc. The

advantages of electrospinning are low cost, high speed, vast material choices, fast operation, versatility, and small space requirements. Electrospun PAN nanofibrous membranes are of particular interest due to their small fiber diameters, concomitant large specific surface areas, and their ability to control the pore sizes between nanofibers. The advantages of PAN polymer are its low density, high polymer strength, elasticity, good solvent resistance and the ability to maintain morphology in the pyrolysis process.

Over the years, photocuring has found industrial application in an increasing number of advanced technologies to meet the required specifications. The main reasons for this increase are its unique benefits such as solvent-free formulations, high curing speed and low temperature requirement. Acrylate-based photocurable formulations with diverse photoinitiators are recently used in most photocurable formulations due to their outstanding reactivity. If using maleimide and its derivatives for photopolymerization, the thermal property of the post-cured materials could be enhanced due to the introduction of rigid five-membered ring of maleimides to polymer chain.

In this thesis, a new type of maleimide monomer containing a perfluorinated aromatic group was synthesized and copolymers were obtained with this monomer in the presence of acrylonitrile and styrene using free radical polymerization. First, N-(4-carboxyphenyl)maleamic acid (CPMA) was obtained from the reaction of maleic anhydride and 4-aminobenzoic acid in DMF. CPMA reacted with sodium acetate and acetic anhydride in DMF at 65 ℃ to form N-(4-carboxyphenyl)maleimide (CPMI). After the reaction of CPMI with thionyl chloride at 80 ℃, excess thionyl chloride was evaporated and N-(4-(chlorocarbonyl)phenyl)maleimide (CPMIC) was obtained. CPMIC reacted with the synthesized 3,5-bis(perfluorobenzyl)oxybenzyl alcohol (FOH) under 0 ℃ to form a new type of monomer, 3,5-bis((perfluorophenyl)methoxy)benzyl-4-(2,5-dioxo-2,5-dihydro-1H-pyrrol-1-yl)benzoate (FMI). The synthesized monomer was characterized by ^{1}H-NMR, ^{13}C-NMR, ^{19}F-NMR and Fourier transform infrared (FT-IR) spectroscopy. The electrospray ionization/mass spectrometry (ESI/MS) proved that the targeted FMI monomer was obtained. FMI monomer dissolved in most organic solvents at room temperature. Following its synthesis and characterization, the new monomer was copolymerized with acrylonitrile and styrene initiated by AIBN at 75 °C. The obtained copolymers were characterized by ^{1}H-NMR and gel permeation chromatography (GPC), and thermal properties were examined by differential scanning calorimetry (DSC) and thermogravimetric analysis (TGA) methods. The Tg values of the copolymers increased as the FMI ratio increased. The maleimide structure prevented the molecular movement of the main chain and increased the glass transition temperature. FMI monomer in copolymers significantly increased thermal stability and residue amount in TGA analyses. UV-Vis analyzes of FMI monomer and FMI-styrene copolymers were performed. The topography of polymers containing FMI monomer was evaluated by scanning electron microscopy (SEM) to examine the effect of fluorine on the structure. In order to investigate the wetting behavior of these polymers, thin films were prepared using the spin coating method and surface contact angle values were measured with distilled water and ethylene glycol. Contact angle measurements of thin films coated by spin coating method showed that the surface wettability of the films decreased significantly with increasing FMI ratio of the polymers.

PAN nanofibers were prepared from polymers using the electrospinning technique. Thermal behavior of the PAN fibers was observed by TGA. From the TGA thermograms of the fibers, the thermal stability of maleimide-containing fibers was improved by the inclusion of maleimide groups. The surface morphologies of the prepared nanofibers were investigated via SEM. It was seen from SEM images that the nanofiber diameter decreased as the fluoride ratio increased. To examine the wetting behavior of nanofibers, surface contact angle values were measured with distilled water and ethylene glycol. Despite the hydrophilic property of the PAN polymer to the nanofibers, the fluorines in the monomer increased the hydrophobicity and oleophobicity of the nanofibers.

In addition, coating applications and characterizations of UV curable epoxy acrylate (EA) and urethane acrylate (UA) containing FMI monomer were performed. The newly synthesized FMI was introduced at different ratios to epoxy acrylate (EA) and urethane acrylate (UA) formulations. The UV-curable epoxy acrylate and urethane acrylate was obtained with oligomer (EA and UA), monomers (FMI, boron methacrylate, TPGDA, TMP3POTA and DPGDA) and photoinitiator (Darocur 1173). The effects of different ratios of the FMI on the coating properties were investigated. UV-curable coatings were applied wooden substrates. The cross-linking degree was analyzed by unsaturation conversion and gel content. High gel content values indicated that a tightly cross-linked network was formed in the films. The physical and mechanical properties of UV-cured coatings such as pencil hardness, pendulum hardness, cross-cut adhesion, water absorption, solvent and chemical resistance were examined. Increasing FMI content of the coating material resulted in higher pencil hardness, pendulum hardness, superior cross-cut adhesion and much less water absorption. The thermal behavior of the UV-cured films was examined by TGA. TGA results revealed that the synthesized FMI can contribute to improve thermal properties at high temperatures, as well as higher char yield to films. The flame retardancy of UV-cured films was characterized by limiting oxygen index (LOI). The LOI results of the UV-curing films showed improved flame retardant characteristics. Contact angles of the UV-cured coatings with distilled water and ethylene glycol were measured. The increasing content of FMI increased contact angle values and surfaces of the coatings became more hydrophobic and oleophobic.

FLOR İÇEREN MALEİMİD POLİMERLERİNİN SENTEZİ, KARAKTERİZASYONU VE UYGULAMALARI

ÖZET

Yeni malzemelerde geliştirilmiş mekanik ve termal özelliklere sahip yeni polimerlerin hazırlanmasına yüksek talep vardır ve bu amaca ulaşmak için kopolimerizasyon tekniği oldukça fazla kullanılmaktadır. Maleimidler, ısıya dayanıklı malzemeler elde etmek amacıyla diğer monomerlerle birlikte polimerize edilen ilginç monomerler haline geldi. Maleimid polimerlerinin omurgalarındaki beş üyeli düzlemsel halka, yüksek bir camsı geçiş sıcaklığı (Tg) ve termal bozunma sıcaklığı sağlar. Maleimid polimerleri, N-sübstitüe edilmiş grupları değiştirerek yeni fonksiyonel gruplar oluşturacak moleküller tasarlar. N-fenil maleimid (PM), N-hidroksifenil maleimid (HPM) ve halojenürle ikame edilmiş N-hidroksifenil maleimid (XHPM) gibi N-aril maleimid (AM) monomerleri genellikle kopolimerleştirilmektedir. Fenil grubunun eklenmesiyle polimerlerdeki ana zincirin moleküler hareketi bloke edilir ve camsı geçiş sıcaklıkları (Tg) arttırılabilir. Bu nedenle maleimid, stiren (St), akrilonitril (AN), metil metakrilat (MMA) ve vinil asetat gibi vinil monomerleriyle polimerleştirilmekte ve polimerlerin kimyasal modifikasyonunda yaygın olarak kullanılmaktadır. Maleimid bazlı kopolimerler havacılıktan tıp ve mikroelektronik alanına kadar çeşitli endüstrilerde çok yönlü uygulamalara sahiptir. Maleimid polimerlerinin diğer uygulamaları arasında yüksek Tg'li foto direnç, termoset polimerler için esnekleştirici, yüksek Tg'li doğrusal olmayan polimer, alev geciktirici vb. yer alır. Bir electron-alıcısı olarak elektron eksikliği olan N-sübstitüe edilmiş maleimidler, stiren ve vinil eter türevleri gibi elektron-verici monomerlerle kopolimerleştirilirler ve radikal başlatıcılar kullanılarak veya kullanılmadan alternatif kopolimerizasyona uğrar. Maleimid ve vinil monomerleri serbest radikal polimerizasyonuyla (FRP) kopolimer oluşturur. Serbest radikal polimerizasyonu, vinil monomerlerden polimer elde etmek için kullanılan yaygın bir yöntemdir. Bir FRP'de, genellikle ısı altında ayrışarak oldukça reaktif türler olan serbest radikaller oluşur. Başlatıcı bir serbest radikalin bir monomere eklenmesine başlatma basamağı denir. Devamında iki radikal kovalent bağlar oluşturur ve yayılmayı durdurmak için karşılıklı olarak yıkıcı bir reaksiyonda etkileşime girerek bir sonlandırma reaksiyonuyla bitirirler.

Floropolimerler olağanüstü termostabilite, kimyasal direnç, düşük yüzey enerjisi, iyi su ve yağ iticiliği gibi bir dizi benzersiz özellik sunar. Bu benzersiz özellikleri nedeniyle florlu polimerler elektronik, optik, biyomalzemeler, kaplamalar ve yüzey aktif maddeler gibi çeşitli uygulamalarda yer bulabilir. Çeşitli çalışmalar, flor içeren moleküllerin maleimid malzemelere dahil edilmesinin, bunların yüzey özelliklerini etkili bir şekilde değiştirebileceğini göstermiştir. Florlu zincirlerin, dipol-dipol etkileşimleri yoluyla diğer florlu malzemelerle etkileşime girme eğilimi yüksektir. Böylece su ve diğer solventlerle istenmeyen etkileşimleri önler. Az miktarda florlanmış grupların veya komonomerlerin varlığı bile yüzey enerjisinde dramatik bir azalmaya, hidrofobiklik ve oleofobiklikte artışa neden olabilir.

Poliakrilonitril (PAN) molekülünün baskın özelliği güçlü polar nitril gruplarının varlığıdır. Poliakrilonitril (PAN), yarı kristalli bir organik polimerdir ve birim yapısı olarak polietilen omurgasına bağlı bir nitril (CN) fonksiyonel grubuna sahiptir. Akrilonitril kopolimer oluşturduğunda sertliğe, sağlamlığa, kimyasal dirence, ışık direncine, ve gaz geçirimsizliğine katkıda bulunur. Ayrıca akrilonitrilin N-fenil maleimid türevleri ile kopolimerizasyonu, yüksek termal stabilite ve mekanik özellikler göstermiştir.

Yüksek peformanslı bir polimerik malzeme olarak polistiren üzerine önemli çalışmalar yapılmıştır. Polistirenin fenil halkaları, zincirlerin karbon-karbon bağları etrafında dönmesini kısıtlayarak polimere önemli bir sertlik kazandırır. Elektronik, uzay taşımacılığı, biyomalzemeler ve diğer alanlarda geniş uygulamaları vardır. Ancak polistirenin termal özelliklerinin eksikliği, belirli koşullar altında uygulanmasını kısıtlamaktadır. Performansının nasıl artırılacağı ve uygulama alanının nasıl genişletileceği ile ilgili araştırmalar yapılmaktadır. N-sübstitüe maleimid ve stirenin, radikal kopolimerizasyon oluşturmaya sahip monomer çiftlerini temsil ettiği iyi bilinmektedir. Ayrıca kopolimerizasyondan sonra, geleneksel bir plastik olarak yaygın şekilde kullanılan polistirenin termal stabilitesi büyük ölçüde artar.

Elektrospinning, nanolifler üretmek için yaygın olarak kullanılan bir tekniktir. Nanoliflerin küçük çap ve son derece yüksek yüzey alanı/hacim oranı dahil olmak üzere özellikleri vardır. Bu nano boyutlu lifler, ayırıcılar, elektrotlar, filtreleme, doku mühendisliği, yara bandı vb. gibi birçok uygulama alanı için iyi adaylardır. Elektrospinning, boyutları mikrometreden nanometreye kadar değişen liflerin üretilmesini sağlar. Elektrospinningin avantajları arasında düşük maliyet, yüksek hız, geniş malzeme seçenekleri, hızlı çalışma, çok yönlülük ve küçük alan gereksinimleri yer almaktadır. PAN'ın lif oluşturma işlemleri, PAN bazlı fonksiyonel malzemelerin üretiminde önemlidir. Elektrospun PAN nanolif membranlar, küçük lif çapları, beraberindeki geniş spesifik yüzey alanları ve nanolifler arasındaki gözenek boyutlarını kontrol etme yetenekleri nedeniyle özellikle ilgi çekicidir. PAN polimerinin avantajları, düşük yoğunluğu, yüksek polimer mukavemeti, elastikiyeti, iyi solvent direnci ve piroliz işleminde morfolojiyi koruma yeteneğidir.

Fotokürleme, yıllar geçtikçe artan sayıda ileri teknolojilerde gerekli özellikleri karşılamak için endüstriyel uygulama alanı bulmuştur. Bu artışın ana nedenleri solvent içermeyen formülasyonlar, yüksek sertleşme hızı ve düşük sıcaklık gereksinimi gibi benzersiz faydalarıdır. Çeşitli fotobaşlatıcılara sahip akrilat bazlı ışıkla kürlenebilir formülasyonlar, olağanüstü reaktiviteleri nedeniyle son zamanlarda çoğu ışıkla kürlenebilir formülasyonda kullanılmaktadır. Fotopolimerizasyon için maleimid ve türevleri kullanılıyorsa, polimer zincirine sert beş üyeli maleimid halkasının eklenmesi nedeniyle sonradan kürlenen malzemelerin termal özelliği artırılabilir.

Bu tezde yeni tip perflorlanmış aromatik grup içeren maleimid monomeri sentezlenmiş ve serbest radikal polimerizasyonu kullanılarak bu monomer ile akrilonitril ve stiren varlığında kopolimerler elde edilmiştir. Önce maleik anhidrit ve 4-aminobenzoik asitin DMF içerisinde reaksiyonundan N-(4-karboksifenil)maleamik asit (CPMA) elde edilmiştir. CPMA, sodyum asetat ve asetik anhidrit ile reaksiyona 65 ℃'de DMF'de reaksiyona girerek N-(4-karboksifenil)maleimidi (CPMI) oluşturmuştur. CPMI'nın tiyonil klorürle 80 ℃ reaksiyonundan sonra tiyonil klorürün fazlası uçurulmuştur ve N-(4-(klorokarbonil)fenil)maleimid (CPMIC) elde edilmiştir. CPMIC sentezlenen 3,5-bis(perflorobenzil)oksibenzil alkol (FOH) ile 0 ℃ altında reaksiyona girerek yeni tip monomer olan 3,5-bis((perflorofenil)metoksi)benzil-4-(2,5-diokso-2,5-dihidro-

1H-pirol-1-il)benzoat (FMI) oluşturmuştur. Sentezlenen monomer Fourier transform kızılötesi spektrometresi (FT-IR), ^{1}H-NMR ^{13}C-NMR, ve ^{19}F-NMR ile karakterize edilmiştir. Elektrosprey iyonizasyon/kütle spektrometresi (ESI/MS), hedeflenen FMI monomerinin elde edildiğini kanıtlamıştır. FMI monomeri oda sıcaklığında çoğu organik çözücüde çözünmüştür. Yeni monomer, sentezi ve karakterizasyonunun ardından AIBN tarafından 75 °C'de başlatılan akrilonitril ve stiren ile kopolimerleştirilmiştir. FMI monomeri akrilonitril ile DMF ile 96 saatte, stiren ile 24 saatte polimerleştirilmiştir. Elde edilen kopolimerler ^{1}H-NMR ve jel geçirgenlik kromatografisi (GPC) ile karakterize edilmiştir ve termal özellikleri diferansiyel taramalı kalorimetri (DSC) ve termogravimetrik analiz (TGA) yöntemleriyle incelenmiştir. Kopolimerlerin Tg değerleri FMI oranı arttıkça artmıştır. Maleimid yapısı, ana zincirin moleküler hareketini engellemiş ve camsı geçiş sıcaklığını arttırmıştır. Kopolimerlerde FMI monomeri, TGA analizlerinde termal stabiliteyi ve kalıntı miktarını önemli ölçüde arttırmıştır. FMI monomerinin ve FMI-stiren kopolimerlerinin UV-Vis analizleri yapılmıştır. FMI monomeri için UV-Vis spektrumdaki önemli absorpsiyona sahip ilk absorpsiyon piki 270 nm'deydi. FMI monomeri içeren polimerlerin topografisi, florun yapıya etkisini incelemek için taramalı elektron mikroskobu (SEM) ile değerlendirildi. Bu polimerlerin ıslanma davranışlarını araştırmak amacı ile spin kaplama yöntemi kullanılarak ince filmleri hazırlanmış ve distile su ve etilen glikol ile yüzey temas açı değerleri ölçülmüştür. Bu sıvıların filmler üzerindeki temas açıları, polar seviyeleri farklı olan bu iki sıvının yüzeyle temas noktasındaki damla profili ile doğrudan ölçülmüştür. Spin kaplama yöntemi ile kaplanmış ince filmlerin temas açısı ölçümleri, polimerlerin artan FMI oranı ile filmlerin yüzey ıslanabilirliğinin önemli ölçüde azaldığını göstermiştir.

Polimerlerden electrospinning tekniği ile PAN nanolifleri hazırlanmıştır. PAN liflerinin termal davranışı TGA ile gözlemlenmiştir. Liflerin TGA termogramlarından, maleimid içeren liflerin termal stabilitesinin, maleimid gruplarının dahil edilmesiyle iyileştiği görülmüştür. Hazırlanan nanoliflerin yüzey morfolojileri SEM ile incelenmiştir. SEM görüntülerinden florür oranı arttıkça nanofiber çapının azaldığı görülmüştür. Nanoliflerin ıslanma davranışlarını incelemek için distile su ve etilen glikol ile yüzey temas açısı değerleri ölçülmüştür. PAN polimerinin nanoliflere verdiği hidrofilik özelliğine rağmen monomer içerisindeki florlar nanoliflerin hidrofobikliğini ve oleofobikliğini arttırmıştır.

Bunlara ek olarak, FMI monomeri içeren UV kürlenebilir epoksi akrilat (EA) ve üretan akrilatın (UA) kaplama uygulamaları ve karakterizasyonları yapılmıştır. Yeni sentezlenen FMI, epoksi akrilat ve üretan akrilat formülasyonlarına farklı oranlarda dahil edilmiştir. UV ile kürlenebilen epoksi akrilat ve üretan akrilat, oligomer (EA ve UA), monomerler (FMI, bor metakrilat, TPGDA, TMP3POTA ve DPGDA) ve foto başlatıcı (Darocur 1173) ile elde edildi. Farklı FMI oranlarının kaplama özelliklerine etkisi araştırılmıştır. Ahşap yüzeylere UV ile kürlenebilen kaplamalar uygulandı. Çapraz bağlanma derecesi, doymamışlık dönüşümü ve jel içeriği ile analiz edildi. Yüksek jel içeriği değerleri, filmlerde sıkı çapraz bağlı bir ağın oluştuğunu göstermiştir. UV ile kürlenen kaplamaların kalem sertliği, pendulum sertliği, cross-cut yapışma, su absorbsiyonu, solvent ve kimyasal direnç gibi fiziksel ve mekanik özellikleri incelenmiştir. Kaplama malzemesinin artan FMI içeriği, daha yüksek kalem sertliği, pendulum sertliği, üstün cross-cut yapışma ve çok daha az su absorbsiyonu ile sonuçlanmıştır. UV ile kürlenen filmlerin termal davranışı TGA ile incelenmiştir. TGA sonuçları, sentezlenen FMI'nın yüksek sıcaklıklarda termal özelliklerin iyileştirilmesine ve ayrıca filmlerde daha yüksek kalıntı verimine katkıda

bulunabileceğini ortaya koymuştur. UV ile kürlenen filmlerin alev geciktiriciliği, sınırlayıcı oksijen indeksi (LOI) ile karakterize edilmiştir. UV ile kürlenen filmlerin LOI sonuçları, gelişmiş alev geciktirici özellikler göstermiştir. UV ile kürlenen kaplamaların distile su ve etilen glikol ile temas açıları ölçülmüştür. Artan FMI içeriği temas açısı değerlerini artırmış ve kaplamaların yüzeyleri daha hidrofobik ve oleofobik hale gelmiştir.

1. INTRODUCTION

Polymers have found many uses in various technological applications. There is a high demand for the preparation of new polymers with improved mechanical and thermal properties in new materials, and the copolymerization technique is widely used to achieve this goal [1]. It has been determined that maleimide and its derivatives polymerize to give thermally stable polymers, and it has been investigated that they copolymerize with various vinyl monomers to improve the thermal properties of the polymers. Thanks to the excellent heat resistance properties of N-substituted maleimides and their derivatives, they have found a place in different application areas such as the rubber and plastic industry. Fluorine-substituted phenyl maleimides were reported to homopolymerize and their homopolymers were thermally stable [2,3]. Fluoropolymers exhibit excellent properties such as remarkable chemical resistance, weather stability, low surface energy, low coefficient of friction, and low dielectric constant. The specific electronic structure of the fluorine atom, the stable carbon-fluorine covalent bond, and the unique intra- and intermolecular interactions between fluorinated polymer segments and main chains provide these properties [4].

1.1 Purpose of Thesis

The aim of the thesis is to synthesize fluorine-containing maleimide polymers and examine their thermal and hydrophobic properties. First of all, a new maleimide monomer containing fluorine was synthesized and its copolymers were obtained by free radical polymerization with acrylonitrile and styrene. The molecular weights and molecular weight distributions of these polymers were measured by GPC. The thermal properties and thermal degradation behaviors of the polymers were investigated by DSC and TGA. The morphological properties of polymers were characterized by SEM. Then, the contact angles of the polymer films were measured to examine the effect of the fluorine atom on the hydrophobicity of the polymers. It was also aimed to examine the thermal properties, hydrophobic and morphological properties of nanofibers prepared using electrospinning technique with acrylonitrile and containing

these polymers. In addition, the aim of the thesis is to prepare UV-curable perfluorinated maleimide-containing epoxy acrylate and urethane acrylate coatings.

1.2 Literature Review

Maleimides are new class of high performance materials having excellent thermal stability and fire resistance. In addition, good toughness, low dielectric constant, low thermal expansion and good adhesion are among the excellent mechanical properties of maleimide [5]. N-substituted maleimides, which are electron deficient as an electron acceptor, are copolymerized with electron-donating monomers such as styrene and vinyl ether derivatives via electron-donor/acceptor polymerization and undergo alternative copolymerization with or without the use of radical initiators [6]. The presence of two adjacent electron-withdrawing carbonyl groups makes the maleimide double bond highly electrophilic. Oishi et al. prepared optically active N-[4-N-(α-methylbenzyl)aminocarbonylphenyl]maleimide from N-[4-(chlorocarbonyl)phenyl]maleimide and obtained its copolymers with styrene and methyl methacrylate. Altintaş et al. prepared UV-curable, non-cracking, hydrophobic and transparent bismaleimide-capped cycloaliphatic epoxy resin using N-(4-carboxyphenyl)maleimide and found that the thermal resistance increased with increasing maleimide ratio. Organic-inorganic hybrid coatings obtained from maleimide-modified epoxy resin have improved thermal, mechanical and other properties such as hardness, gloss, contact angle and abrasion resistance [5]. There has been great interest in the free radical polymerization and copolymerization of N-substituted maleimide (RMI). Poly(N-substituted maleimide)s has excellent thermal stability because of a rigid backbone consisting of a five-membered ring structure [7]. Free-radical polymerizations have technically many advantages. Free-radical polymerizations can be performed at convenient temperatures of 20-80 °C. Free-radical initiators are usually not very expensive and often relatively easy to store [8]. Fluorine-containing phenyl maleimide monomers have been reported to be synthesized and polymerized. Fluorine imparts extreme hydrophobicity and water insolubility to polymers. It increases thermal and oxidative stability. Mokhtar et al. have synthesized a new fluoro-maleimide monomer of 4,(4’-trifluoromethyl)phenoxy N-phenyl maleimide (FPMI) that is readily polymerized by free radical mechanism using 2,2’-azobisisobutyronitrile as initiator in 1,4-dioxane. PFPMI exhibits high glass

transition temperature, (Tg=236), good solubility, and high thermal stability and photostability [9]. Electrospinning can be easily and directly used to produce nanosized fibers from a polymeric solution. Electrospinning is an effective technique to produce fibers with diameters ranging from micrometer to nanometer. In the electrospinning process, the voltage applied to the polymeric solution, then a charged jet starts from the needle, undergoes spiral motion after a certain distance. Finally, it is collected on a screen placed at a certain distance from the needle. Polymeric nanofibers are used in many applications such as battery separation, tissue engineering, wound dressing etc. Solution composition, flow rate, applied voltage, solvent type, and distance between tip and the collector affect the morphology and properties of nanofiber membranes [10-12]. Many polymers are used to obtain electrospun fibers. One of them, polyacrylonitrile, is used as a separator material. Polyacrylonitrile (PAN) fibers have been widely used in industry because of good conductivity, good thermal stability, solvent resistance, high strength and good compatibility with Li metal. Electrospun PAN nanofibrous membranes have extraordinary properties such as small fiber diameters and accompanying large specific surface areas. PAN fibers have been of interest due to their ability to control pore sizes between nanofibers and incorporate antimicrobial agents at the nanoscale [10,13,14].

1.3 Hypothesis

Maleimides provide a high glass-transition temperature (Tg) and high thermal degradation temperature to their polymers because they have a rigid backbone consisting of a five-membered ring structure. The formation of copolymers of maleimides with various vinyl monomers such as styrene and acrylonitrile give these copolymers improved heat resistance and mechanical properties. Since the C-F bond has low polarization and low surface energy, fluorine-containing polymers are both hydrophobic and oleophobic. In addition, if UV curable materials containing maleimide are prepared and coated on wooden surfaces, thermal, hardness and solvent and chemical resistance properties are increased.

2. THEORETICAL PART

2.1 Maleimide

The IUPAC name of maleimide is 1H-pyrrole-2,5-dione with a melting point 91-93 °C (Figure 2.1). Maleimide is a reactive vinyl monomer used in polymerizations initiated by free radicals. Substituted cyclic five-membered imide rings are found in various polymers used for high-temperature aerospace applications [15]. N-substituted maleimides are an important group of electron acceptor monomers that can form charge transfer complexes with different vinyl monomers. Maleimides undergo free radical-initiated copolymerization with electron donors, often forming alternative copolymers. Maleimide and its derivatives give stable thermal polymers. In addition to being used as monomers in the preparation of various polymers and copolymers, N-substituted maleimides also serve as biologically active compounds. For case, N-ethylmaleimide is a diuretic and potentially nephrotoxic agent in dogs [16]. Maleimides have also been used in the manufacture of aerospace and electronic components, in the preparation of vitrimers and complex architectural polymers [17].

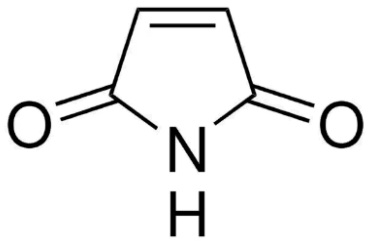

Figure 2.1 : Chemical structure of maleimide.

2.2 Polymaleimide

Polymaleimides have a polar five-membered imide ring structure. This structure allows them to have good thermal stability with a high glass transition temperature (Tg). In addition, the high dipole moment and cyclic structure of the maleimide unit at right angles to the backbone provide great rigidity to the polymer chain. Functional polymaleimides containing diverse maleimide monomers provide certain desirable

properties. Maleimide polymers design molecules to form new functional groups by replacing N-substituted groups. N-aryl maleimide (AM) monomers, such as N-phenyl maleimide, N-hydroxyphenyl maleimide, and halide-substituted N-hydroxyphenyl maleimide, were usually copolymerized with ethylene or propylene monomers to enhance their heat and fire resistance. To date, many studies have been conducted on copolymers of N-aryl maleimide monomers with styrene, methyl methacrylate or vinyl acetate (Figure 2.2).

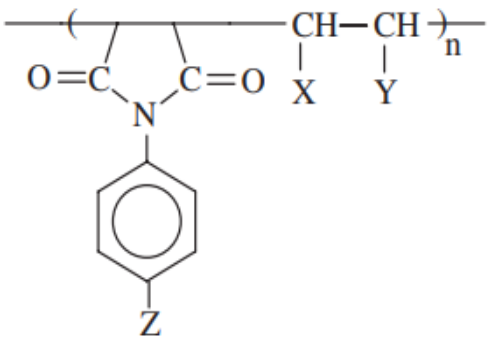

Figure 2.2 : Copolymers of AM with vinyl monomers [18].

The AM segment is rigid and has high thermal stability properties, giving its copolymers higher softening points (or Tg) and good fire resistance. AM and styrene comonomers have electron-poor and electron-rich double bonds, respectively, and form an almost complete alternative copolymer by free radical copolymerization [18,19]. Maleimide polymers, as in thermoplastic resins, generally exhibit very good thermal stability, good chemical and solvent resistance and excellent mechanical properties. It was also reported that polymaleimides with long alkyl groups on the nitrogen atom have the ability to form tough and thin films [20,21]. So far, N-substituted maleimide polymers have applications photo-resist with high Tg, flexibilizer for thermosetting polymers, nonlinear polymer with high Tg and flame retardant, etc. Some N-protected polymaleimides can be applied as thermally stable resist materials in the deep ultraviolet region according to the chemical amplification concept. Photoresist film should have high resolution, high sensitivity, high etching resistance, good thermal stability and high adhesion for use in lithographic processes. By incorporating silicon into the polymaleimide structure, good dry-etch resistance and better adhesion to substrates can be achieved [18]. In order to avoid the toxicity of small maleimide molecules and to improve reactivity, heat and impact resistance, a multifunctional, oligomeric maleimide resin was synthesized in addition to

bismaleimides. These maleimide resins are often toughened by allyl compounds. The most common bismaleimide resin is commercially available 4,4-bis(maleimidodiphenyl)methane toughened by diallylbisphenol A. Studying the thermostability of materials and the change in their properties at high temperatures of use has always aroused great interest. Research on the pyrolysis behavior and mechanism of maleimide resins is important for processing and performance evaluation [22]. The polymaleimides have variable applications in many fields, such as aerospace, medical and microelectronic industry. Among these polymers, poly[N-(4-carboxyphenyl)maleimide] and poly[N-(4-hydrophenyl)maleimide] are the most important polymer classes. By adding the phenyl group, the molecular movement of the main chain in the polymers was blocked and the glass transition temperatures (Tg) could be increased. That is, if functional groups are incorporated into polymers, their practical applications also expand [7].

2.3 Thermal Stability of Maleimide Polymers

Maleimide polymers have good thermal stability. Maleimide polymer chains are restricted by the rigid five membered ring and this structure increases glass transition (Tg) and initial thermal degradation temperatures of the copolymers containing maleimide. The excellent heat resistance properties of N-substituted maleimides and their derivatives have made them important in different application fields such as the rubber and plastic industry. Omayu and Matsumato synthesized alternative copolymers derived from phenylmaleimides containing isobutene hydroxy and carboxy substituents and showed that their thermal stability properties were excellent. The initial degradation temperatures of these compounds are higher than 350 °C, and glass transition temperatures (Tg), are over 220 °C. The structure and position of polar groups in the N-phenyl group affected thermal stability (Figure 2.3) [3].

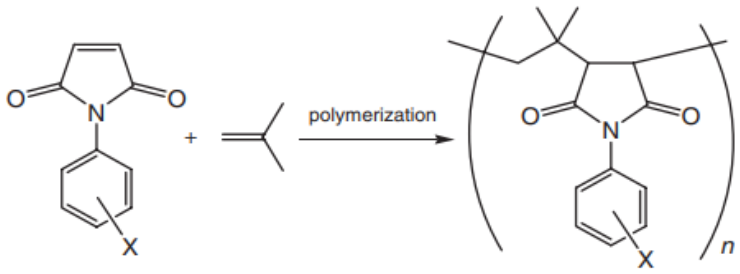

Figure 2.3 : The alternating copolymers of N-(substituted phenyl)maleimides [23].

2.4 Fluoropolymers

Fluoropolymers are olefinic polymers containing fluorines that replace some hydrogen atoms. The very strong carbon-fluorine bond and the high electronegativity of fluorine determine the properties of fluoropolymers. Therefore, these polymers have non-stick and water-repellent properties, low refractive indexes and low dielectric constants. They exhibit excellent specific heat resistance, combustion resistance and chemical resistance. These properties are not usually seen in organic compounds [24]. Adding fluorine to polymers produces many high-performance materials i.e. polytetrafluoroethylene (PTFE, Teflon) and polyvinylidene fluoride (PVDF) (Figure 2.4). The strong C-F bond provides fluoropolymers with resistance to acid, base, oxidation, corrosion and heat. Fluoropolymers have variety of structures ranging from semi-crystalline to amorphous, and form thermoplastics, thermosets, and elastomers. They were fabricated into various nanostructures on the substrate surface to obtain superhydrophobic and chemical-resistant surfaces. These surfaces are difficult to wet with water and non-fluorine solvents and allow for water collection, anti-fouling and self-cleaning applications [25]. Fluoropolymers have been involved in many applications: elastomers, protective coatings, biomaterials, lubricants, surfactants, fuel cell membranes, fabrics, specific items in the automotive industries, aerospace and aeronautics, petrochemical, microelectronics, high performance membranes, textile treatment, protective building coatings (e.g. paints or films resistant to UV) and optics (core and cladding of optical fibres) [26].

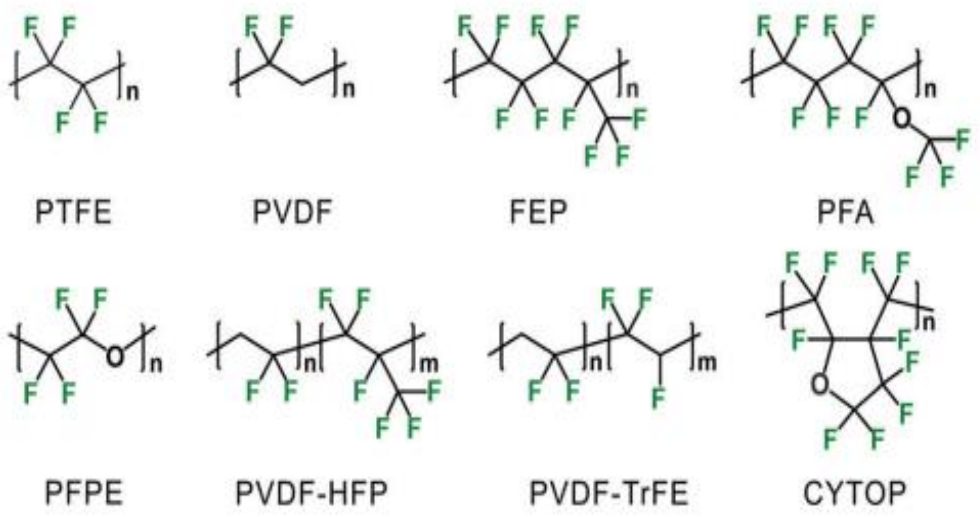

Figure 2.4 : Chemical structures of well-known fluoropolymers [25].

2.5 C-F Bonds

Fluorine is the most electronegative element known on the periodic table. It has an atomic size close to the atomic size of hydrogen. It can be incorporated into organic compounds to replace hydrogen without significantly changing the size of the molecule. The bond between carbon and fluorine is the strongest in organic chemistry. Fluorine, with its strong electronegativity, firmly holds three lone pairs with its nucleus. The C-F bond is a highly polarized and unreactive bond. The C-F bond with ionic character interacts with others through dipole-dipole or charge-dipole interactions. Fluoridation of chemicals offers unique properties such as high stability under extreme conditions. One of the characteristics of the C-F bond is that it has low surface energy. For example, the fact that the surface energy of a trifluoromethyl group ($-CF_3$) is only one quarter of the surface energy of a methyl group ($-CH_3$) proves these properties. That is, highly fluorinated compounds are both hydrophobic and oleophobic. They produce phase separation in both aqueous solutions and most organic solvents; this phenomenon is generally called the "fluorous effect". Fluorinated chains have a high tendency to interact with other fluorinated materials through dipole-dipole interactions. Thus, it prevents undesirable interactions with water and other solvents. The phase separation and fluorophilic behavior of fluorinated materials have enabled their widespread use in green chemistry for chemical synthesis, catalysis, and separation [25].

2.6 Free Radical Polymerization

The most widely used method for polymer synthesis is free radical polymerization (FRP). It is less affected by random impurities [27]. Free radical polymerization is a common method used to obtain polymers from vinyl monomers. The most important feature of an FRP is an adjustable radical source, which often decompose under heating to form free radicals, that is highly reactive species with an unsatisfied electron valence pair. Free radicals are added to a monomer molecule to initiate propagation and become one of the end groups of a linear chain. Vinyl monomers to polymerize, with the addition of each monomer resulting in a free radical. The resulting free radical maintains the same structure as the attacking radical and retains the ability to add new molecules. Electron-withdrawing substituents will make easy the addition of nucleophilic species, while electron-donating substituents will provide the addition of

electrophilic species. The addition of an initiator free radical to a monomer is called the initiation step. The two radicals then form covalent bonds and interact in a mutually destructive reaction to stop propagation, ending with a termination reaction. Peroxides and azo compounds are usually produced as monomer initiators. Commonly used initiators are shown in Figure 2.5 [28].

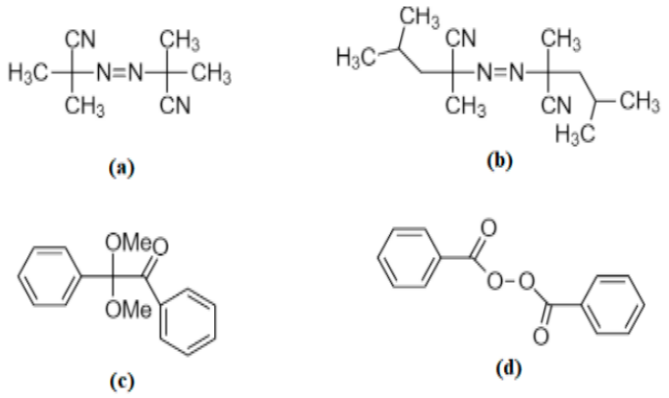

Figure 2.5 : Commonly used initiators: (a) azobisisobutyronitrile (AIBN), (b) azobisdimethylvaleronitrile, (c) benzildimethylacetal, (d) benzoyl peroxide [29].

2.7 Basic Mechanism of Free Radical Polymerization

The basic mechanism of chain formation contains the generation of free radicals, the initiation, propagation and termination. Radical formation and first monomer addition to an initiating radical form the initiation step. Successive monomer additions onto a new free radical and termination of chain growth by disproportionation and/or coupling actually constitute the formation of chains (Figure 2.6) [28].

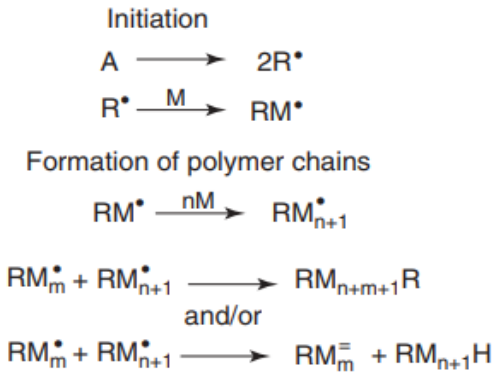

Figure 2.6 : Reaction induced by an initiating radical generated from the initiator A [28].

2.7.1 Initiation

Chemical initiation involves the dissociation of initiator molecules A to form primary radicals R•, which can initiate new polymer chains. If any two radicals produced are in such close proximity, not all of them can escape the solvent "cage" to react with the monomer molecules. Some radicals will self-destruct or react with other near-neighboring molecules. In the initiation step, only some R• radicals form RM•, which becomes the precursor of a polymer chain [28].

2.7.2 Propagation

It is an addition reaction that generates the polymer chain by a series of fast successive steps of monomer addition over the propagating radical. The addition of a monomer unit creates a radical that is structurally similar to the radical before the addition. Thus, there is no change in the stability of the growing radical. The group substituent (G) affects the stability of both the double bond and the resulting radical (Figure 2.7) [28].

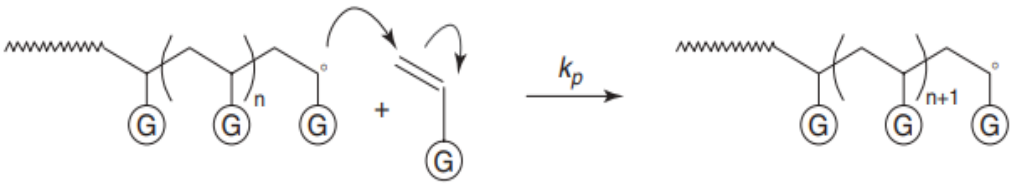

Figure 2.7 : Schematic representation of the propagation reaction [28].

2.7.3 Termination

This reaction has very high rate constants. The very low concentration of propagating chains is critical for the radical to survive for a few seconds or less before encountering another radical species. Termination usually involves coupling and disproportionation reactions. However, a propagating radical can also participate in abstraction reactions that end in growth deactivation. Chain transfer is this type of reaction. Termination reaction and inherent side reactions self-regulate size or molecular weight. An increase of temperature causes faster AIBN decomposition and lower molecular weight is obtained as more chains are observed. However, higher pressure increases dissipation and inhibits termination, resulting in higher molecular weight. The increase of AIBN concentration also has the same effect as the increase of temperature [28].

2.8 Copolymers

Polymerization of two or more monomers is called copolymerization. Those using more than two monomers are called multicomponent copolymers. When three monomers are used, the term terpolymer is used. The molecular arrangement is the same at each end of the monomer molecule. In a copolymer, monomers can be in a head-to-tail, head-to-head or tail-to-tail arrangement. Copolymers can be classified as alternating copolymer, random copolymer, block copolymer and graft copolymer according to the arrangement of repeating units along the chain. The addition of more than one monomer type to the reaction causes increased complexity in the kinetic reaction mechanisms. This complexity consists of different polymerization rates depending on the structure of each monomer as well as the radicals. This affects the polymer composition, the monomer sequence distribution, and the polymer molecular weight [30,31].

2.8.1 Acrylonitrile copolymers with maleimide

Polyacrylonitrile (PAN) is a semi-crystalline organic polymer and has a strong polar nitrile (CN) functional group attached to the polyethylene backbone as its unit structure (Figure 2.8). The nitrile group behaves as a hydrogen bond acceptor due to a lone pair on the nitrogen atom. In the nitrile group, there is a large dipole moment between the electron-deficient carbon atom and the electron-rich nitrogen atom and is used for relatively strong attractive interactions. PAN is predominantly white powder up to 250 ℃ and exhibits thermoplastic properties. It does not melt under normal conditions, but above this temperature it becomes darker due to decomposition before melting. PAN has a relatively high glass transition temperature (around 100 ℃). It has low thermal plasticity and cannot be used as a plastic material due to the high melting point (317 ℃) of crystallized PAN. Commercial PAN is synthesized via free radical polymerization without control over the molecular structure. Acrylonitrile incorporated into a comonomer contributes to hardness, rigidity, chemical resistance, light resistance, gas impermeability and melt viscosity [32,33].

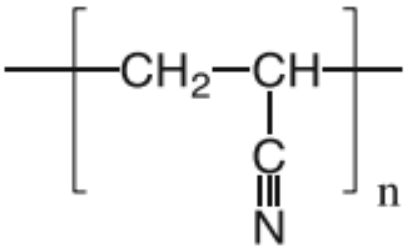

Figure 2.8 : Molecular structure of PAN [32].

Chiang and Ding copolymerized N-(4-carboxyphenyl)maleimide (N-4-CPMI) with AN using azobisisobutyronitrile (AIBN) in DMF at 60 ℃ (Figure 2.9). In addition to having good film-forming ability, acrylonitrile also has a strong polar group. Therefore, N-4-CPMI copolymer with AN produces good thermal resistance and strong films. In addition, the copolymer of CPMI (containing hydrophilic group) and acrylonitrile (containing hydrophobic group) was applied in pervaporative separation [34].

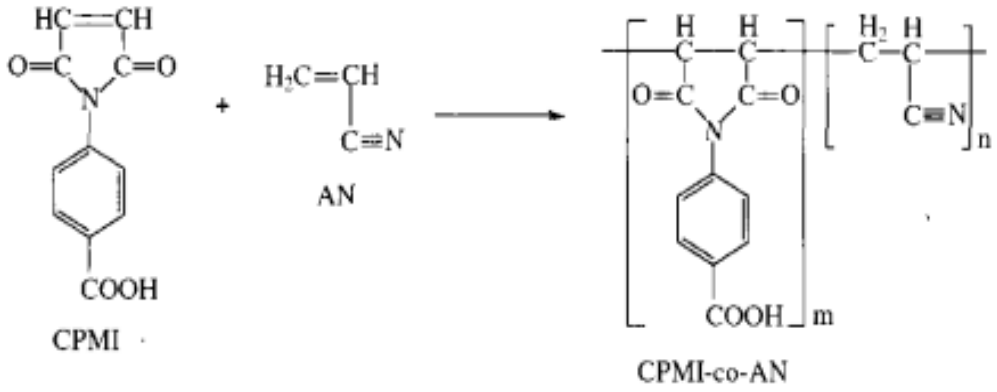

Figure 2.9 : Copolymerization of CPMI with AN [34].

Abdel-Naby prepared some amino phenyl maleimide and amino phenyl-2,3-dimethyl maleimide derivatives in order to be copolymerized with acrylonitrile using power ultrasound for the purpose of improving the PAN thermal property. Thermogravimetric data reveal that the addition of small amounts of N-aryl amino maleimides and N-aryl amino-2,3 dimethyl maleimides into the PAN matrix leads to a remarkable improvement in thermal stability compared to the PAN homopolymer. Because the percentage weight loss values at 500℃ decreased and also the initial decomposition temperature increased [35].

2.8.2 Styrene copolymers with maleimide

Styrene, a liquid hydrocarbon produced commercially from petroleum, is the monomer of polystyrene. At room temperature, polystyrene (pSt) is normally a solid thermoplastic. However, it can be melted at higher temperatures for molding or extrusion and then resolidified. Since styrene is an aromatic monomer, polystyrene is also an aromatic polymer [36]. Solid polystyrene is transparent. This is because large ring-shaped molecular groups prevent polymer chains from packing into close crystalline arrangements. The phenyl rings of polystyrene restrict the rotation of chains around carbon-carbon bonds, giving the polymer significant rigidity. Significant research is being conducted on polystyrene due to its wide applications in electronics, space transportation, biomaterials and other fields. However, the deficiency of thermal properties for polystyrene restricts its application under specific conditions. Research is being conducted on how to increase its performance and expand its application area. The thermal stability of polystyrene forming copolymerization is greatly increased and is widely used as a conventional plastic. Polystyrene is easily obtained from styrene by free radical polymerization using free radical initiators. Styrene, with or without diluent, is mixed with a free radical initiator such as dibenzoyl peroxide and heated. Several stages of polymerization result in a polymer dissolved in monomer or diluent solution (Figure 2.10) [37-39].

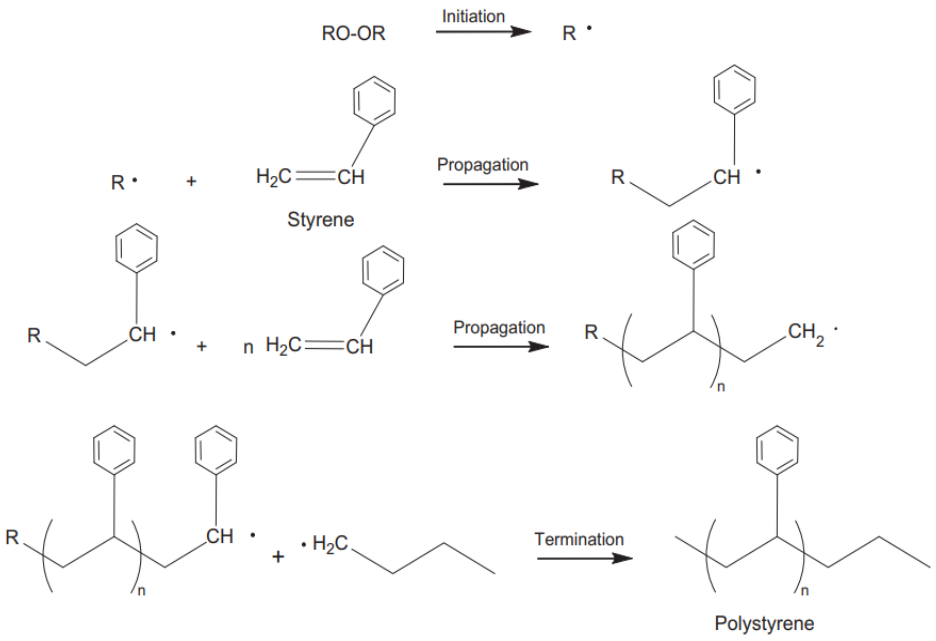

Figure 2.10 : Free radical polymerization of polystyrene [38].

Li et al. synthesized a novel monomer N-[4-(N'-8-quinolinyl)aminocarbonylphenyl]maleimide from CPMI and 8-aminoquinoline. The radical copolymerization of this monomer with styrene was investigated. It was found that the onset decomposition temperature for the copolymer was 380 °C, which showed that the copolymer had excellent thermal stability. The Tg value of the copolymer was found to be 229 °C. Because the bulky N-substituted group prevented molecular movement and increased the Tg value [7]. Cılgı et al. investigated thermal degradation stages of N-(4-(3-thienyl methylene)-oxycarbonylphenyl) maleimide monomer and an alternating copolymer of this monomer with styrene (Figure 2.11). Thermal stabilities of both monomer and copolymer were investigated. The thermal stability of the copolymer was higher than the monomer. Intermolecular forces play an important role in macromolecules and increase the thermal stability of polymers. Thermal stability of the polymer has enhanced highly with the aid of copolymerization [3].

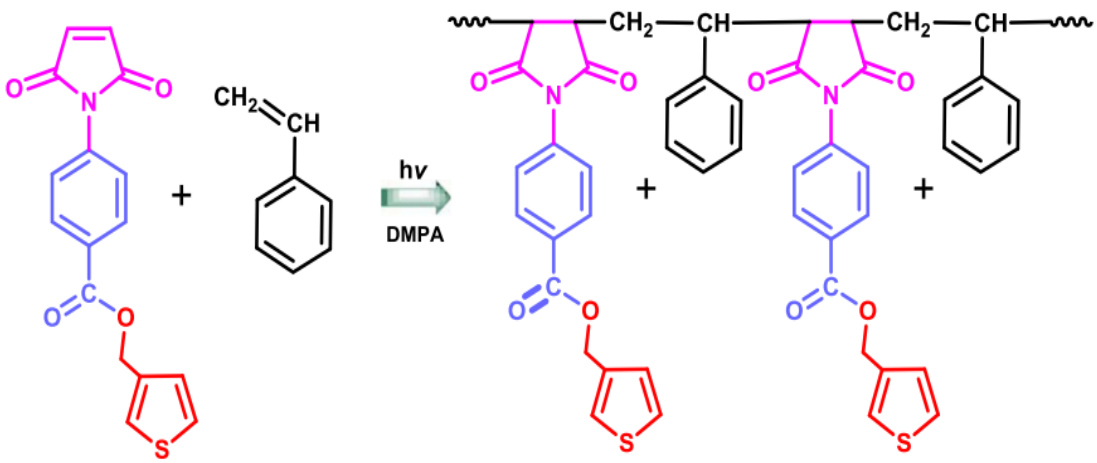

Figure 2.11 : Synthesis of alternating copolymer of N-(4-(3-thienyl methylene)-oxycarbonylphenyl) maleimide and styrene [3].

2.9 Molecular Weight of Polymers

The molecular weight of a polymer is the sum of the atomic weights of the individual atoms that make up a molecule. It represents the average length of the polymer chains. Not all polymer molecules of a given grade have exactly the same molecular weight. There is a range or distribution of molecular weights. There are two different ways to calculate molecular weight: number average molecular weight and weight average molecular weight. Figure 2.12 shows a molecular weight distribution diagram with two different molecular weight measurements. The ratio Mw/Mn is called the molar-

mass dispersity index (polydispersity). When the polydispersity is 1, if all polymer chains are exactly the same, the number average and weight average molecular weights are exactly the same. If the molar-mass distribution index becomes larger, the molecular weight distribution also becomes wider [40].

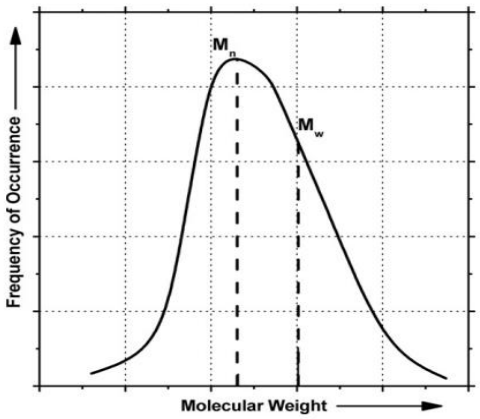

Figure 2.12 : Hypothetical molecular weight distribution plot showing number- and weight-average molecular weights [40].

2.10 Ultraviolet-Visible Spectroscopy

Ultraviolet-visible (UV-vis) spectroscopy includes absorption spectroscopy and reflection spectroscopy in the UV-vis spectral region. Molecules containing p-electrons or nonbonding electrons (n-electrons) absorb ultraviolet or visible light energy. These electrons can be excited into higher antibonding molecular orbitals. Only certain functional groups (chromophores) in molecules containing valence electrons with low excitation energy can absorb ultraviolet and visible radiation. UV-vis spectroscopy should not be confused with IR spectroscopy in terms of excitation wavelengths. Molecules undergo electronic transitions in the ultraviolet or visible region and vibration transitions in the IR region. Information about various adsorption bands and transitions based on the presence of various functional groups is provided using UV-vis [41].

2.11 Electrospinning

Electrospinning is a widely used technique to produce nanofibers. Nanofibers have properties such as small diameter and extremely high surface area to volume ratio. The experimental setup for the electrospinning process is shown in Figure 2.13. In the

electrospinning technique, high voltage is applied to the polymer solution. The polymer solution is fed to the needle tip and the solution droplet turns into a conical shape (Taylor cone) under the electric field. When the critical voltage is reached, polymeric jets are formed and come to the collector. In the presence of an electric field, the jets get thinner, the solvent evaporates and nano-sized fibers are produced on the collector.

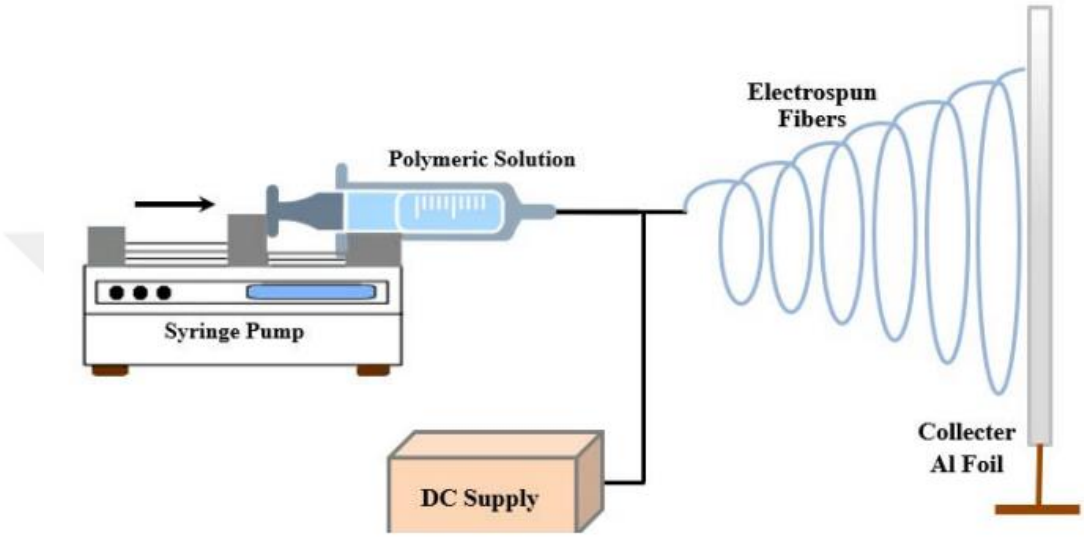

Figure 2.13 : Schematic view of electrospinning process [11].

The advantages of electrospinning are low cost, high speed, vast material choices, fast operation, versatility, and small space requirements. In addition, thanks to this technique, control is achieved in fiber diameter and microstructure. Process and solution parameters including solution composition, polymer solution feed rate, applied voltage, and distance between tip and the collector affect average nanofiber diameters. The type of solvent also affects the morphology and properties of nanofiber membranes. The dipole moment, conductivity, boiling point, viscosity and surface tension of solutions determine electrospinnability. Mechanical, chemical and thermal stability of nanofiber membranes are critical properties that affect the performance of nanofiber membranes. Nanofiber membranes are used in many applications, especially battery separation, filtration, protective clothing, sensors, composite reinforcement, tissue engineering, wood dressing etc. Polyacrylonitrile, polyvinylidene fluoride, polyethylene oxide, polyvinyl alcohol, polyurethane etc. are involved in the production of nanofiber membranes [11,12].

2.12 Electrospinning of PAN for Nanofiber Production

Polyacrylonitrile (PAN) polymer has low density, high polymer strength, elasticity, good solvent resistance, high ionic conductivity, good thermal stability and good compatibility with Li metal. Thus, PAN nanofiber is widely used in membrane air filters, water filters and carbon fibers [13,42]. Fiber forming processes of PAN are important in the production of functional materials based on PAN. The discovery of aprotic polar solvents suitable for spinning PAN, such as N,N-dimethylformamide (DMF), dimethyl sulfoxide (DMSO), N,N-dimethylacetamide (DMAc) and dimethylsulfone, which were developed for the production of PAN fibers, is important. This soon led to the invention of electrospinning, a technique invented in 1934 to produce nanofibers from polymer materials by applying high voltage to a polymer solution until a small jet of polymer solution ejects. There are other methods for the production of PAN nanofibers such as vapor growth, arc discharge, laser ablation, and chemical vapor deposition. But compared to them, electrospinning can easily generate nanofibers with diameters from 10 nm to several mm under the application of an electrostatic force. Significant electrostatic forces occur between the dipoles of adjacent nitrile groups, and this intramolecular interaction leads to a stiffer chain due to restricting bond rotation [43].

2.13 Contact Angle and Wettability Behavior

Contact angle is important to determine wettability behavior. The angle between the liquid and solid material is measured. Additionally, the effect of ambient air and gravity should also be kept in mind. In other words, the contact angle is the angle formed by solid, liquid and gas phase materials with the effect of gravity. The forces of attraction between the liquid own molecules are called cohesion forces, and the forces of attraction between the liquid and the solid are called adhesion forces. The magnitude of the angle depends on these attraction forces. If the magnitude of cohesion forces is greater than adhesion forces, the contact angle between the liquid and the solid also increases. When the liquid-solid attraction forces are low, the contact angle increases, and when these forces are high, the contact angle decreases. The wettability properties of solid materials occur depending on the value of the contact angle created by the liquid dropped on the solid material. When the contact angle value is below 90°,

the solid is hydrophilic, and it is above 90°, it is hydrophobic. In Figure 2.14, wetting behavior conditions are shown based on contact angle values [44].

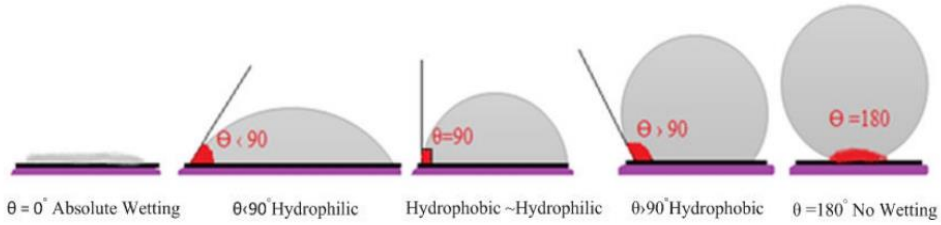

Figure 2.14 : The representation of the wetting behavior based on the value of the contact angles [44].

2.14 UV Curing of Maleimide Containing Systems

Photocuring has found numerous industrial applications and will continually find new applications in advanced technologies. The photopolymerization system generally consists of photoinitiator, reactive oligomer and mono/multifunctional monomer. The photoinitiator absorbs UV light, producing reactive species, free radicals and ions, and converts the monomer or oligomer into a cross-linked network [45]. The advantages of photocuring are its unique benefits such as solvent-free formulations, high-cure rate and low temperature processing. Acrylate-based photocurable formulations with various photoinitiators are currently used in most photocurable formulations due to their superior reactivity [46]. Photoinitiators do not react completely in photocuring and small molecular byproducts are formed by photolysis. Residual photoinitiator and small molecular by-products turn the light-cured product yellow, age it, give it odor and deteriorate its appearance and performance. Maleimide (MI) and its derivatives, due to the presence of active polymerizable groups, can generate free radicals to initiate photopolymerization and copolymerize with photocurable resin. These can increase the thermal property of post-cured materials due to the incorporation of photopolymerization-hardened five-membered maleimide rings (MIs) into the polymer chain [47]. Bismaleimide is widely used in adhesive, packaging and aerospace industries with its other important properties such as low moisture absorption, highly cross-linked structures, high chemical resistance, high mechanical stability [48]. The electron-withdrawing maleimide group has unique homo- and copolymerization properties and has been used as an attractive monomer to design special phenolic polymers. N-(4-hydroxyphenyl)maleimide (HPM) is designed to

modify the thermal stability and fire resistance of organic matrix materials. They also incorporate pendant phenol functions into the polymer backbone through copolymerization with selected comonomers. The precursor phenolic functions themselves combine with many other functional groups such as cyanate, epoxies, isocyanates [49]. Epoxy acrylate (EA) resins are one class of the most important and extensively used reactive oligomers in UV-curing systems because of their networks possessing high stiffness and strenght, excellent chemical and solvent resistance, good adhesion properties and so on. Therefore, UV-curable epoxy acrylate coatings are widely use for protective coatings. Epoxy acrylate is synthesized by adding vinyl ester groups and carbon-carbon double bonds to epoxy resin and can be cured with radical photoinitiators. However, flammability is one of the principal disadvantages of epoxy acrylates. Therefore, it is essential to generate epoxy acrylates with excellent flame retardance [50-52]. Urethane acrylate oligomers have been the most widely used components in the preparation of UV-curable coatings. This is due to they provide good adhesion to various substrates, flexibility, impact strenght, weatherability, water resistance and solvent resistance compared to other oligomers [53,54].

3. EXPERIMENTAL PART

3.1 Materials and Chemicals

3.1.1 Monomers

Acrylonitrile (AN):

It was distilled in vacuo and kept cold before use.

Styrene (St, Organik Kimya):

It was distilled in vacuo and kept cold before use.

Tripropylene glycol diacrylate (TPGDA, Photomer 4061 F, Cognis):

It is a difunctional acrylate that shows good flexibility, abrasion, scuff resistance and high reactivity in coatings given in Figure 3.1. It was used as received.

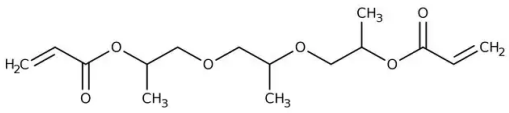

Figure 3.1 : Chemical structure of tripropylene glycol diacrylate.

Trimethylolpropane [3 PO] triacrylate (TMP3POTA, Photomer 4072 F, Cognis):

It is an aliphatic trifunctional acrylate of low viscosity with high crosslinking properties given in Figure 3.2. It was used as received.

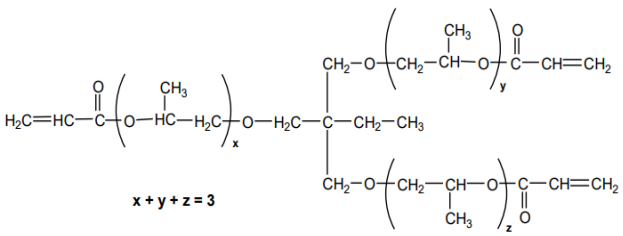

Figure 3.2 : Chemical structure of trimethylolpropane [3 PO] triacrylate.

Dipropylene glycol diacrylate (DPGDA):

DPGDA seen in Figure 3.3 is used in coatings and inks with improved flexibility, good cure response adhesion and high moisture resistance. It was used as received.

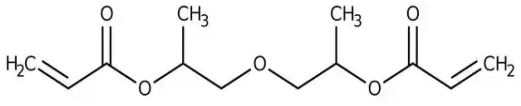

Figure 3.3 : Chemical structure of dipropylene glycol diacrylate.

3.1.2 Solvents

Acetone (≥99.5%, Honeywell):

It was dried and distilled.

N,N-Dimethylformamide (DMF, 99%, Merck):

It was distilled in vacuo before use.

Ethyl acetate (99.9%, Carlo Erba):

It was used as received.

Toluene (≥99.9%, Merck):

It was dried and distilled.

Dichloromethane (DCM, 99.9%, Carlo Erba):

It was used as received.

n-Hexane (≥96%, Isolab):

It was used as received.

Chloroform ($CHCl_3$, ≥99.0%, Sigma Aldrich):

It was used as received.

Tetrahydrofuran (THF, ≥99.9%, Honeywell):

It was used as received.

Methanol (≥99.9%, Merck):

It was used as received.

3.1.3 Other chemicals

Maleic anhydride (≥99%, Merck):

It was used as received.

4-Aminobenzoic acid (99%, Alfa Aesar):

It was used as received.

Acetic anhydride (>98%, Merck):

It was used as received.

Sodium acetate (99.3%, VWR Chemicals):

It was used as received.

Thionyl chloride ($SOCl_2$, ≥99.0%, Merck):

It was used as received.

Triethyl amine (TEA, ≥99.0 %, Merck):

It was used as received.

3,5-Dihydroxybenzyl alcohol (99%, Aldrich):

It was used as received.

18-Crown-6 (99%, Aldrich):

It was used as received.

2,3,4,5,6-Pentafluorobenzylbromide (98%, abcr):

It was used as received.

Potassium carbonate (99+%, Lancaster):

It was used as received.

Magnesium sulfate ($MgSO_4$, Carlo Erba):

It was used as received.

Sodium sulfate (Na_2SO_4, ≥99.0, Merck):

It was used as received.

2,2′-Azobis(2-methylpropionitrile) (AIBN, 98%, Acros Organics):

It was used as received.

Ethylene glycol (99.9%, ACROS)

It was used as received.

Polyacrylonitrile (PAN, average Mw 150,000 Typical, Aldrich):

It was used as received.

Polystyrene (pSt, average Mw 192,000, Aldrich):

It was used as received.

Bisphenol A epoxy diacrylate diluted with 20% TPGDA (Photomer 3016 20 RF, Cognis):

It exhibits high gloss, chemical resistance and improved flexibility. It was used as received.

Aliphatic urethane diacrylate diluted in 12% 1,6-hexanediol diacrylate (HDDA) (Doublemer 584, Filli Boya):

It exhibits excellent flexibility, good toughness, excellent durability and is non-yellowing. It was used as received.

2-Hydroxy-2-methyl-1-phenyl-propan-1-one (Darocur 1173, Ciba):

It is a variant in effective liquid photoinitiator which is used to initiate the photopolymerization of unsaturated prepolymers given in Figure 3.4. It was used as received.

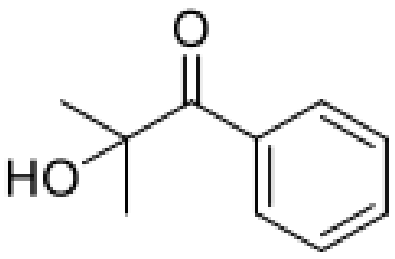

Figure 3.4 : Chemical structure of 2-hydroxy-2-methyl-1-phenyl-propan-1-one.

3.2 Characterization Methods, Equipment and Analysis

3.2.1 Infrared analysis (IR)

IR spectroscopy provides information about functional groups present in organic or inorganic molecules. FT-IR spectrum was recorded using Nicolet FT-IR iS10 spectrometer in a range of 4000-400 cm^{-1} with a range resolution of 4 cm^{-1}.

3.2.2 Nuclear magnetic resonance (NMR)

^{1}H-NMR, ^{13}C-NMR and ^{19}F-NMR spectra were obtained from Agilent VNMRS 500 MHz spectrometer using deuterated dimethyl sulfoxide (DMSO-d_6) and deuterated chloroform ($CDCl_3$) as solvent.

3.2.3 Gel permeation chromatography (GPC)

Gel permeation chromatography (GPC) analyses were performed with an Agilent pump equipped with three Agilent Zorbax PSM 1000S, 300S and 60S columns at a flow rate of 0.5 mL/min and the temperature of the refractive index detector of 30 ℃, and THF as eluent. The molecular weights of the polymers were calculated with the aid of polystyrene (pSt) standards.

3.2.4 Differential scanning calorimetry (DSC)

The glass transition temperatures of the polymers were measured by differential scanning calorimetry (TA, DSC Q10) in a flowing nitrogen atmosphere at a scanning rate of 10 °C/min.

3.2.5 Thermogravimetric analysis (TGA)

The thermal stability of the polymers was measured by thermogravimetric analysis (TA, TGA Q50) in a flowing nitrogen atmosphere at a heating rate of 20 °C/min.

3.2.6 Spin coating

Plexiglass substrates were coated with the prepared polymer solutions using spin coater. The spin coating process was performed using a SCS P6700 Series model device in 27 seconds at 1000 RPM.

3.2.7 Contact angle measurements

Contact angles of distilled water and ethylene glycol were measured at room temperature with a KSV Attension Theta Lite contact angle instrument. Distilled water and ethylene glycol drops were dropped onto the surfaces from a distance of 0.5 mm in a 1000 μL syringe.

3.2.8 Gel content

Gel content measurements were determined by weighing a cured film sample (m_1) accurately. The cured film was immersed in acetone for 48 h at room temperature. The film was then dried at 60 ℃ until its weight was constant to get the weight m_2. Gel content of the UV-cured film was calculated by equation 3.1:

$$Gel\ content\ (\%) = \frac{m_2}{m_1} x\ 100\% \tag{3.1}$$

where m_1 is the weight of the cured film sample; m_2 is the residual weight of the cured film sample.

3.2.9 Chemical and solvent resistance

Chemical and solvent resistance of the UV-cured films was determined by weighing a cured film sample (m_a) and then immersing into various chemicals and solvents at 25 ℃. The samples were kept in various chemicals and solvents for 24 h and then dried. Chemical and solvent resistance values were calculated by the equation 3.2:

$$Weight\ loss\ (\%) = \frac{m_a - m_b}{m_a}\ x100\% \tag{3.2}$$

where m_a and m_b are weights of the dry sample before and after immersion into various chemicals and solvents, respectively. Materials used for chemical resistance: 10% HCl and 10% NaOH; materials used for solvent resistance: xylene, methanol and chloroform.

3.2.10 Water absorption

Water absorption measurements of UV-cured samples were carried out in distilled water at 25 ℃ according to ASTM D 570. Weighed samples were kept in distilled

water at 25 ℃ for 24 h until equilibrium absorption was obtained. The films were then removed, the surface water was wiped off with a piece of filter paper and weighed again. In addition, water resistance values were calculated by equation 3.3:

$$Water\ absorption\ (\%) = \frac{m_b - m_a}{m_a}\ x\ 100\% \tag{3.3}$$

where m_a denotes the initial weight of cured films and m_b represents the weight of the UV-cured films after immersion in water.

3.2.11 Hardness

The pendulum hardness of the UV-cured films was determined with a pendulum hardness tester (BYK-Gardner) according to ASTM D 4366 (pendulum weight=200 ± 0.2 g, amplitude limitation angle (deflection)=6-3°, oscillation period=1.4 s). The pencil hardness of the UV-cured films was determined by ASTM D 3363. Pencil hardness test was applied on coated wooden plates.

3.2.12 Cross-cut adhesion

Adhesion testing was performed using a cross-cut adhesion tester to check the adhesion of the coating to the wood substrate according to ASTM D 3359.

3.2.13 Limiting oxygen index

Limiting oxygen index (LOI) test was conducted with an MARESTEK instrument according to ASTM D2863-17-Oxygen Index Test standard.

3.3 Preparation Methods

3.3.1 Synthesis of (Z)-4-(3-carboxyacrylamido)benzoic acid (N-(4-carboxyphenyl)maleamic acid, CPMA)

50 mL of dimethylformamide (DMF) was added to 4-aminobenzoic acid (13.71 g, 0.1 mol) under nitrogen. Maleic anhydride (9.81 g, 0.1 mol) and 25 mL DMF were taken into a dropping funnel and dropped onto the mixture containing 4-aminobenzoic acid and DMF, which was prepared before. The mixture was allowed to stir at room temperature for 4 hours under a nitrogen atmosphere. At the end of the reaction, the mixture was precipitated with ice. It was filtered and dried under vacuum at 60 ℃.

Yield: 95 %; FT-IR ν (cm^{-1}): 3310, 2997, 1685, 1534, 1508, 1290, 845, 674; ^{1}H-NMR (DMSO-d_6), δ (ppm): 12.82 (s, 2H), 10.62 (s, 1H), 7.91 (d, 2H), 7.73 (d, 2H), 6.49 (d, 1H), 6.32 (d, 1H) ppm.

3.3.2 Synthesis of 4-(2,5-dioxo-2,5-dihydro-1H-pyrrol-1-yl)benzoic acid (N-(4-carboxyphenyl)maleimide, CPMI)

Sodium acetate (1.61 g, 0.019 mol) and acetic anhydride (17.8 mL, 0.189 mol) were added under nitrogen, respectively. They were dissolved by adding 13 mL DMF. The temperature was set to 40 ℃. CPMA (12 g, 0.051 mol) were added to the reaction mixture. The mixture was left to stir for 5 hours under nitrogen at 65 ℃. The reaction mixture was filtered after precipitation with ice water. The product was boiled with 350 ml of ethyl acetate, filtered and allowed to crystallize. The product was dried in a vacuum at 60 °C. Yield: 81.1 %; FT-IR ν (cm^{-1}): 3101, 1775, 1701, 1603, 1515, 1380, 1300, 1214, 1176, 952, 697; ^{1}H-NMR (DMSO-d_6), δ (ppm): ^{1}H-NMR (DMSO-d_6), δ (ppm): 13.10 (s, 1H), 8.04 (d, 2H), 7.50 (d, 2H), 7.22 (s, 2H) ppm.

3.3.3 Synthesis of 4-(2,5-dioxo-2,5-dihydro-1H-pyrrol-1-yl)benzoyl chloride (N-(4-(chlorocarbonyl)phenyl)maleimide, CPMIC)

CPMI (15.70 g, 0.072 mol) and thionyl chloride ($SOCl_2$) (131 mL, 1.807 mol) were mixed under nitrogen gas. The reaction was carried out in an oil bath fixed at 80 °C. It was refluxed for approximately 4.5 hours. Unreacted $SOCl_2$ was separated by vacuum distillation. After drying in a vacuum at 40 °C, it was crystallized with toluene. Then it was dried in vacuum at 60 ℃. Yield: 72.78%, m.p: 168-169 ℃; FT-IR ν (cm^{-1}): 3168, 3108, 1771, 1709, 1596, 1506, 1388, 1370, 1136, 951, 876, 821, 761, 684; ^{1}H-NMR (DMSO-d_6), δ (ppm): 8.04 (d, 2H), 7.49 (d, 2H), 7.21 (s, 2H) ppm.

3.3.4 Synthesis of 3,5-bis(perfluorobenzyl)oxybenzyl alcohol (FOH)

3,5-dihydroxybenzyl alcohol (1.71 g, 12.2 mmol) and 18-crown-6 (0.32 g, 1.21 mmol) were dissolved by mixing in 100 mL of acetone. Pentafluorobenzyl bromide (6.62 g, 25.3 mmol) and K_2CO_3 (3.52 g, 25.4 mmol) were added to the prepared mixture. The mixture was allowed to stir vigorously under nitrogen. After 3 days, the acetone was removed in vacuo. The residue was partitioned between water (40 mL) and CH_2Cl_2 (40 mL), the aqueous layer was extracted with CH_2Cl_2 (3x 200 mL). CH_2Cl_2 extracts were collected, dried with $MgSO_4$, concentrated in vacuo. The product, (FOH), was

obtained by crystallization from 50% hexane/CH_2Cl_2. Yield: 72%, m.p: 98 °C; FT-IR ν (cm^{-1}): 3299, 2958, 2895, 1658, 1596, 1524, 1502, 1378, 1285, 1081, 1038, 934, 828, 687; ^{1}H-NMR (DMSO-d_6), δ (ppm): 6.67 (d, 2H), 6.50 (t, 1H), 5.11 (s, 4H), 4.67 (d, 2H), 1.74 (t, 1H) ppm.

3.3.5 Preparation of (3,5-bis((perfluorophenyl)methoxy)benzyl-4-(2,5-dioxo-2,5-dihydro-1H-pyrrol-1-yl)benzoate (Perfluoromaleimide Monomer, FMI)

FOH (2.1g, 4.2 mmol) and 15 mL $CHCl_3$ were mixed in a flask over a salt-ice bath. After adding triethylamine (0.7 mL, 4.6 mmol), the reaction temperature was waited to drop below 0 °C. CPMIC (1.0 g, 4.2 mmol) dissolved in 100 mL of chloroform was added to the dropping funnel and added to the mixing flask by controlling the temperature. The reaction mixture was allowed to stir in a salt-ice bath for 2 hours. After 2 hours, the salt-ice bath was removed and the reaction system was allowed to stir at room temperature for 1 day. At the end of the reaction, the mixture was extracted with water and chloroform. After drying by adding Na_2SO_4, it was filtered, the solvent was evaporated, and dried under vacuum at 40 °C. Yield: 68%, m.p: 84±1 °C; FT-IR ν (cm^{-1}): 2890, 1713, 1684, 1658, 1598, 1523, 1502, 1381, 1234, 1132, 823, 753, 689; ^{1}H-NMR (DMSO-d_6), δ (ppm): 8.04 (d, 2H), 7.50 (d, 2H), 7.21 (s, 2H), 6.65 (d, 2H), 6.62 (t, 1H), 5.17 (s, 4H), 4.45 (s, 2H). ^{13}C-NMR (DMSO-d_6), δ (ppm): 169.95, 166.72, 158.80, 146.13, 145.79, 144.16, 142.06, 140.05, 138.08, 136.09, 135.53, 134.86, 129.89, 129.59, 126.10, 110.32, 105.89, 100.05, 62.63, 57.43. ^{19}F-NMR (DMSO-d_6) δ = -143.13 (m, 4F, ortho-F), -153.46 (m, 2F, para-F), -162.31 (m, 4F, meta-F) ppm.

3.3.6 Synthesis of AN and FMI copolymers (p(AN-co-FMI) copolymers)

Dry nitrogen and vacuum were applied three times to the dry Schlenk tube, which was mixed with a magnetic stirrer. Under nitrogen, certain amounts of FMI monomer, DMF, AN, AIBN (1.5 mol % of total monomer) were added, respectively. The tube with the polymerization mixture was placed in a silicone oil bath preheated to 75 °C. After 96 hours, the tube was removed from the oil bath and allowed to cool to room temperature. The polymers were precipitated in distilled water, filtered and dried under vacuum at 40 °C.

3.3.7 Synthesis of St and FMI copolymers (p(St-co-FMI) copolymers)

Dry nitrogen and vacuum were applied to the dry Schlenk tube three times under a magnetic stirrer. Determined amounts of FMI monomer, toluene, styrene, and AIBN (2.5 mol % of total monomer) were added. The tube containing the polymerization mixture was placed in an oil bath preheated to 75 ℃. After 24 hours, the tube was removed from the oil bath, cooled to ambient temperature, the reaction mixture was diluted with THF. Polymers were precipitated in methanol and allowed to dry under vacuum.

3.3.8 Film preparation in spin coater

Solutions of the synthesized acrylonitrile containing copolymers were prepared concentrations of 50 mg in 3 mL of THF. Solutions of the synthesized styrene containing copolymers were prepared of 30 mg in 3 mL of THF. Thin polymer films were spin coated (1000 rpm for 27 s) on clean and dry glass substrate using an SCS P6700 spin coater. After spin coating, the films were placed in the oven at 90 ℃ for 2 hours. Thus, the glass substrates was coated with polymer.

3.3.9 Preparation of PAN nanofibers

Polymer/PAN nanofibers containing p(AN-co-FMI)-30/70 and pFMI polymers at 5% and 20% by weight were prepared. Additionally, 100 wt% PAN, 20 wt% pSt/PAN, 20 wt% p(St-co-FMI)-50/50/PAN and 20 wt% p(St-co-FMI)-25/75/PAN fibers was prepared. PAN and polymers were dissolved in DMF and stirred at ambient temperature for 24 hours to obtain solutions of the fibers. The polymer/PAN solution was then electrospun into nanofiber with the following process parameters: flow rate of 1 mL h^{-1}, voltage of 12 kV, and tip-to-collector distance of 10 cm.

3.3.10 Film preparation by UV-curing

UV curable formulations were prepared by mixing varying proportions of bisphenol A epoxy diacrylate diluted with 20% TPGDA, aliphatic urethane diacrylate diluted in 12% 1,6-hexanediol diacrylate, FMI, TMP3POTA, TPGDA, DPGDA, boron methacrylate, and photoinitiator. Each formulation was prepared in a beaker with adequate stirring. In order to remove air bubbles formed during mixing, the beaker content kept under gentle vacuum for 10 min without disturbing the composition. After removal of air bubbles, the prepared formulations were coated onto wood panels using

a glass baguette obtaining a layer thickness of 100 μm. The applied wet coatings were cured by high pressure UV lamp situated 15 cm above the panels. Moreover, hybrid free films were prepared by pouring the UV curable liquid formulations on to a Teflon mold (10 mm x 50 mm x 1 mm). In order to prevent the inhibiting effect of oxygen, the mixture in the mold and on the wood panels was covered by transparent, thin polyester film before irradiation with a high pressure UV-lamp (OSRAM 300W, λ_{max}=365 nm). A glass plate was placed over to obtain a smooth thin surface. The formulations were irritated under a high-pressure UV lamp for 300 s. After irradiation under UV-lamp, 1000 μm thick free hybrid films were obtained.

4. RESULTS AND DISCUSSION

4.1 Synthesis of Perfluoromaleimide Monomer (FMI)

N-(4-carboxyphenyl)maleimide (CPMI) were obtained by the reaction of an equimolecular mixture of maleic anhydride with 4-aminobenzoic acids followed by cyclodehydration, in the presence of acetic anhydride and sodium acetate in DMF solvent [1, 39]. A mixture of N-(4-carboxyphenyl)maleimide (CPMI) and thionyl chloride ($SOCl_2$) was refluxed at 80°C. Unreacted thionyl chloride was evaporated to yield the residual product N-[4-(chlorocarbonyl)phenyl]maleimide (CPMIC) which was recrystallized from toluene (Figure 4.1).

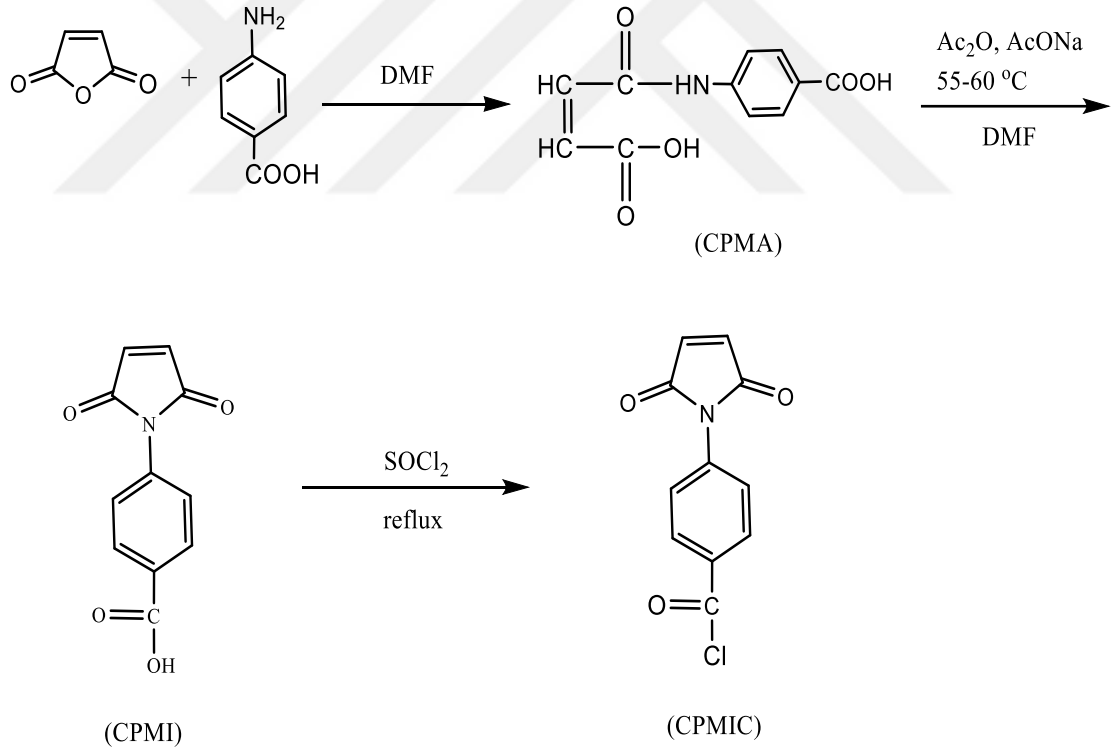

Figure 4.1 : Synthesis of N-[4-(chlorocarbonyl)phenyl]maleimide (CPMIC).

The FT-IR spectrum of CPMA showed absorptions at 3200-2700 (carboxylic acid O-H), 3310, 1534, 1508 (amide N-H), 1685 (carboxylic acid and amide), 1290 (carboxylic acid C-O), 845 (CH=CH), 674 (C-H bending) in cm^{-1}.

The ^{1}H-NMR spectrum of CPMA in DMSO-d_6 is given in the Figure 4.2. The double-bonded -CH proton attached to the carboxylic acid group was observed at 6.34-6.31 ppm, and the other double bonded -CH proton was observed at 6.50-6.48 ppm. In the ring structure, carbon protons in the meta position to the carboxylic acid were found to be at 7.74-7.72 ppm, and carbon protons in the ortho position were found to be at 7.92-7.90 ppm. A sharp peak at 10.62 ppm belonging to the N-H group and a broad peak at 12.82 ppm belonging to the protons of the carboxylic acid OH groups were observed.

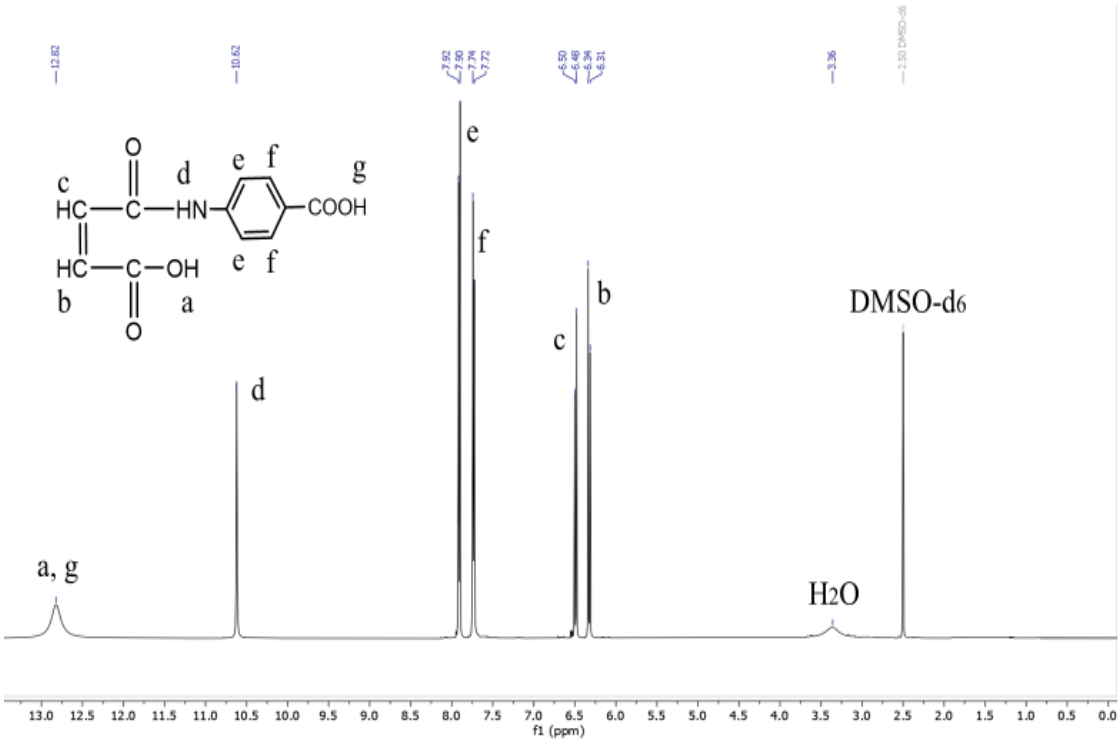

Figure 4.2 : ^{1}H-NMR (in DMSO-d_6) spectrum of CPMA.

The IR spectrum of CPMI showed absorptions at 3500-2500 (carboxylic acid O-H), 1775 (C=O stretch, 5-membered imide ring), 1701 (-CONCO- imide I), 1603, 1515 (aromatic C=C), 1380 (C-N-C imide II), 1300 (C-N stretching imide III), 1214 (carboxylic acid C-O), 1176 (C-O), and 952, 697 (CH=CH) cm^{-1}.

The ^{1}H-NMR spectrum of the obtained CPMI was taken in DMSO-d_6. The ^{1}H-NMR spectrum of the product shown in Figure 4.3 showed that the structure was correct. OH proton at 13.10 ppm (s, 1H), -CH protons in maleimide (s, 2H) at 7.22 ppm, -CH protons in ortho position to the electron withdrawing group (-COOH) at 8.05-8.04 ppm (d, 2H), -CH protons in meta position to the electron withdrawing group at 7.51-7.49

ppm (d, 2H) were observed. The absence of N-H protons signaling at 10.62 ppm in the spectrum also confirmed the completeness of the cyclodehydration reaction. Thus, the imidization could be monitored by ^{1}H-NMR spectroscopy.

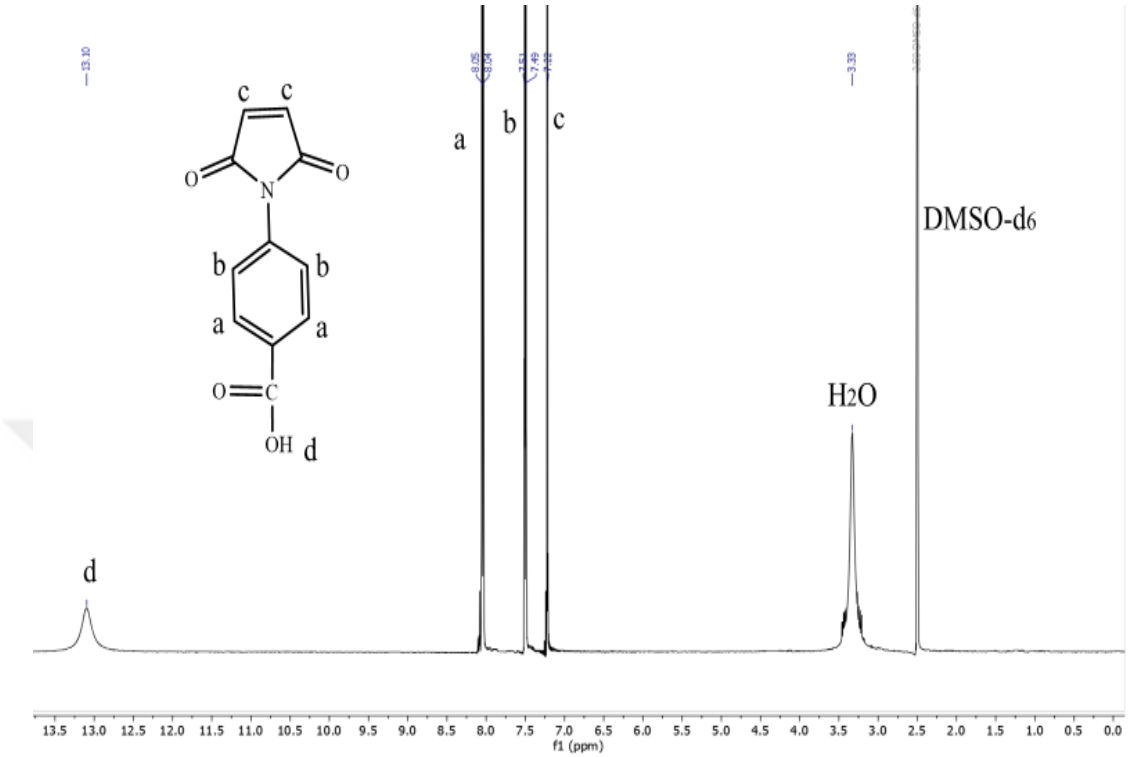

Figure 4.3 : ^{1}H-NMR (in DMSO-d_6) spectrum of CPMI.

The IR spectrum of CPMIC showed absorptions at 3168 (olefinic C-H), 3108 (aromatic C-H), 1771 (COCl), 1709 (-CONCO- imide I), 1596, 1506 (aromatic C=C), 1388 (C-N imide II), 1370 (CH), 1136 (C-N-C imide III), 951 (CH=CH), 876 (C-Cl), 821 (aromatic C-H), 761 (bending C=O imide IV), 684 (CH=CH) cm^{-1}. The shift of the carbonyl stretching peak and the absence of the OH peak at 3500-2500 cm^{-1} confirmed the formation of acyl chloride in the structure.

The disappearance of the signal at 13.10 ppm belonging to the OH proton in the ^{1}H-NMR of the structure taken in DMSO-d_6 showed that acyl chloride was formed instead of the carboxylic acid group. Protons belonging to maleimide gave signals at 7.21 ppm (s, 2H), aromatic protons in the ortho position to the acyl chloride at 8.05-8.03 ppm (d, 2H), and protons in the meta position to the acyl chloride at 7.50-7.49 ppm (d, 2H) (Figure 4.4).

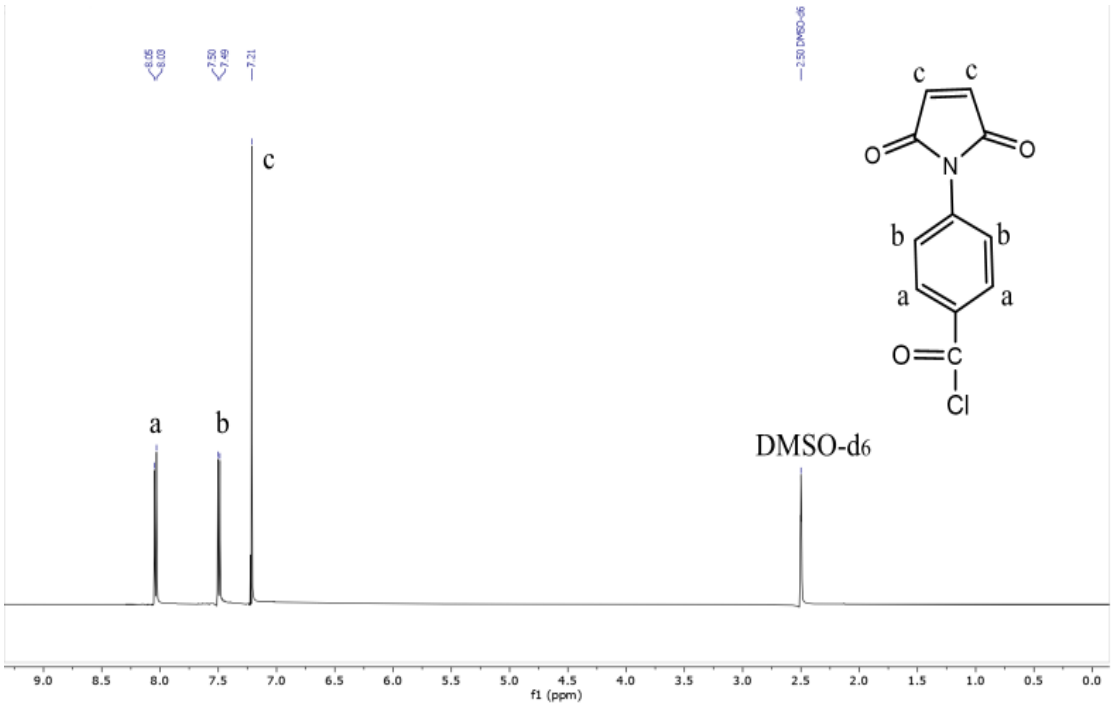

Figure 4.4 : ^{1}H-NMR (in DMSO-d_6) spectrum of CPMIC.

In this study, a new maleimide monomer containing a perfluoroaromatic group was synthesized using 3,5-bis(perfluorobenzyl)oxybenzyl alcohol (FOH) (Figure 4.5) [55].

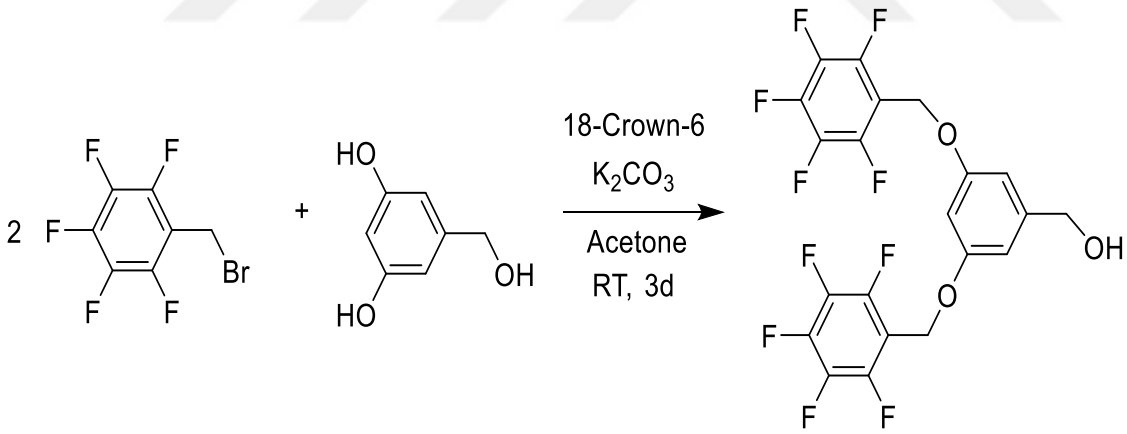

Figure 4.5 : Synthesis of FOH.

^{1}H-NMR of FOH in $CDCl_3$ is shown in the Figure 4.6. The signal of 1.74 ppm belonged to the OH proton of the alcohol. The carbon proton belonging to the hydroxyl group gave a signal at 4.67 ppm, the aromatic carbon protons in the ortho position to the primary alcohol group gave a signal at 6.67 ppm, the carbon protons in the para position gave a signal at 6.50 ppm, and the protons of the carbons attached to the ether group gave a signal at 5.11 ppm.

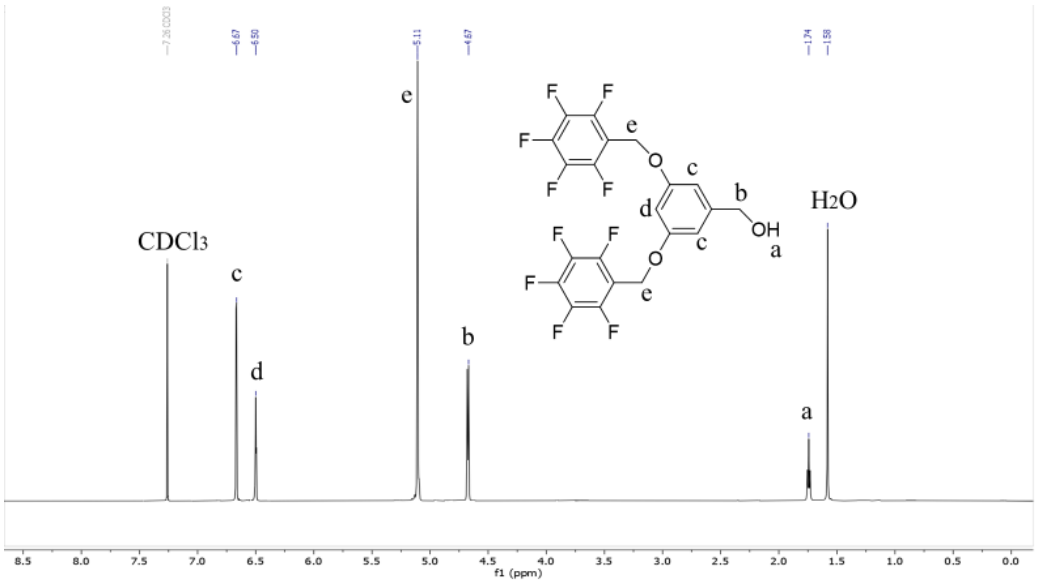

Figure 4.6 : ^{1}H-NMR (in $CDCl_3$) spectrum of FOH.

Perfluoromaleimide monomer containing perfluorinated aromatic group was synthesized from the esterification of N-[4-(chlorocarbonyl)phenyl]maleimide (CPMIC) with 3,5-bis(perfluorobenzyl)oxybenzyl alcohol (FOH) (Figure 4.7).

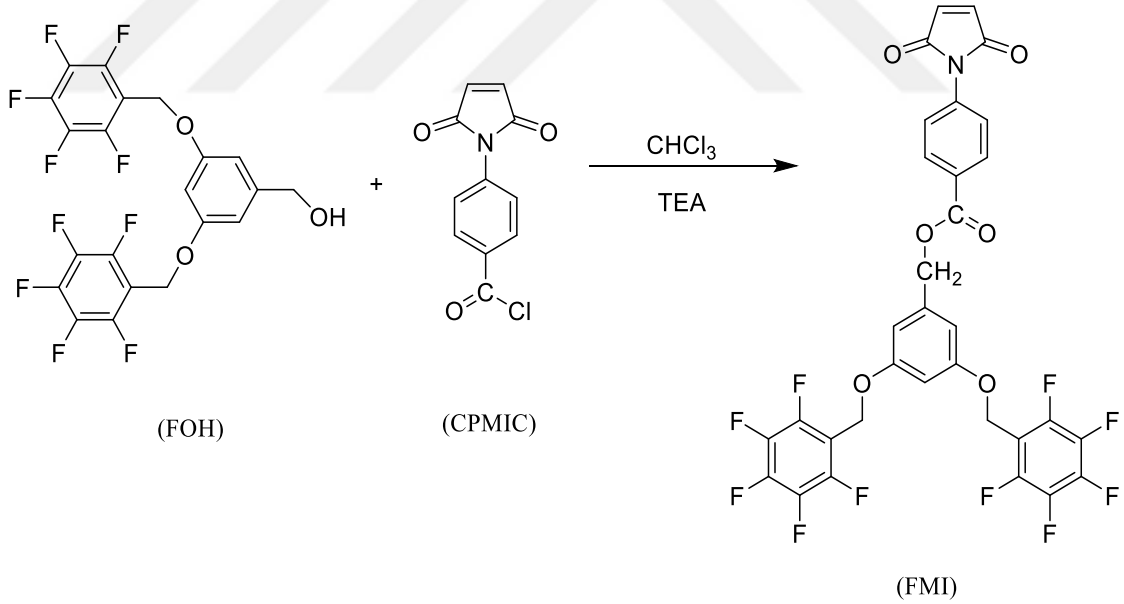

Figure 4.7 : Synthesis of FMI.

FT-IR spectra of FOH and FMI are shown in Figure 4.8. FOH, whose FT-IR spectrum gave a broad signal belonging to the -OH group at 3299 cm^{-1}. The absence of a signal belonging to the OH group in the FT-IR spectrum proved that FOH was bound. The FT-IR spectrum of FOH showed C-O-C band at 1285 cm^{-1} and bending in the C-H plane at 1081 and 1038 cm^{-1}. Aliphatic C-H bands at 2958, 2895 cm^{-1}, aromatic C=C

stretching bands at 1658, 1614, 1596, 1524 cm^{-1}, aromatic C-C stretching bands at 1502 cm^{-1} were seen in the FT-IR spectrum of FOH and FMI. The structure of FMI monomer was confirmed by FT-IR spectroscopy. The disappearance of the signal at 876 cm^{-1} belonging to N-[4-(chlorocarbonyl)phenyl]maleimide in the FT-IR spectrum proved the absence of acyl chloride. In addition, the FT-IR spectrum gave a characteristic C=O signal at 1713 cm^{-1}, indicating that an ester was formed instead of acyl chloride. The peak at 823 cm^{-1} corresponded to the disubstitution vibration of benzene (C-H_{arom}). And the absorption at 689 cm^{-1} was attributed to the CH=CH vibration of the maleimide ring. The peak at 1684 cm^{-1} showed the imide I carbonyl band (CONCO), the peak at 1234 cm^{-1} showed the C-O-C ester band, the peak at 1381 cm^{-1} showed the C-N imide II band, the peak at 1132 cm^{-1} showed the C-N-C imide III band and the peak at 753 cm^{-1} showed the C-O imide IV band.

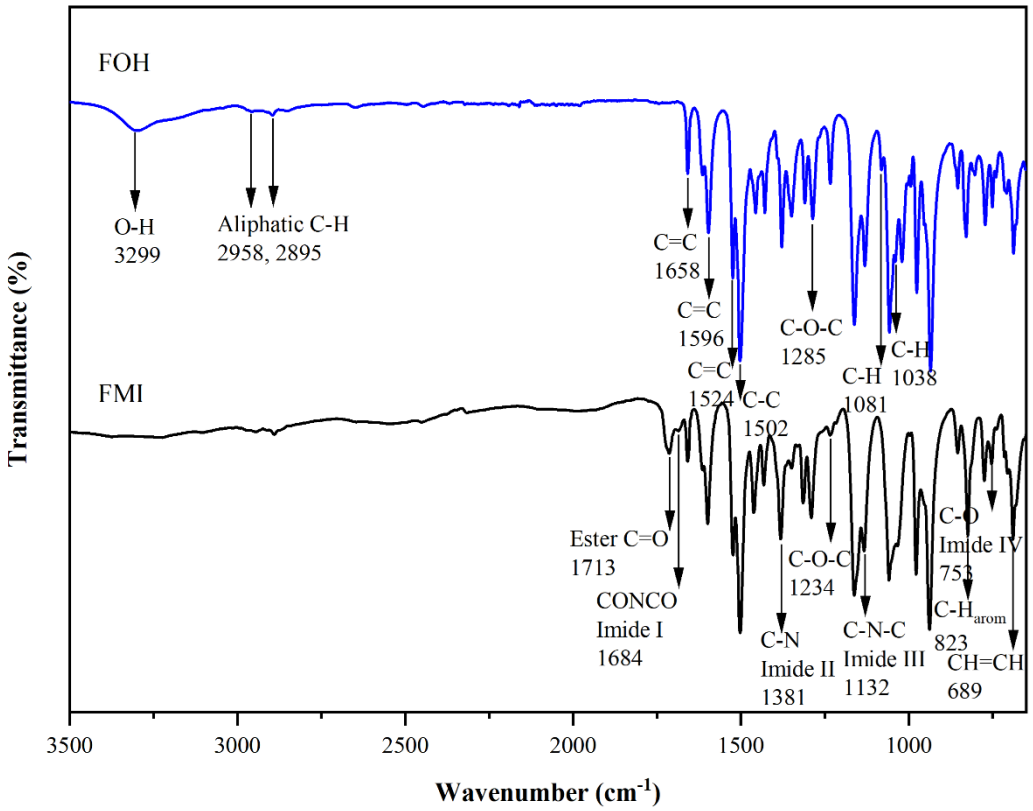

Figure 4.8 : FT-IR spectrum of FOH and FMI.

In the ^{1}H-NMR spectrum of FMI taken in DMSO-d_6, maleimide vinyl protons are at 7.21 ppm, Ar-H protons in the ortho position to the ester group are at 8.05-8.03 ppm, Ar-H protons in the meta position to the ester group are at 7.51-7.49 ppm were seen. OCH_2 protons attached to the ester group peaked at 4.45 ppm, two Ar-H protons

groups peaked at 6.65 ppm, one Ar-H proton peaked at 6.62 ppm, and -OCH_2 protons attached to ether groups peaked at 5.17 ppm. The absence of the -OH group peak at 1.74 ppm proved that FOH was bound to the structure (Figure 4.9).

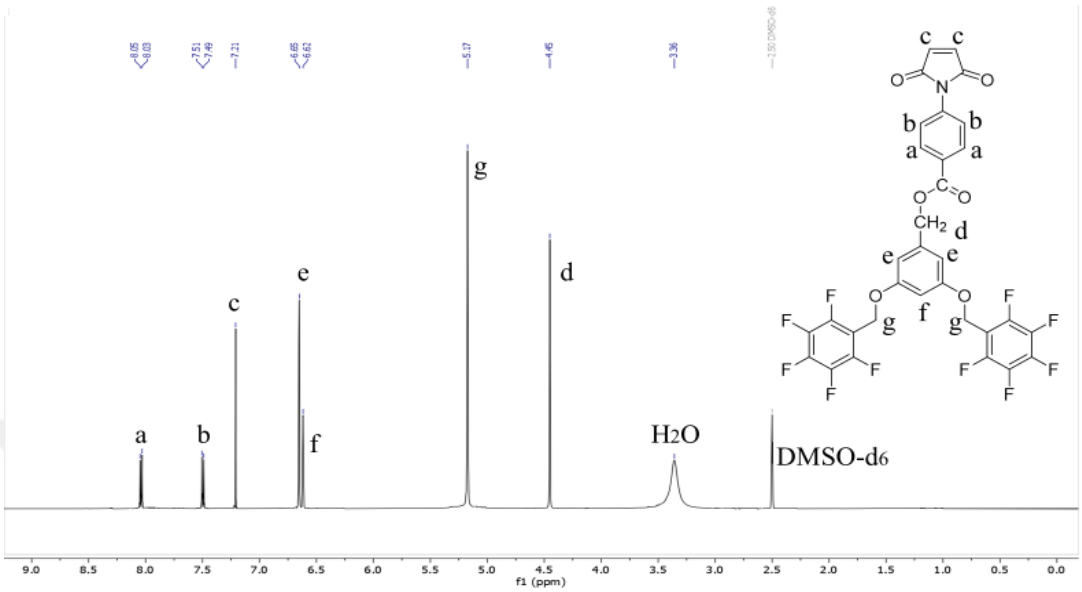

Figure 4.9 : ^{1}H-NMR (in DMSO-d_6) spectrum of FMI.

In ^{13}C-NMR taken in DMSO-d_6, carbonyl carbons of maleimide were seen at 169.95 ppm, vinylic carbons of maleimide at 134.86 ppm, aryl carbon attached to the imide group of maleimide at 135.53 ppm, and aryl carbon attached to the ester group at 129.59 ppm. The aryl carbons in the ortho position to the ester group gave peak at 129.89 ppm, the aryl carbons in the meta position to the ester group gave peak at 126.10 ppm, the ester carbon at 166.72 ppm, the -CH_2 carbon attached to the ester group at 62.63 ppm, and the aryl carbon attached to the CH_2 group at 145.79 ppm. It was observed that the aryl carbons attached to the ether group were at 158.80 ppm, the other carbon was at 100.05 ppm and two -OCH_2 carbons were at 57.43 ppm. Aryl carbons attached to the -OCH_2 groups were at 110.32 ppm, aryl carbons in the ortho position to the -OCH_2 group were at 146.13-144.16 ppm, aryl carbons in the meta position to the -OCH_2 group were at 142.06-140.05 ppm, aryl carbons in the para position to the -OCH_2 group were at 138.08-136.09 ppm (Figure 4.10).

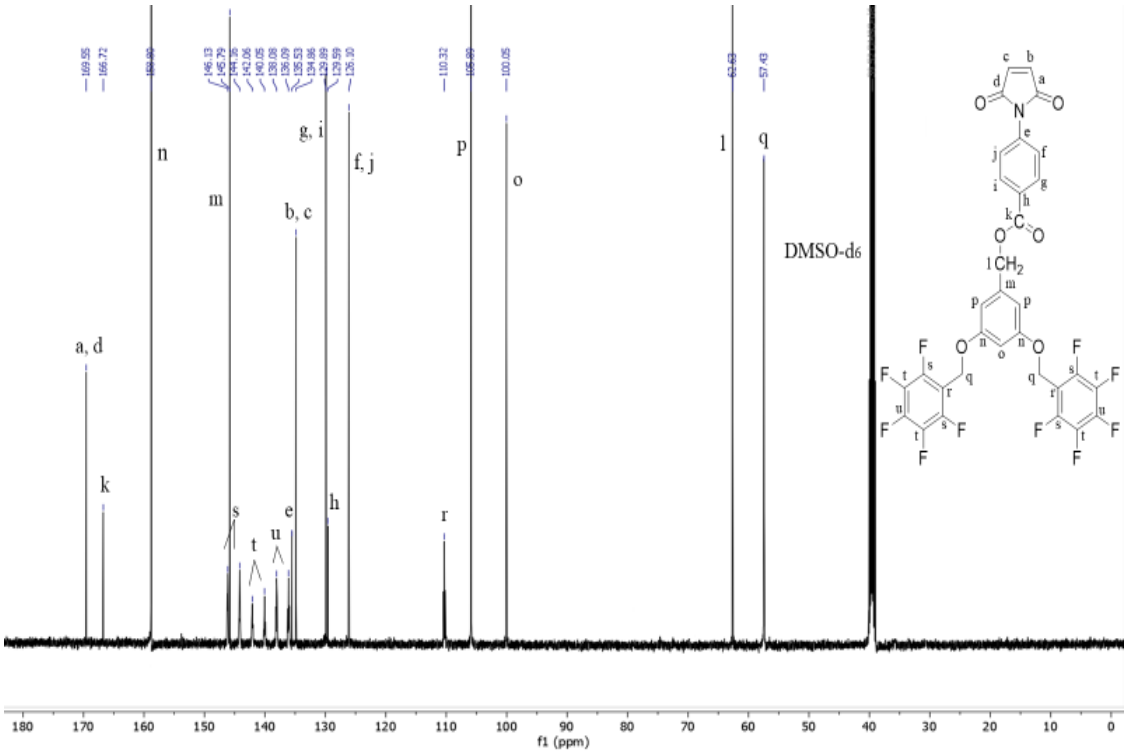

Figure 4.10 : ^{13}C-NMR (in DMSO-d_6) spectrum of FMI.

In Figure 4.11, ^{19}F-NMR (in DMSO-d_6) spectrum showed signals at -143.13, -153.46, -162.31 ppm assigned to ortho-F, para-F, meta-F atoms in the aromatic ring respectively.

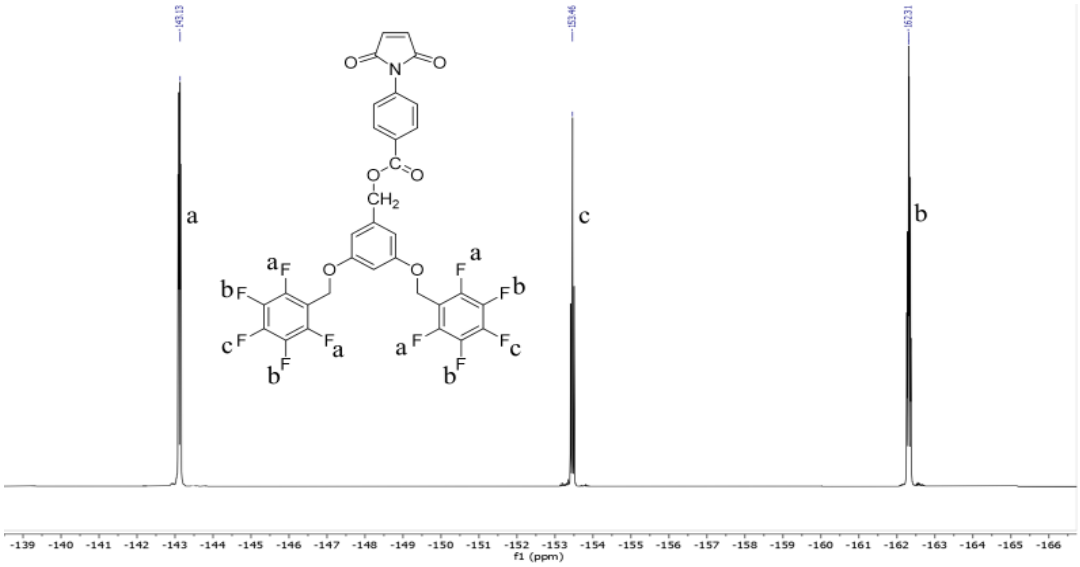

Figure 4.11 : ^{19}F-NMR (in DMSO-d_6) spectrum of FMI.

Mass spectrum of the FMI monomer showed the sodium adduct in electrospray positive ionization (ESI^+). Electrospray ionization/mass spectrometry (ESI/MS)

analysis pointed to the expected ion peak at m/z 722.06299 for $[M-Na]^+$, which led us to believe that the FMI was obtained. Additionally, in source fragmentation of the product ion resulted in a fragment ion with a mass-to-charge ratio of 718.09399, corresponding to the loss of four hydrogens. (m/z): Calculated for $C_{32}H_{15}F_{10}NO_6Na$ 722.443, Found: 722.0699 $[M-Na]^+$.

Solubility of the synthesized FMI monomer was tested in different solvents at room temperature and by heating. The results can be seen in Table. 4.1. FMI monomer dissolved at room temperature in a variety of solvents except n-hexane and diethyl ether.

Table 4.1 : Solubility of the synthesized FMI monomer in different solvents at room temperature and by heating.

Solvents	Solubility at room temperature	Solubility by heating
Acetone	+	+
DCM	+	+
Chloroform	+	+
THF	+	+
n-Hexane	-	-
Methanol	+	+
Ethanol	+	+
Diethyl ether	-	-
DMF	+	+
Toluene	+	+
Ethyl acetate	+	+

+, soluble; -, insoluble.

4.2 Free Radical Copolymerization of FMI Monomer with Acrylonitrile and Styrene

As seen in Figure 4.12, homopolymerization of FMI were carried out in DMF solution using AIBN as free radical initiator at 75 °C.

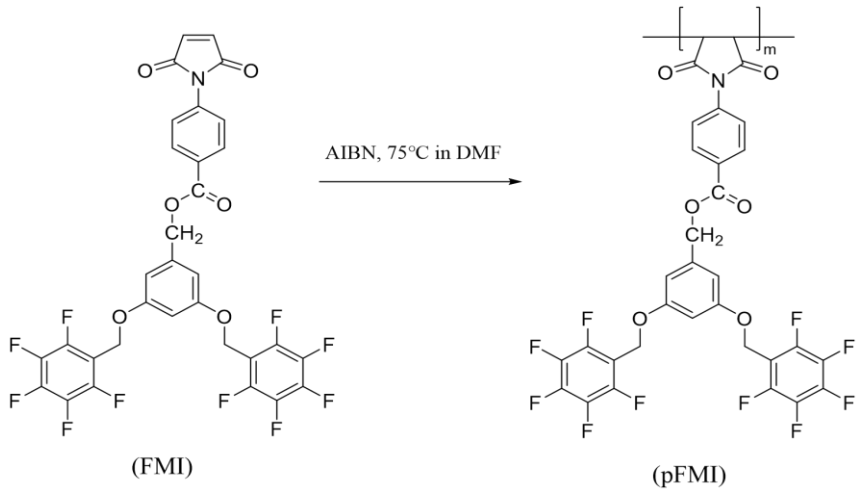

Figure 4.12 : Synthesis of pFMI homopolymer.

The ^{1}H-NMR spectrum of homopolymer pFMI is shown in Figure 4.13. The double bond in the maleimide structure became a single bond during polymerization. After polymerization, the absorption peak of the unsaturated bond of the maleimide ring disappeared at low field 7.21 ppm, and the single bond peaked at high field 3.90 ppm for the cis form and 4.28 ppm for the trans form. δ at 7.67-7.25 and 8.17-7.91 ppm corresponded to 2Ar-H ortho- and meta- to maleimide group, respectively. The δ at 4.45 ppm appeared for 2H in -$COOCH_2$- group of FMI segment. The δ at 6.76 ppm was for 2Ar-H, ortho- to ester group; at δ 6.63 ppm was for 1Ar-H, para- to ester group. -CH_2- group protons attached to the ether group were seen at 5.18 ppm.

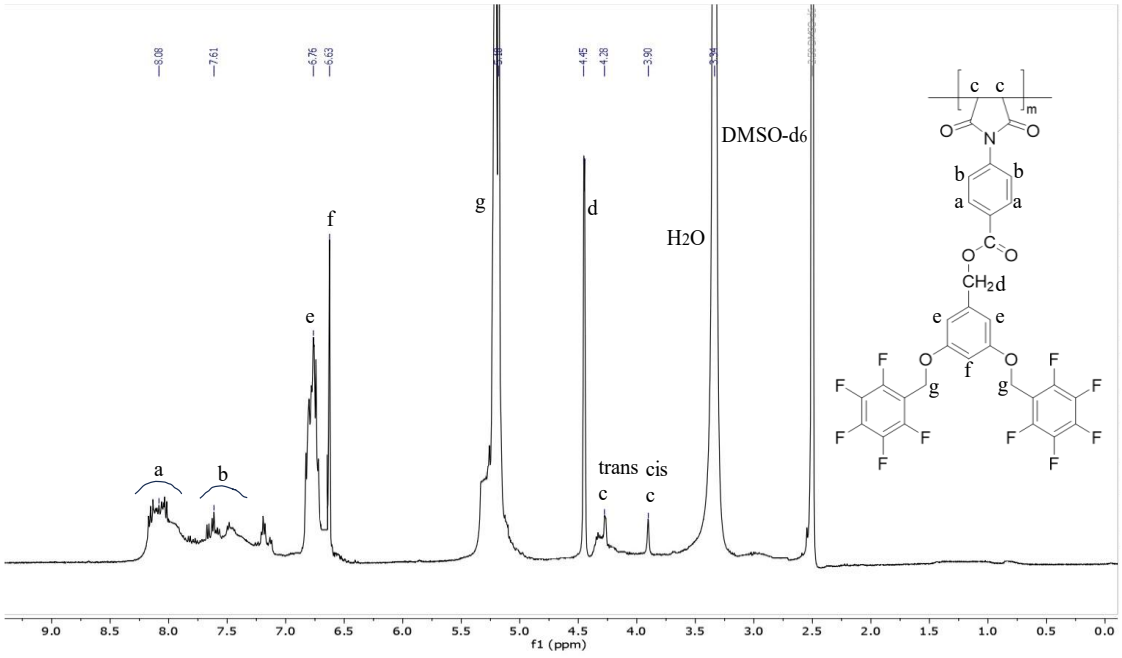

Figure 4.13 : ^{1}H-NMR (in DMSO-d_6) spectrum of pFMI homopolymer.

FMI was copolymerized with acrylonitrile initiated by AIBN in DMF at 75 °C (Figure 4.14).

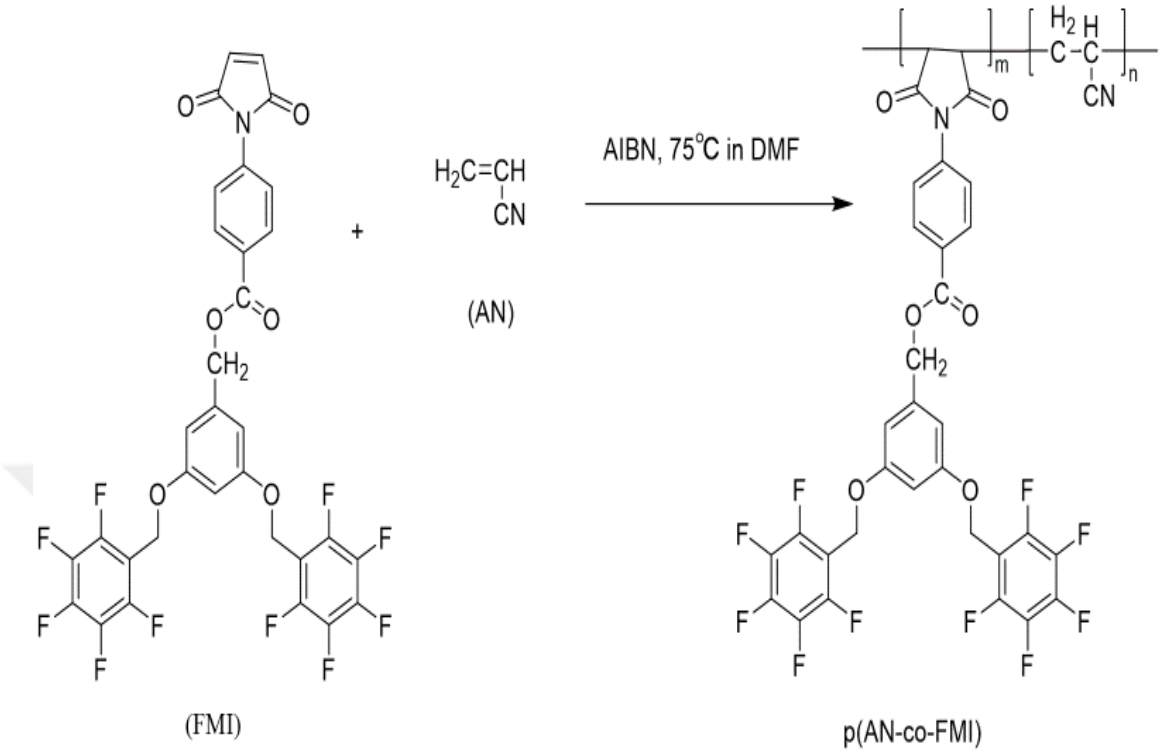

Figure 4.14 : Synthesis of p(AN-co-FMI) copolymers.

The ^{1}H-NMR spectrum of the copolymer formed by FMI monomer and acrylonitrile p(AN-co-FMI), taken in DMSO-d_6, is given in the Figure 4.15. In the ^{1}H-NMR spectrum, the peak at 2.04 ppm belonged to the -CH_2 protons of acrylonitrile, and the peak at 3.02 ppm belonged to the -CH proton of acrylonitrile. The double bond in the maleimide structure became a single bond during polymerization. In the maleimide unit, -CH=CH- protons were seen at 7.21 ppm when it was a monomer, while in p(AN-co-FMI) methine protons were seen at 3.90 ppm in the cis form and 4.27 ppm in the trans form. The peak at 8.17-7.95 ppm was assigned to 2Ar-H protons ortho to the ester group, and the peak at 7.72-7.26 ppm was assigned to 2Ar-H protons ortho to the maleimide. The signal at 4.45 ppm was observed for -OCH_2 protons, the signal at 6.76 ppm was observed for two Ar-H protons, the signal at 6.62 ppm was observed for one Ar-H protons, and the signal at 5.18 ppm was observed for -OCH_2 protons of ethers.

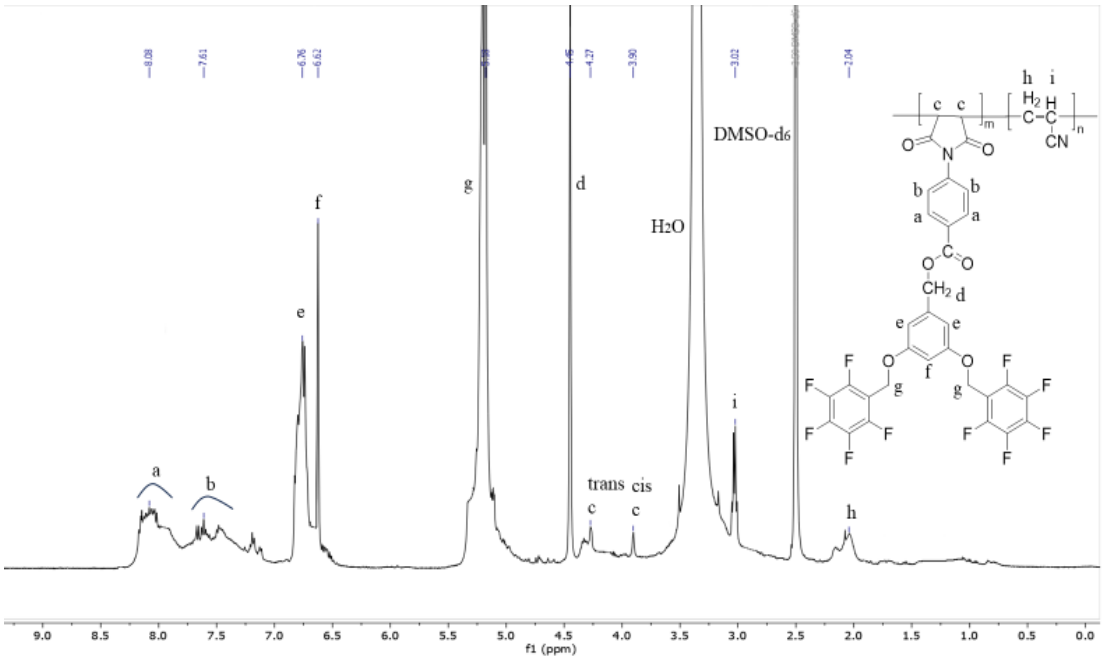

Figure 4.15 : ^{1}H-NMR (in DMSO-d_6) spectrum of p(AN-co-FMI) copolymers.

FMI monomer was copolymerized with styrene at 75 °C using AIBN as the initiator in toluene. Comparing the electron-poor and electron-rich double bonds of N-aryl maleimide and styrene comonomers, respectively, a complete alternative copolymer can be formed by free radical copolymerization (Figure 4.16) [18].

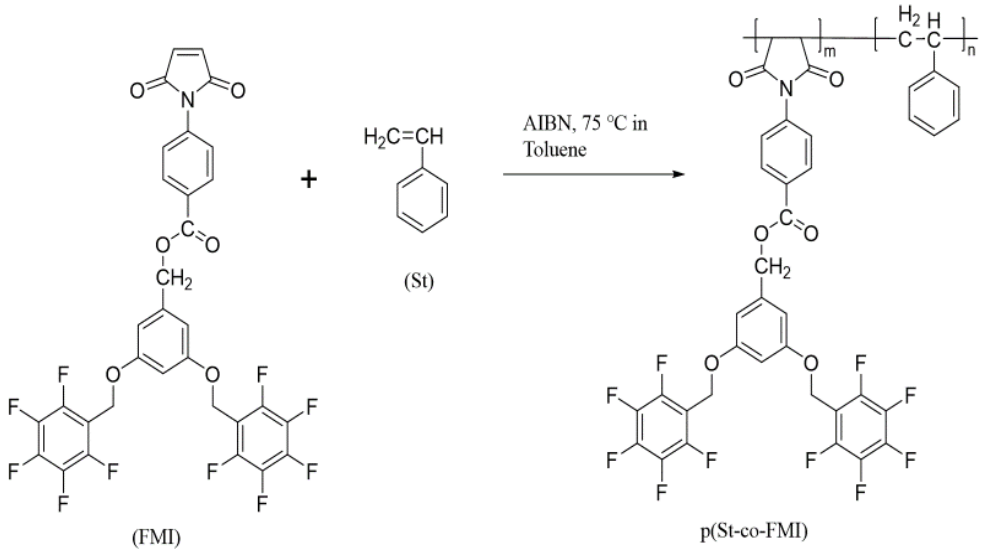

Figure 4.16 : Synthesis of p(St-co-FMI) copolymers.

The Figure 4.17 shows the ^{1}H-NMR of the p(St-co-FMI) polymer taken in DMSO-d_6. In p(St-co-FMI) samples, the chemical shift at 7.21 ppm due to CH=CH in maleimide monomer has disappeared and appeared at 4.25 ppm for trans form and 3.92 ppm for

cis form, that confirm polymerization is through the vinyl group. The observed at 2.00-1.67 ppm corresponded to 1H (-CH) and at 1.62-1.32 ppm for 2H of methylene group of St segment. -CH protons in the position ortho to the -CH group in the St unit appeared at 6.56 ppm, and other -CH aromatic protons appeared at 7.36-7.11 ppm. The δ at 7.96 ppm was for 2Ar-H, meta- to N of imide group while at 7.36-7.11 ppm for 2Ar-H, ortho- to N of imide group. The δ at 6.72 ppm was for 2Ar-H, ortho- to -OCH_2 group and at δ 6.63 ppm was for 1Ar-H, para- to -OCH_2 group. Ether -OCH_2- protons signaled at 5.18 ppm.

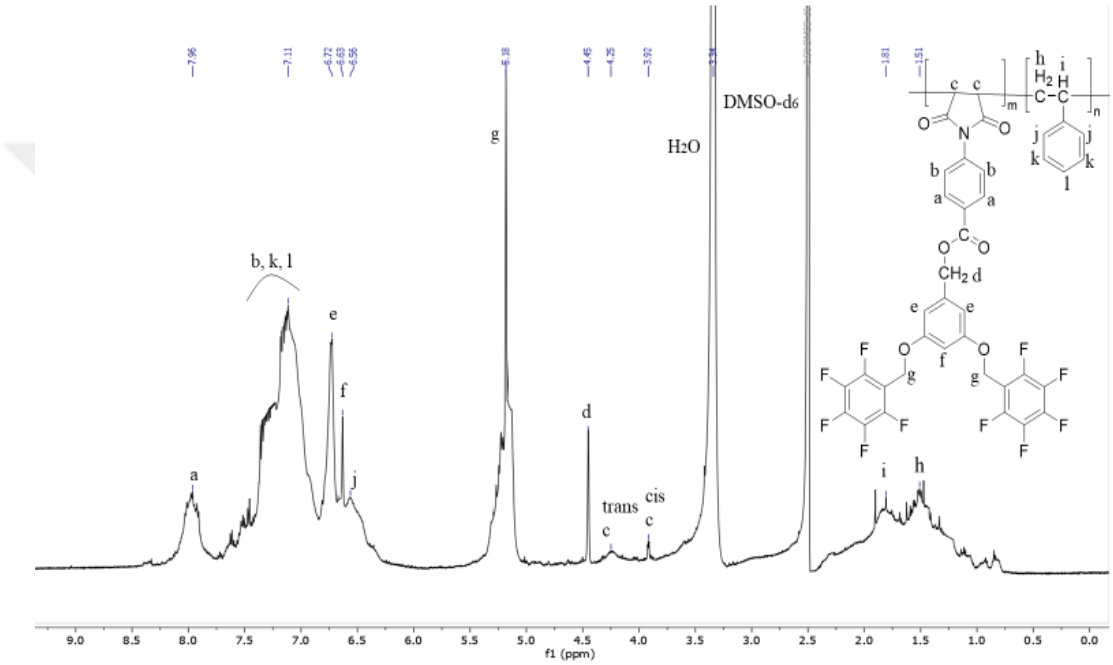

Figure 4.17 : ^{1}H-NMR (in DMSO-d_6) spectrum of p(St-co-FMI) copolymers.

The nine polymer samples synthesized by using different feed ratios of monomer FMI, AN and St, are listed in Table 4.2 and Table 4.3. The effect of different feed ratios of monomers on the properties of copolymers was investigated. The number average and weight average molecular weight of the prepared homopolymer and copolymers were determined by gel permeation chromatography. From Tables 4.2 and 4.3, PDI values between 1.0 and 10 clearly indicate that the polymerization proceeds through free radical polymerization. The number average molecular weights (Mn) of p(AN-co-FMI) and pFMI polymers were approximately same. Since the molecular weights of p(AN-co-FMI) polymers were measured in GPC with THF instead of DMF and with polystyrene standard, relative results were obtained.

Table 4.2 : Free Radical Copolymerization of AN (M_1) and FMI (M_2) at 75 °C in DMF[a].

Polymer	Monomer Feed (mol%)		Mn[b]	Mw/Mn[b]
	AN (M_1)	FMI (M_2)		
p(AN-co-FMI)-80/20	80	20	23160	1.04
p(AN-co-FMI)-50/50	50	50	23517	1.05
p(AN-co-FMI)-30/70	30	70	23110	1.05
pFMI	-	100	23136	1.05

[a] Initiator: AIBN (mol %1.5), time 96 hours.

[b] Determined by means of GPC calibrated with pSt standards.

The number average molecular weights of p(St-co-FMI) copolymer series were approximately in the range 2.9-7.4x10^4 (g/mol). In the polymerizations, well-defined polymers with narrow polydispersity were obtained. The Mn value in p(St-co-FMI) copolymers gradually decreased with the increase of maleimide monomers in the feed. The average molecular weight was affected by side chain effect and steric hindrance due to maleimide and styrene segments, making polymerization difficult. The interlocking of chains has decreased. Additionally, this may be because FMI monomer can easily cause chain transfer during the copolymerization reaction.

Table 4.3 : Free Radical Copolymerization of St (M_1) and FMI (M_2) at 75 °C in Toluene[a].

Polymer	Monomer Feed (mol%)		Mn[b]	Mw/Mn[b]
	St (M_1)	FMI (M_2)		
pSt	100	-	4318	1.57
p(St-co-FMI)-90/10	90	10	74679	1.52
p(St-co-FMI)-75/25	75	25	67647	2.92
p(St-co-FMI)-50/50	50	50	62666	2.15
p(St-co-FMI)-25/75	25	75	29696	1.37

[a]Initiator: AIBN (mol %2.5), time 24 hours.

[b]Determined by means of GPC calibrated with pSt standards.

The UV-Visible analysis was accomplished by using DCM as a solvent at 2 mg/100 ml concentrations (Table 4.4). In FMI monomer, the maleimide unit has -C=C- and -C=O chromophore groups responsible for electronic absorption. For FMI monomer, the first band in the spectra with a significant absorption was associated with a $\pi_1 \rightarrow \pi_1^*$ transition. This absorption peak was at 270 nm [56]. The important thing is that

the absorbance wavelength matches the emitting wavelength of the source. The absorbance increased with the decrease of molecular weight of p(St-co-FMI). P(St-co-FMI)-90/10 has a weaker absorbance compared to other p(St-co-FMI) copolymers, which is a consequence decreasing maleimide concentration [57]. Bathochromic effect was observed in p(St-co-FMI)-25/75 and p(St-co-FMI)-50/50 copolymers. Moreover, as the styrene ratio increased in the copolymers, the hypochromic effect increased (Figure 4.18).

Table 4.4 : UV-Visible analysis of FMI monomer and p(St-co-FMI) copolymers.

Compound	Wavelength (nm)	Absorbance
FMI	270.00	0.683
p(St-co-FMI)-25/75	274.50	0.685
p(St-co-FMI)-50/50	274.50	0.500
p(St-co-FMI)-75/25	270.00	0.168
p(St-co-FMI)-90/10	270.00	0.140

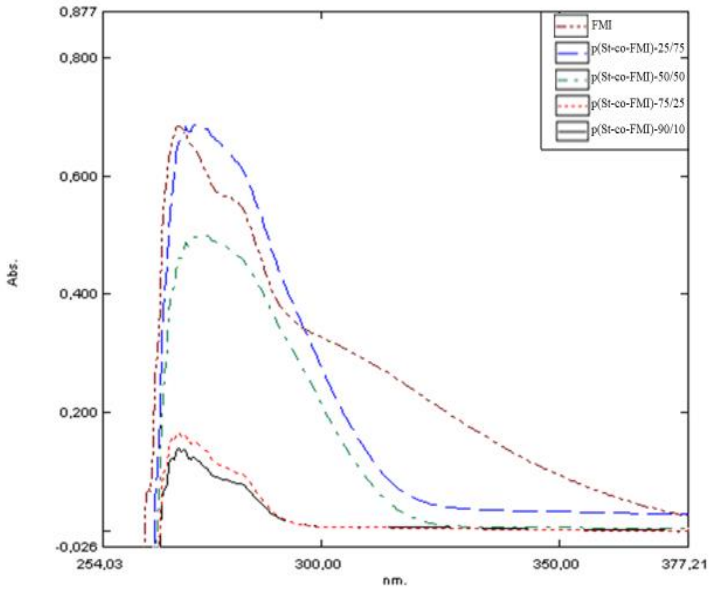

Figure 4.18 : Overlayed UV absorbance spectra of FMI monomer and p(St-co-FMI) copolymers in DCM.

Thermal behaviors of polymers were analyzed by DSC and TGA measurements. The results of thermal analysis are summarized in Table 4.5.

Table 4.5 : DSC and TGA results for p(AN-co-FMI) and pFMI polymers.

Polymers	Tg (°C)	5% weight loss temp. (°C)	10% weight loss temp. (°C)	50% weight loss temp. (°C)	Residue at 500 °C (%)
p(AN-co-FMI)-80/20	49.7	203	236	377	39.7
P(AN-co-FMI)-50/50	64.1	201	233	377	39.4
P(AN-co-FMI)-30/70	52.1	227	247	404	42.5
pFMI	45.4	222	245	393	41.9

The DSC curves of the p(AN-co-FMI) and pFMI polymers during cooling are reported in Figure 4.19. The Tg of polyacrylonitrile was 98 °C and the Tg of pFMI homopolymer was 45.4 °C. The fact that the Tg values of p(AN-co-FMI) copolymers were between these two values showed that a random copolymer was obtained [58]. In the case of pFMI, fluorine containing groups increased the hydrodynamic volume, increased molecular motion and decreased the Tg value. When FMI formed a copolymer with acrylonitrile, the hydrodynamic volume decreased and Tg values increased due to the effect of the rigid maleimide group. The segmental movements of the copolymer chains were effectively blocked by the rigid maleimide unit, leading to an increase in the Tg value of the copolymers. In the p(AN-co-FMI)-50/50 copolymer, AN and FMI showed the best compatibility with each other and obtained the highest Tg value. Since the molecular weights of all p(AN-co-FMI) copolymers were around 2.3 x 10^4, their Tg values were close to each other.

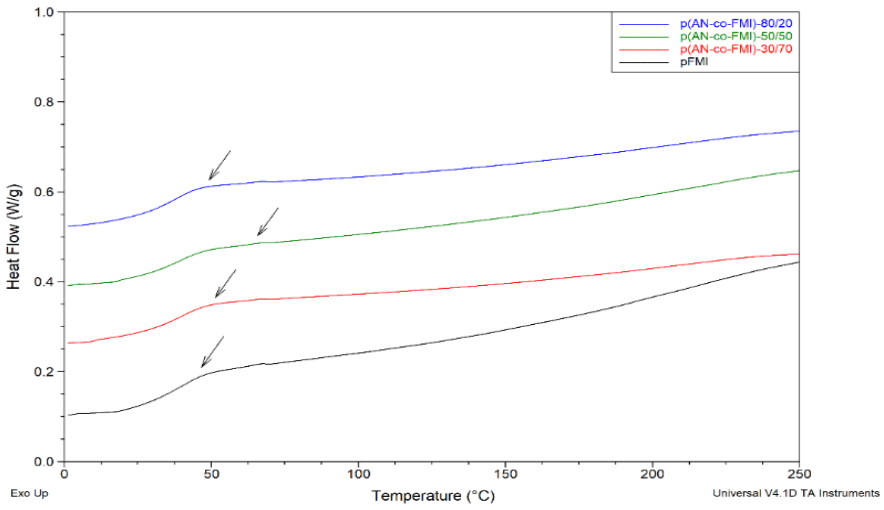

Figure 4.19 : DSC curves of p(AN-co-FMI) and pFMI polymers.

The thermal analysis data of the pSt and p(St-co-FMI) copolymers are reported in Table 4.6.

Table 4.6 : DSC and TGA results for p(St-co-FMI) and pFMI polymers.

Polymers	Tg (°C)	5% weight loss temp. (°C)	10% weight loss temp. (°C)	50% weight loss temp. (°C)	Residue at 500 °C (%)
pSt	100.0	263	351	421	0.2
p(St-co-FMI)-90/10	55.8	201	242	408	27.4
p(St-co-FMI)-75/25	56.7	212	250	417	40.6
p(St-co-FMI)-50/50	102.4	352	370	616	61.9
p(St-co-FMI)-25/75	66.5	315	357	583	58.4
pFMI	45.4	222	245	393	41.9

The DSC curves of the p(St-co-FMI) and pFMI polymers during cooling are presented in Figure 4.20. All these copolymers showed a single Tg. This indicates that the maleimide segments and styrene segments in the copolymers are completely compatible. Maleimide and styrene with poor electron and rich electron density, respectively, formed alternating copolymer [18]. Since the p(St-co-FMI)-50/50 copolymer had a higher molecular weight than the p(St-co-FMI)-25/75 copolymer, the Tg value of the p(St-co-FMI)-50/50 copolymer was higher. The Tg value was lowest due to fluorine-containing groups in pFMI. When FMI copolymerized with styrene, the rigid property of maleimide became significant and Tg increased.

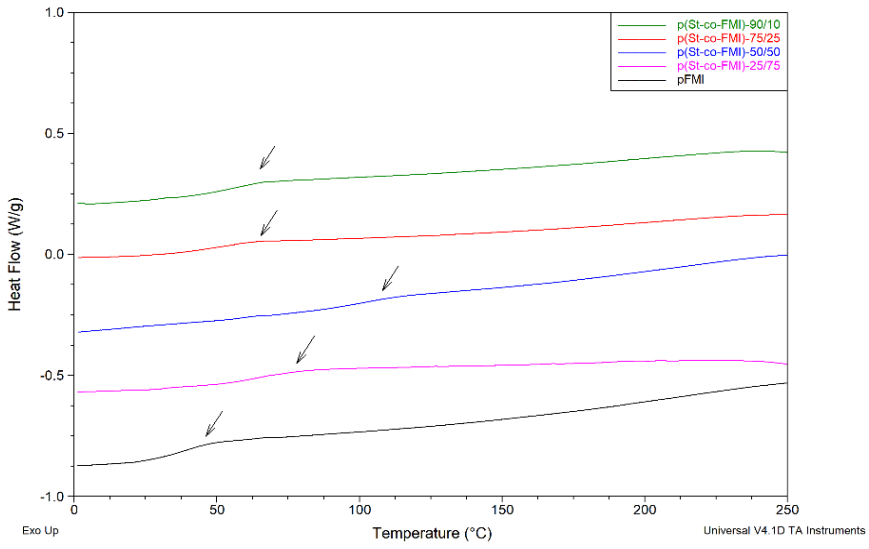

Figure 4.20 : DSC curves of p(St-co-FMI) and pFMI polymers.

The thermogravimetric analysis (TGA) and derivative thermogravimetry (DTG) curves for p(AN-co-FMI) and pFMI are presented in Figure 4.21 and Figure 4.22, respectively. The TGA thermograms were obtained by heating the polymers in N_2 at a rate of 20 °C/min. The temperatures for 5% decomposition T_5, 10% decomposition T_{10}, 50% decomposition T_{50}, and residue at 500 °C determined from TGA for polymers are showed in Table 4.4. T_{10} is the onset temperature at which 10% degradation occurs, T_{50} is the midpoint temperature corresponding to 50% degradation. The degradation of acrylonitrile copolymers and pFMI homopolymer occurred in three steps. The first degradation occurred at 180-325 °C regarding to nitrile oligomerization and decomposition of the ester linkages in FMI segment. The second decomposition step started from 325 °C continued to 410 °C related with the decomposition or condensation of aromatic rings. Also, degradation of maleimide ring and dehydrogenetion of the structure were observed from 410 °C continued to 710 °C.

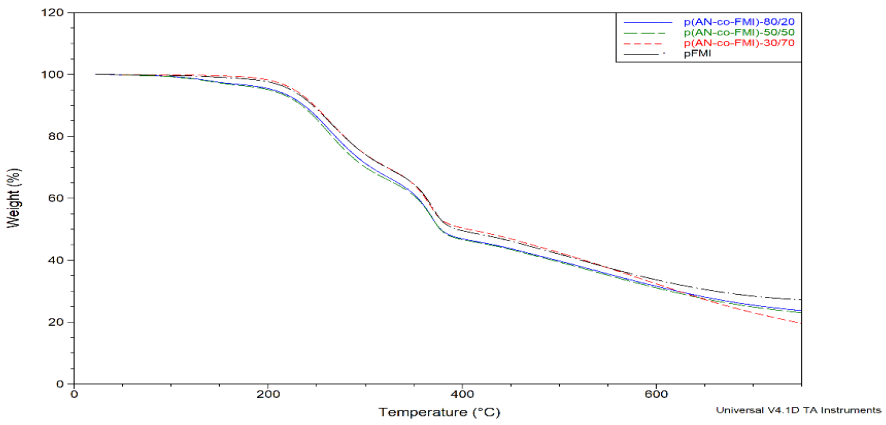

Figure 4.21 : TGA curves of p(AN-co-FMI) and pFMI polymers.

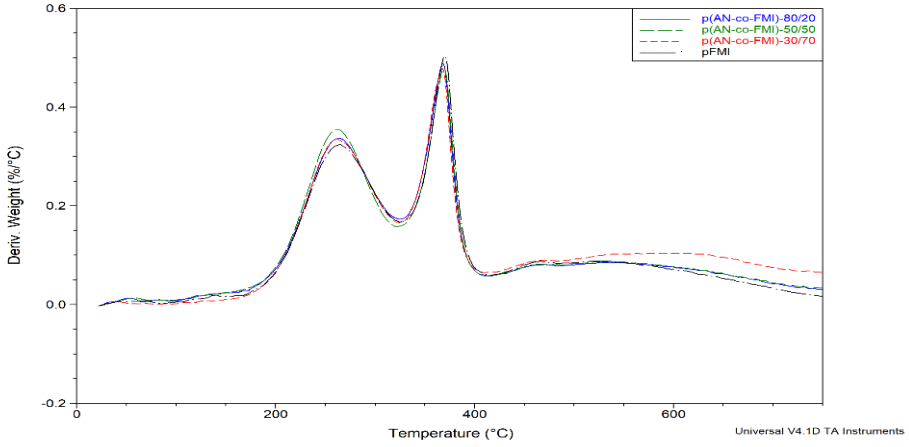

Figure 4.22 : DTG curves of p(AN-co-FMI) and pFMI polymers.

The thermal stability of p(AN-co-FMI)-80/20 and p(AN-co-FMI)-50/50 copolymers was close to each other. In detail, T_{10} and T_{50} values of p(AN-co-FMI) copolymers increased from 236 to 247 ℃ and from 377 to 404 ℃, respectively as FMI ratio rises from 20 to 70%. It can be clearly found that the introduction of FMI monomer can enhance the decomposition temperature of copolymers. The corresponding char residue of copolymers at 500 ℃ rises from 39.7 mass% for p(AN-co-FMI)-80/20 to 42.5 mass% for p(AN-co-FMI)-30/70. Although the p(AN-co-FMI)-30/70 copolymer contained fewer maleimide units, it showed better thermal properties than the pFMI homopolymer due to the presence of acrylonitrile. The char yields of p(AN-co-FMI) samples were increased slightly with the increasing FMI content. As a result, FMI-monomer significantly increased thermal stability and char residue amounts.

The TGA and DTG curves of p(St-co-FMI) polymers are shown in Figure 4.23 and Figure 4.24, respectively. Single phase degradation was observed at 350-480 ℃ for the pure polystyrene. This phase attributed to the decomposition of polystyrene matrix to volatile styrene monomers. The degradation of the p(St-co-FMI) copolymers proceeded in three consecutive stages. The first weight loss in p(St-co-FMI) copolymers at 180-325 ℃ resulted from the decomposition of the ester linkages in FMI segment. The second step of decomposition of the aromatic rings of styrene and aromatic rings of FMI occurred at 325-405 ℃. The third step of fragmentation of the maleimide ring and dehydrogenation of the structure seen in the p(St-co-FMI) copolymers occurred at 405-480 ℃.

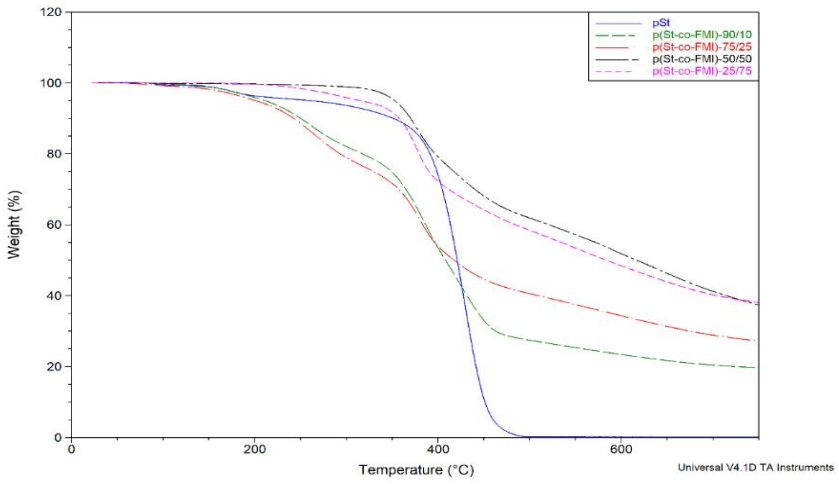

Figure 4.23 : TGA curves of p(St-co-FMI) polymers.

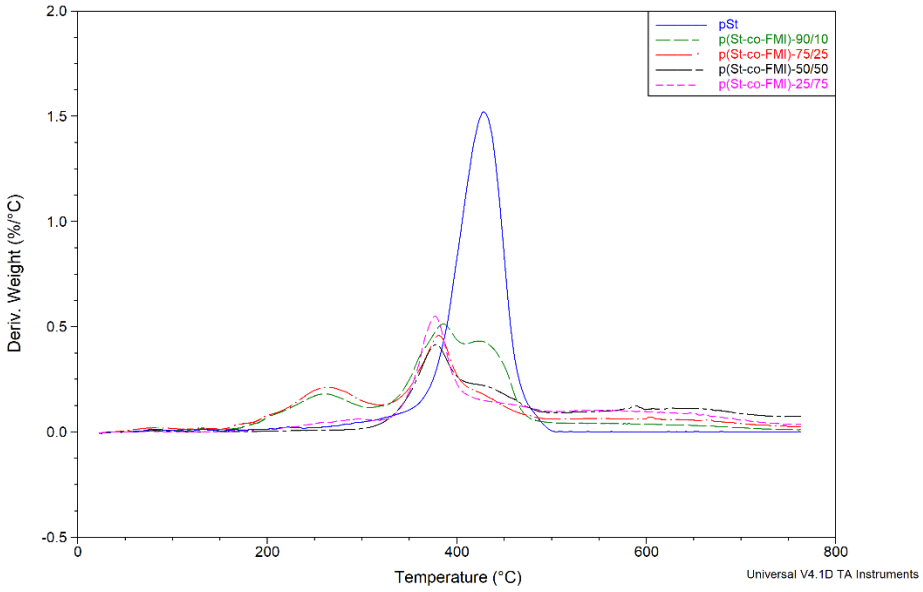

Figure 4.24 : DTG curves of p(St-co-FMI) polymers.

Although 5%, 10% and 50% weight loss of p(St-co-FMI)-90/10 and p(St-co-FMI)-75/25 polymers were less than pSt, as the FMI ratio in the content increased in the feed, the decomposition of p(St-co-FMI)-50/50 and p(St-co-FMI)-25/75 polymers occurred at higher temperatures. The degradation temperatures of the copolymers increased as the FMI unit increased. This revealed that the addition of the maleimide ring increased the thermal stability of the copolymers. This maleimide structure restricts the movement of the pSt chains, hence retarding the onset of thermal decomposition and improving the mechanical properties of the copolymers. Moreover, the residues of the copolymer at approximately 500 °C were all higher than those of pSt due to the presence of thermally stable maleimide units. P(St-co-FMI)-50/50 showed better thermal properties than p(St-co-FMI)-25/75 as its molecular weight was significantly higher.

As can be seen in Figure 4.25, from the scanning electron miscroscope (SEM) for the polymers, different topographies were observed. It has been observed that as the FMI monomer ratio increases in polymers, F atoms affect the texture and cover the surface due to the way the fluorines orient towards the surface. Therefore, it was concluded that the emergence of F atoms to the surface leads to a more sponge-like structure for the pFMI homopolymer.

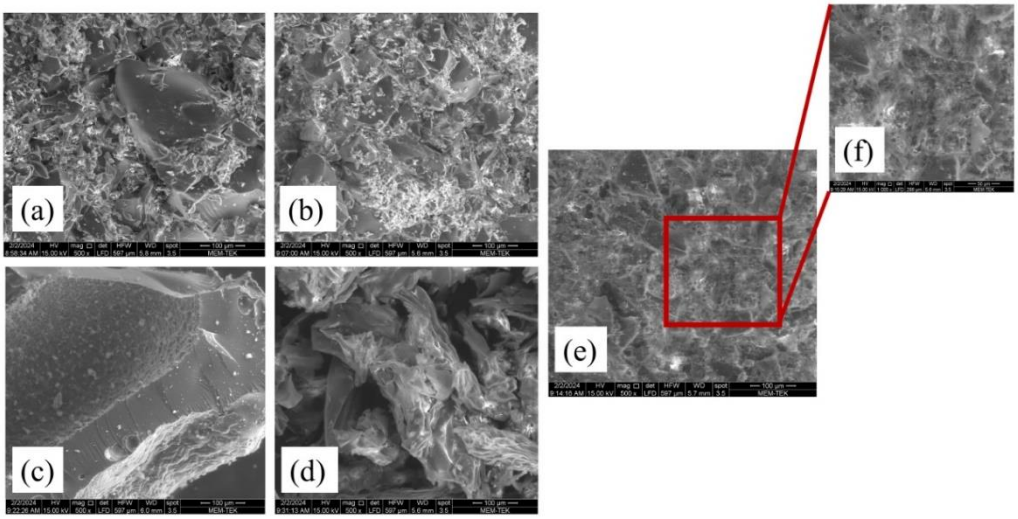

Figure 4.25 : SEM images of polymer samples, (a) p(AN-co-FMI)-80/20 with x500 magnification, (b) p(AN-co-FMI)-50/50 with x500 magnification, (c) p(St-co-FMI)-75/25 with x500 magnification, (d) p(St-co-FMI)-50/50 with x500 magnification, (e) pFMI with x500 magnification, (f) pFMI with x1,000 magnifications.

It can be seen that the fluorine-containing chain could remain on the surface of the film, which could reduce the surface tension of the film and improve the hydrophobic and oleophobic performance of the coating significantly. The hydrophobic properties of polymers were examined by measuring contact angles. Contact angles of the spin cast polymer films with distilled water and ethylene glycol were measured. Distilled water and ethylene glycol have different level of polarity. The contact angles of these liquids on the films were directly measured by the drop profile at the contact point of these two liquids having different polar levels with the surface. Contact angle values of films are listed in Table 4.7.

Table 4.7 : Contact angles θ (°) with distilled water and ethylene glycol of spin cast polymer films.

Material	Contact Angle θ (°) with	
	Distilled Water	Ethylene Glycol
p(AN-co-FMI)-80/20	80.1	67.5
p(AN-co-FMI)-50/50	81.4	68.6
p(AN-co-FMI)-30/70	83.5	68.7
pFMI	91.6	71.1
pSt	75.2	63.4
p(St-co-FMI)-90/10	77.1	65.5
p(St-co-FMI)-75/25	81.1	67.9
p(St-co-FMI)-50/50	89.8	65.9
p(St-co-FMI)-25/75	92.9	68.3

Results of measuring contact angle for spin cast polymer films in W (water) and EG (ethylene glycol) are presented in Figure 4.26 and Figure 4.27. The contact angles of films were evaluated in 5 μL drops in distilled water and ethylene glycol. It is known that the higher the contact angle of the polymer, the better the hydrophobicity of the polymer. Fluorine groups are migrated to the surface and are segregated at polymer surfaces [59].

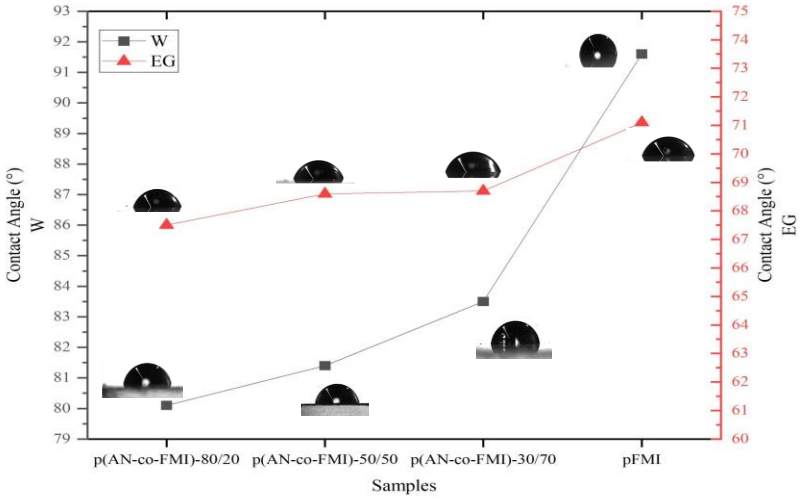

Figure 4.26 : Contact angle of water and ethylene glycol on spin cast p(AN-co-FMI) and pFMI polymer films.

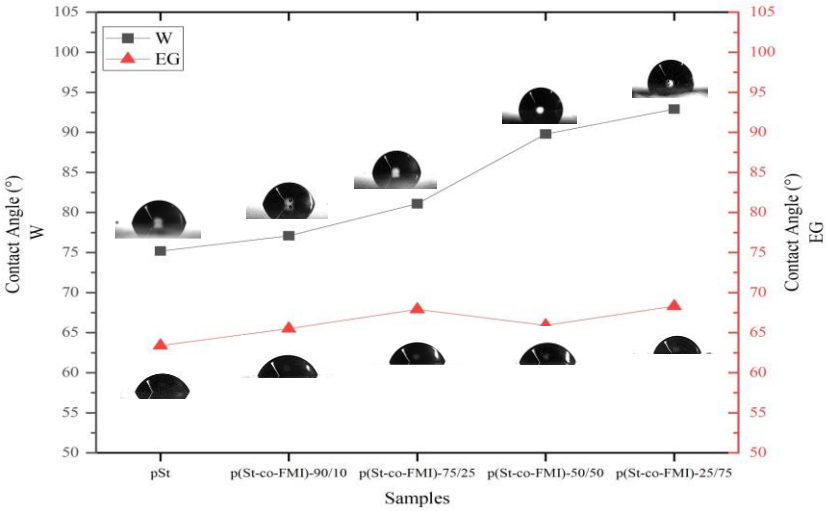

Figure 4.27 : Contact angle of water and ethylene glycol on spin cast pSt and p(St-co-FMI) polymer films.

Fluorinated polymers exhibited excellent hydrophobic performance, which was attributed to the presence of hydrophobic groups such as fluorine-containing groups in

the main chains. Due to the unique property of the fluorine atom that reduces the surface energy of polymers, the polymer exhibits prominent hydrophobicity. As the FMI ratio increased in the films coated with p(AN-co-FMI) copolymers, the contact angles with distilled water increased from 80.1° to 83.5°, and the contact angles with ethylene glycol increased from 67.5° to 68.7°. The film coated with pFMI synthesized under these conditions had the highest values of 91.6° and 71.1° with distilled water and ethylene glycol, respectively. Spin coated film of pure pSt showed a contact angle of 75.2° for water and 63.4° for ethylene glycol while fluorinated p(St-co-FMI) films had contact angle values between 77.1°-92.9° for distilled water and 65.5°-68.3° for ethylene glycol.

4.3 Preparation of PAN Nanofibers

Figure 4.28 shows photographs and zoomed-in photographs of PAN nanofibers containing each different polymer contents.

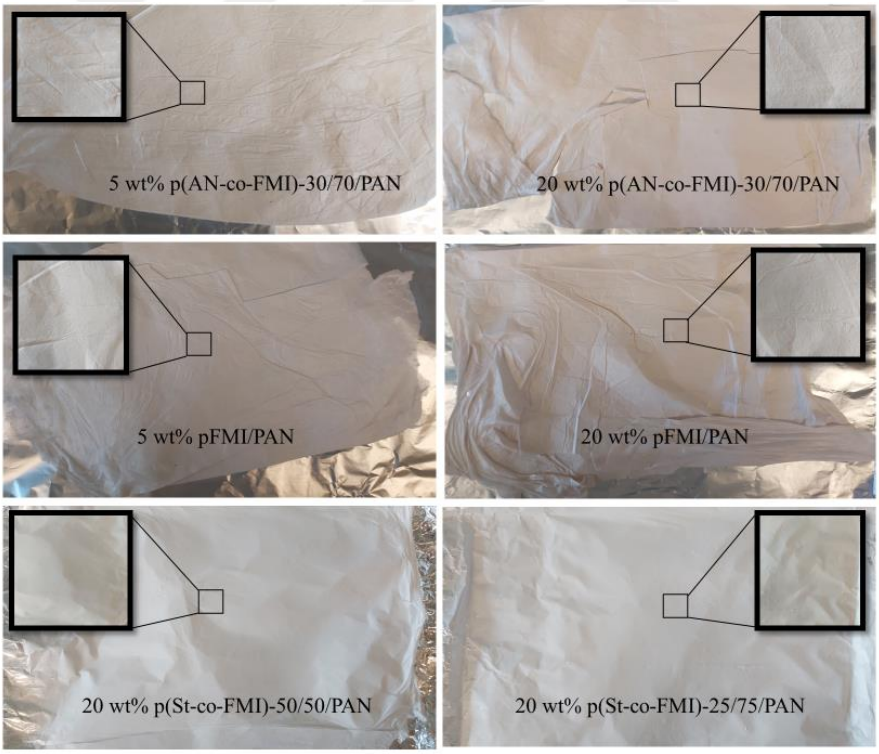

Figure 4.28 : Photographs of PAN nanofibers with different polymer contents.

The 5% weight loss temperature, 10% weight loss temperature, 50% weight loss temperature, the char residue at 500 ℃ and the char residue at 600 ℃ of PAN nanofibers are listed in Table 4.8.

Table 4.8 : TGA results for PAN nanofibers.

Fibers	5% weight loss temp. (℃)	10% weight loss temp. (℃)	50% weight loss temp. (℃)	Residue at 500 ℃ (%)	Residue at 600 ℃ (%)
100 wt% PAN	286	288	402	38.7	36.1
5 wt% p(AN-co-FMI)-30/70/PAN	299	308	401	40.0	37.1
20 wt% p(AN-co-FMI)-30/70/PAN	242	301	636	54.8	51.6
5 wt% pFMI/PAN	306	310	402	42.1	39.4
20 wt% pFMI/PAN	244	305	666	59.4	55.1
20 wt% p(St-co-FMI)-50/50/PAN	304	307	430	43.5	40.1
20 wt% p(St-co-FMI)-25/75/PAN	311	315	585	52.7	49.5

The TGA traces of p(AN-co-FMI)/PAN and pFMI/PAN nanofibers are shown in Figure 4.29 and Figure 4.31. The DTG curves are shown in Figure 4.30 and Figure 4.32. TGA curve of the PAN illustrated two main decomposition steps. In the initial step, the degradation of PAN was the range between 265 ℃ and 362 ℃ in the second step was in the range of 362 ℃ and 490 ℃. The p(AN-co-FMI)/PAN and pFMI/PAN nanofibers showed a three step weight loss profile. The first step represented the decomposition of the ester linkages in pFMI segment at 180-290 ℃. The second step attributed to the cyclization of PAN molecules at between 290-370 ℃. The third step was observed between 370 ℃ and 500 ℃ due to the decomposition of maleimide ring and degradation of PAN.

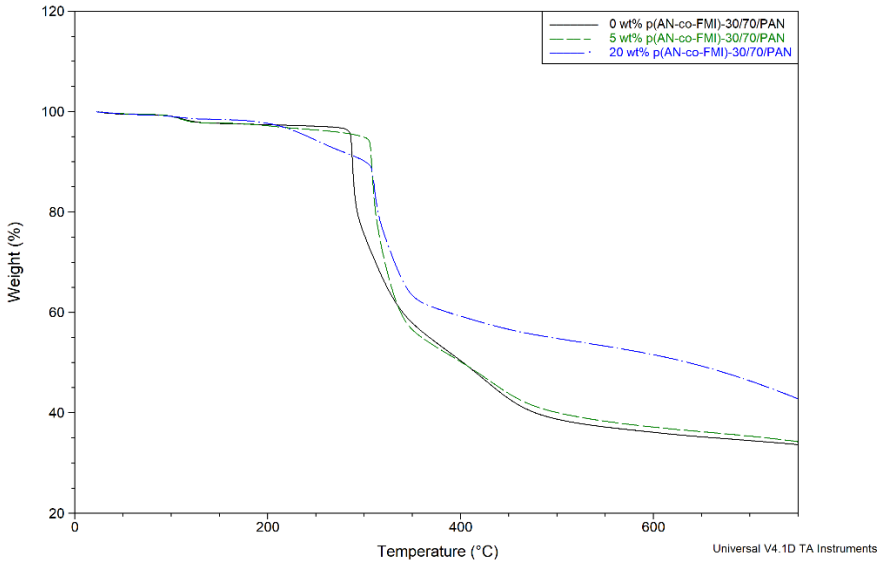

Figure 4.29 : TGA curves of p(AN-co-FMI)-30/70/PAN nanofibers.

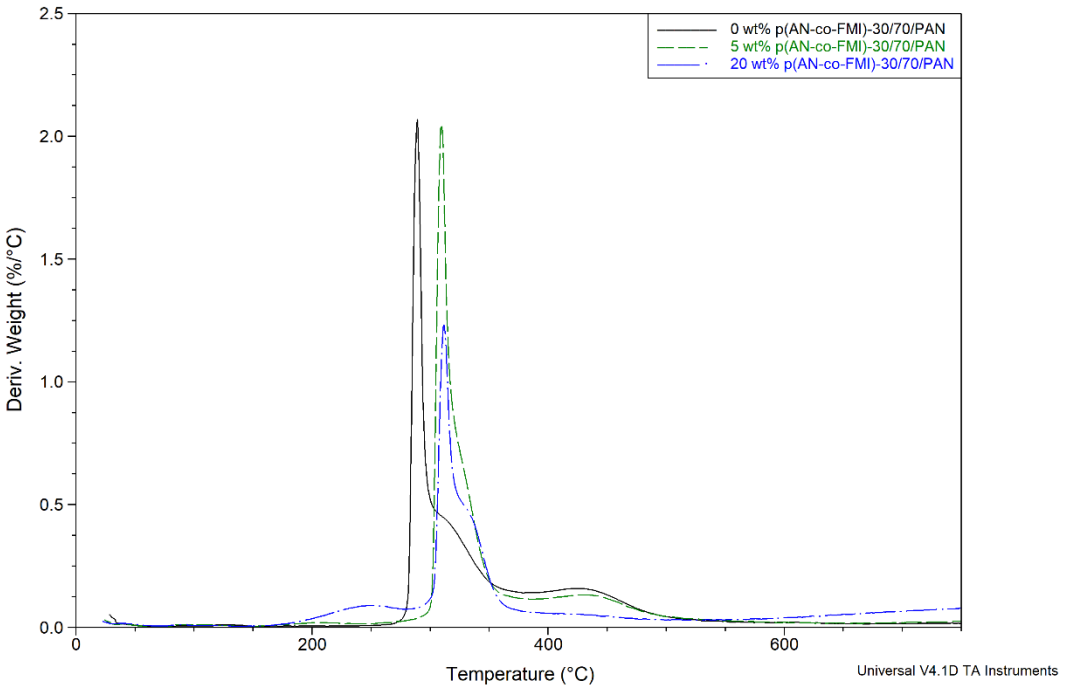

Figure 4.30 : DTG curves of p(AN-co-FMI)-30/70/PAN nanofibers.

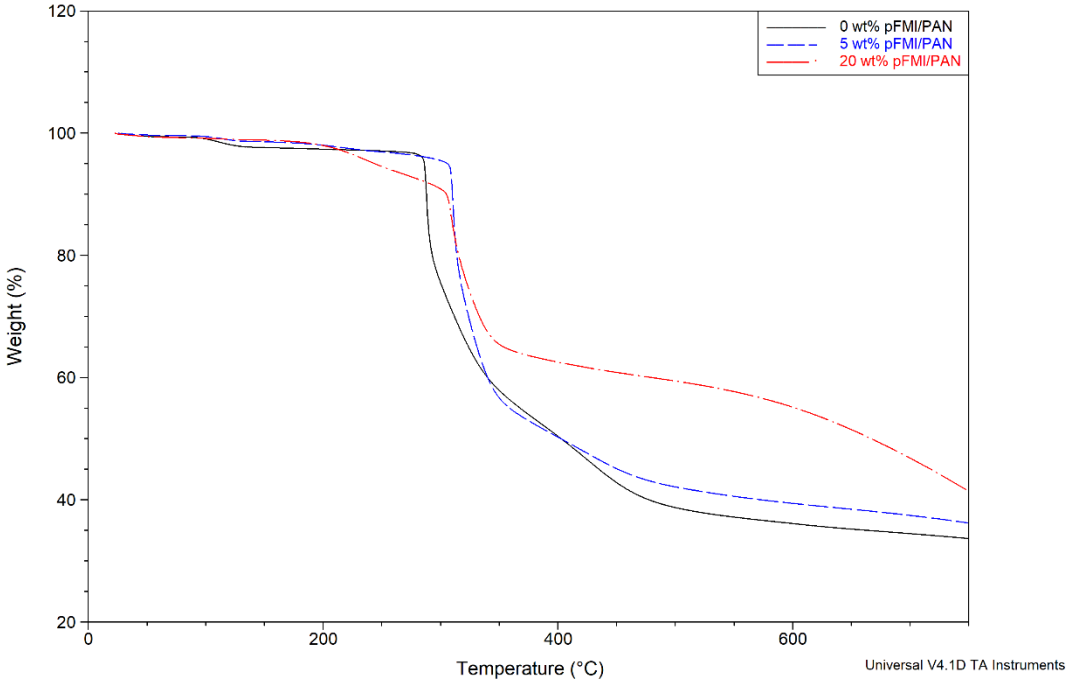

Figure 4.31 : TGA curves of pFMI/PAN nanofibers.

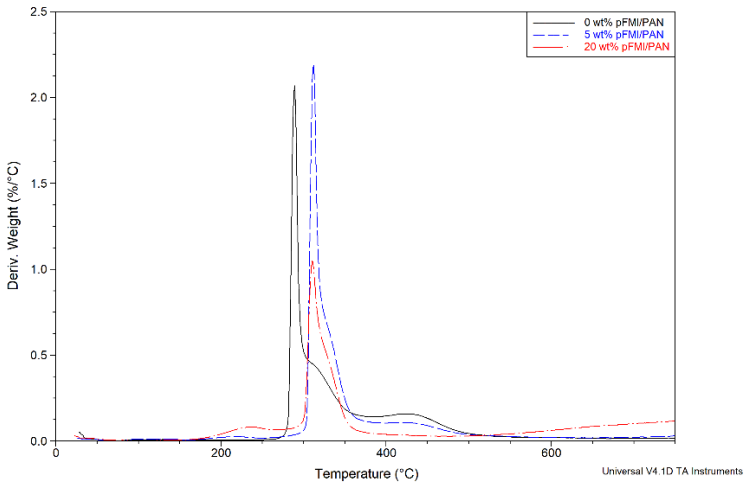

Figure 4.32 : DTG curves of pFMI/PAN nanofibers.

The degradation temperature of 10 wt.% loss for the p(AN-co-FMI)/PAN and pFMI/PAN fibers increased from 288 ℃ for the pure PAN nanofiber to 308 ℃ (5 wt% p(AN-co-FMI)-30/70/PAN), 301 ℃ (20 wt% p(AN-co-FMI)-30/70/PAN), 310 ℃ (5 wt% pFMI/PAN) and 305 ℃ (20 wt% pFMI/PAN). The temperature of 5% weight loss for 20 wt% polymer/PAN nanofibers are lower than that of PAN nanofiber. This can be attributed to the polymers promoted the dehydrogenation reaction to a certain extent. The T_{50} for the fibers increased to 636 ℃ (20 wt% p(AN-co-FMI)-30/70/PAN), 666 ℃ (20 wt% pFMI/PAN) from 402 ℃ for the pure PAN nanofiber. It could be also found from Table 4.8 that the yield of char residue at 500 ℃ and 600 ℃ for the polymer/PAN fibers is higher than that of pure PAN nanofiber, and the yield of char residue remarkably increased with the increasing copolymer amount. From the TGA thermograms of the fibers, it was clearly observed the thermal stability of the maleimide containing fibers was improved with the incorporation of maleimide groups. This was mainly due to the benzene ring substituent and the imide structure of N-phenyl maleimide, which improved the thermal performance of the resulting nanofibers.

The TGA curves of p(St-co-FMI)/PAN nanofibers are shown in Figure 4.33. The DTG curves are shown in Figure 4.34. P(St-co-FMI)/PAN nanofibers exhibited two step thermal degradation profile. The first step resulted from the cyclization of PAN molecules and decomposition of the aromatic rings of styrene at 290-390 ℃. The second step came from the decomposition of maleimide ring and degradation of PAN from 390 ℃ to 500 ℃.

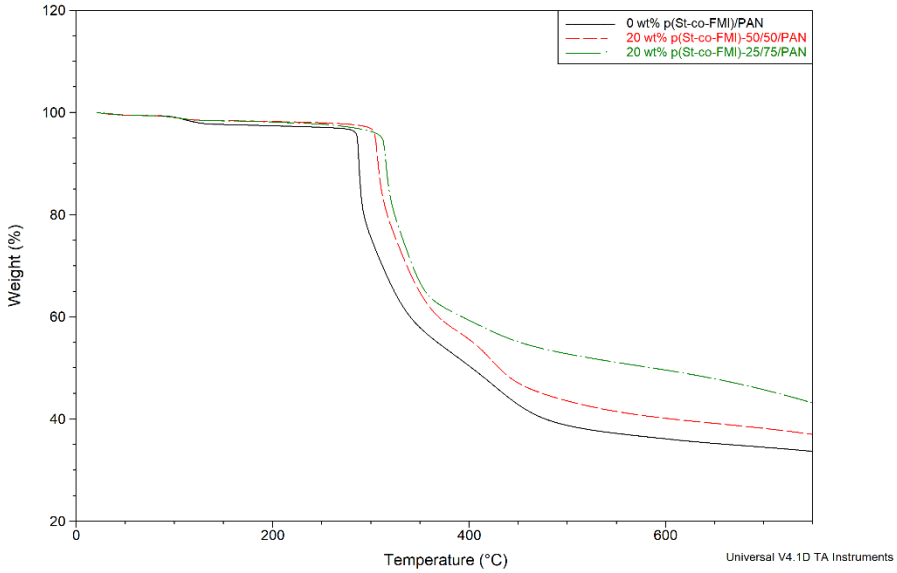

Figure 4.33 : TGA curves of p(St-co-FMI)/PAN nanofibers.

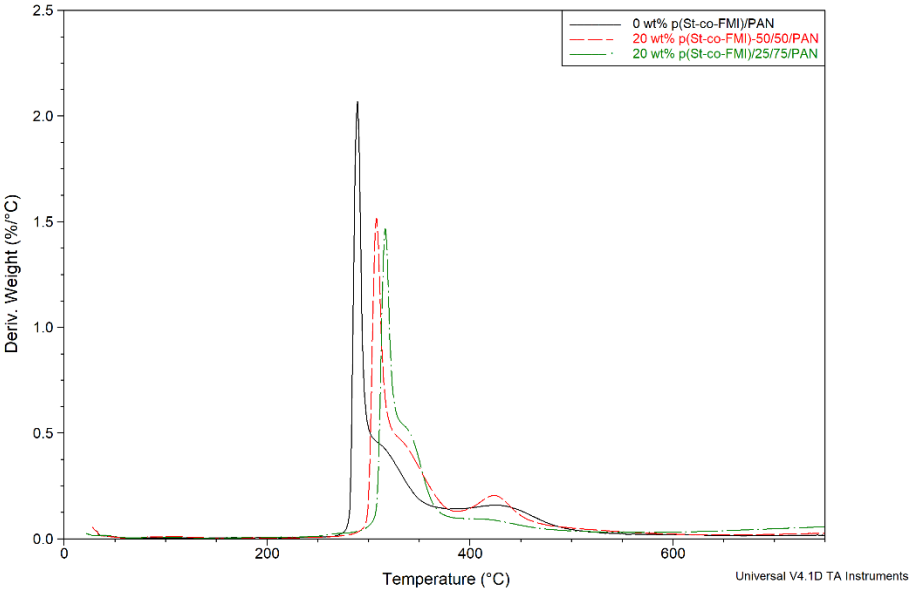

Figure 4.34 : DTG curves of p(St-co-FMI)/PAN nanofibers.

It can be found that the T_5, T_{10} and T_{50} for 20 wt% p(St-co-FMI)-25/75/PAN fiber were higher than those values for the 20 wt% p(St-co-FMI)-50/50/PAN fiber. The residues at 500 ℃ and 600 ℃ for the 20 wt% p(St-co-FMI)-25/75/PAN fiber were higher than 20 wt% p(St-co-FMI)-50/50/PAN, and the residue increased with the increasing FMI amount in the copolymer. 20 wt% pFMI/PAN fiber showed higher 50% weight loss temperature than 20 wt% p(St-co-FMI)-50/50/PAN and 20 wt% p(St-

co-FMI)-25/75/PAN fibers. Additionally, the 20 wt% pFMI/PAN fiber had higher residue values at 500 ℃ and 600 ℃.

The morphology of electrospun nanofibers is characterized by SEM in Figure 4.35 and Figure 4.36. Polymers containing FMI monomer have been shown to be suitable with PAN to form ultrafine nanofibers.

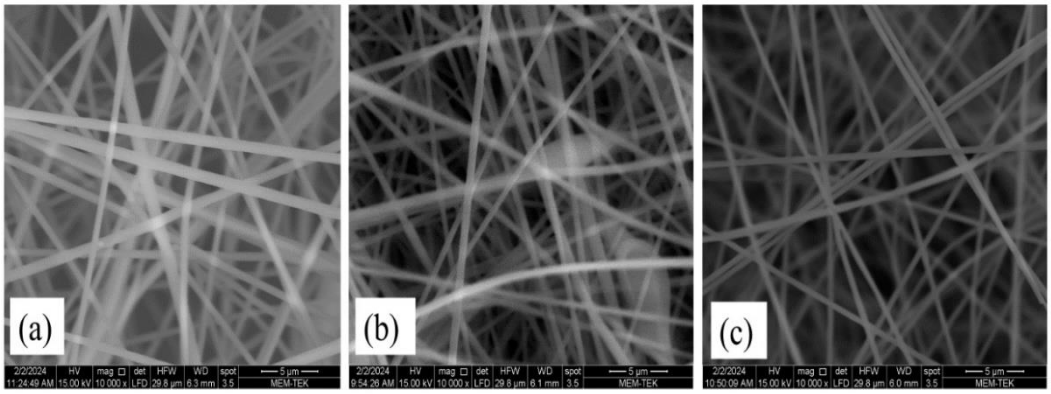

Figure 4.35 : SEM images of PAN nanofibers, (A) 100 wt% PAN with x10,000 magnification, (B) 20 wt% p(AN-co-FMI)-30/70/PAN with x10,000 magnification, (C) 20 wt% pFMI/PAN with x10,000 magnifications.

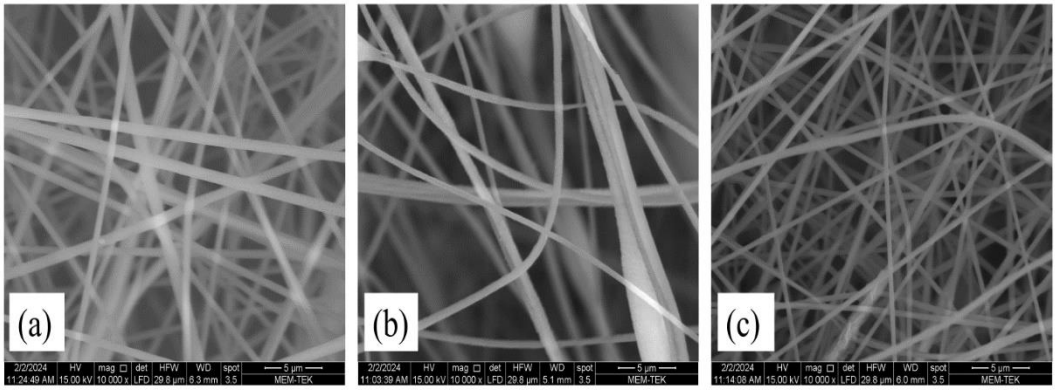

Figure 4.36 : SEM images of PAN nanofibers, (a) 100 wt% PAN with x10,000 magnification, (b) 20 wt% p(St-co-FMI)-50/50/PAN with 10,000 magnification, (c) 20 wt% p(St-co-FMI)-25/75/PAN with x10,000 magnifications.

Polymer concentration is one of the important factors affecting viscosity and surface tension. The relationship between viscosity and nanofiber diameter can be expected to be similar. This is because the viscosity of fluorine-containing polymers decreases due to the low chain packing density caused by the bulky fluorine groups in the polymer backbone [60]. The nanofiber diameters (nm) based on chemical composition are summarized in Table 4.9. 100 wt% PAN had the highest nanofiber diameter. It was

observed that the diameters of the nanofibers decreased as the FMI monomer ratio increased in the polymers used in nanofibers. The reason why the diameter of nanofibers of styrene-containing copolymers are less than the 20 wt% pFMI/PAN nanofiber may be due to different intrinsic polymer properties.

Table 4.9 : Nanofiber diameters (nm) based on their chemical composition.

Samples	Nanofiber diameter (nm)
100 wt% PAN	751.84 ± 184.0521
20 wt% p(AN-co-FMI)-30/70/PAN	610.98 ±78.2102
20 wt% pFMI/PAN	478.9 ± 59.9320
20 wt% p(St-co-FMI)-50/50/PAN	442.167 ±127.4212
20 wt% p(St-co-FMI)-25/75/PAN	403.6167 ± 81.3526

The detailed data of distilled water and ethylene glycol contact angles θ (°) of nanofiber surfaces are listed in Table 4.10.

Table 4.10 : Contact angle θ (°) with distilled water and ethylene glycol of PAN nanofibers.

Material	Contact Angle θ (°) with	
	Distilled Water	Ethylene Glycol
5 wt% p(AN-co-FMI)-30/70/PAN	112.6	120.1
20 wt% p(AN-co-FMI)-30/70/PAN	118.3	124.3
5 wt% pFMI/PAN	128.2	125.7
20 wt% pFMI/PAN	137.3	138.3
20 wt% pSt/PAN	118.4	0
20 wt% p(St-co-FMI)-50/50/PAN	131.7	0
20 wt% p(St-co-FMI)-25/75/PAN	139.2	136.0

About 5 μL droplet of distilled water ethylene glycol were used to determine the contact angle of nanofibers. PAN has a high dipole moment and is a semi-crystalline polymer with highly polar nitrile groups. The high polarity of PAN polymers increases the hydrophilicity of the nanofibre layer [61]. In general, fluorine-containing monomers are used to improve the hydrophobicity of the fibers. It is known that the high electronegativity of the fluorine atom, its strong fluorine-carbon bond and its large van der Waals radius compared to hydrogen create a significant repulsive force against water [62]. Distilled water and ethylene glycol contact angles θ (°) of nanofiber surfaces are shown in Figure 4.37 and Figure 4.38. Compared to copolymers containing acrylonitrile, 20 wt% pFMI/PAN fiber had the highest contact angle values

of 137.3° in distilled water and 138.3° in ethylene glycol. While the addition of polystyrene to PAN increased the repellency of the fiber towards water but it did not provide repellency towards ethylene glycol. The 20 wt% p(St-co-FMI)-25/75/PAN fiber showed high contact angle values of 139.2° in distilled water and 136.0° in ethylene glycol. In Figure 4.39 there are two different images of droplets on nanofibers.

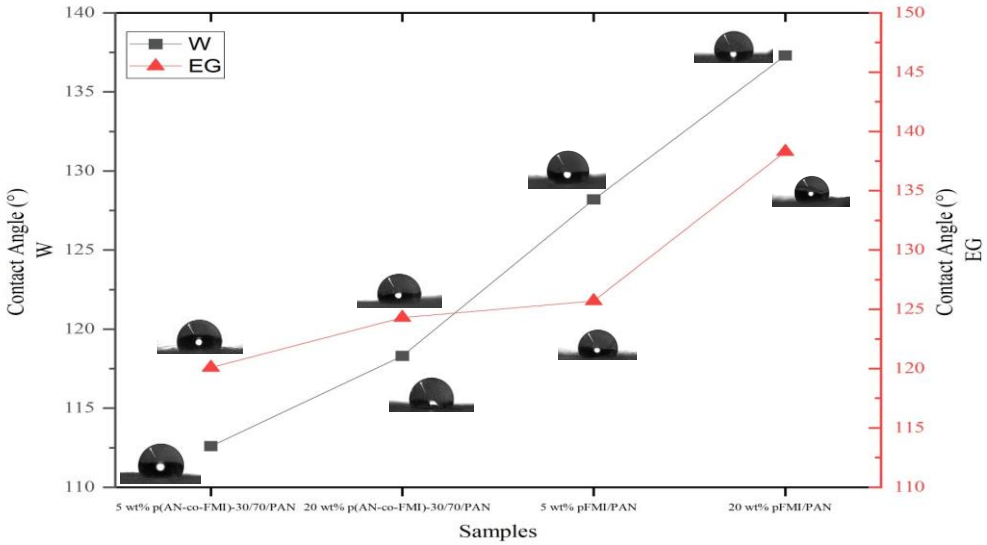

Figure 4.37 : Contact angle of water and ethylene glycol on p(AN-co-FMI)/PAN and pFMI/PAN nanofibers.

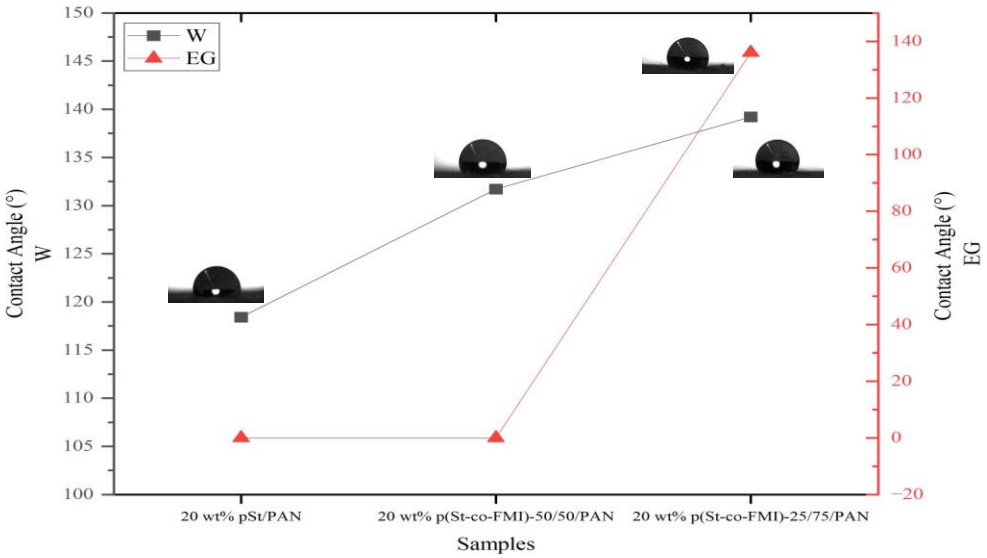

Figure 4.38 : Contact angle of water and ethylene glycol on pSt/PAN and p(St-co-FMI)/PAN nanofibers.

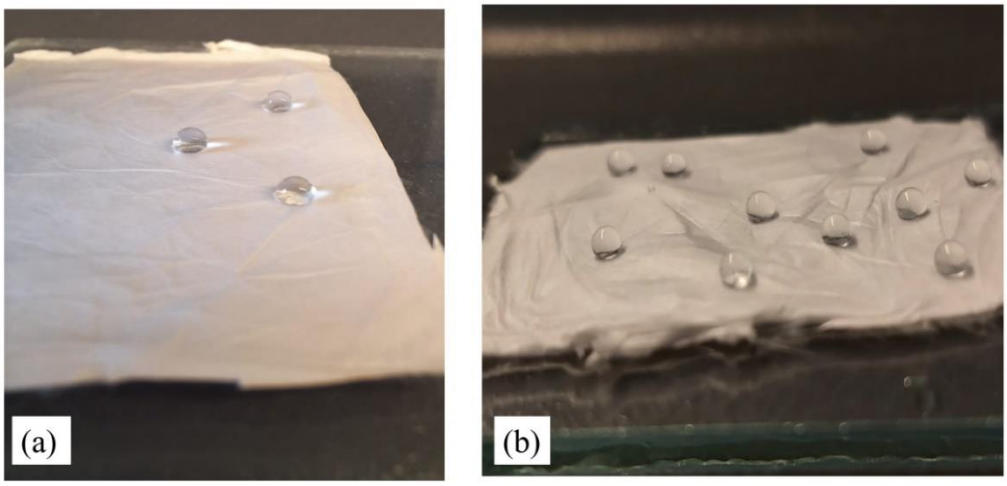

Figure 4.39 : Photograph of 5 µL drop of water on p(AN-co-FMI)/PAN nanofiber (a) and photograph of 5 µL drop of ethylene glycol on p(St-co-FMI)/PAN nanofiber (b).

4.4 Preparation and Characterization of UV-Curable Epoxy Acrylates and Urethane Acrylates Containing FMI for Coating Applications

Wood samples were coated using UV photopolymerization technique with various combinations of coating formulations. Newly synthesized fluorine-containing maleimide monomer (FMI) has been incorporated into epoxy acrylate (EA) and urethane acrylate (UA) coating formulations and their physical and mechanical properties were examined. Additionally, TPGDA, TMP3POTA, DPGDA, boron methacrylate (BAc) monomer were added to the FMI monomer at different rates in the coating formulations. Tripropylene glycol diacrylate (TPGDA), trimethylol propane [3PO] triacrylate (TMP3POTA) and dipropylene glycol diacrylate (DPGDA) were used as reactive diluents and Darocur 1173 as photoinitiator. Boron methacrylate monomer is classified as a saturated cyclic borate ester. It was synthesized from the esterification of 2,2-dimethyl-1,3-propanediol (neopentyl glycol) and boric acid (Figure 4.40) [63].

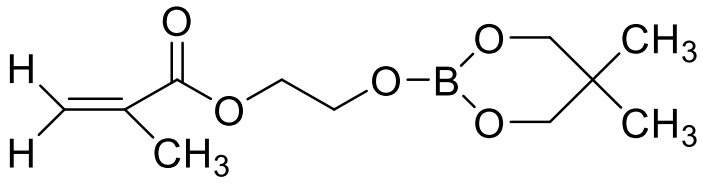

Figure 4.40 : Chemical structure of BAc.

Two different types of formulations were prepared and the compositions of formulations are given in Table 4.11. As seen in the table, there are 13 different formulations. The photoinitiator ratio was kept constant. Control formulations did not contain fluorine-containing maleimide monomer and boron methacrylate, and significant changes in the coating properties of the materials could be observed. Photographs of UV-cured EA and UA films are given in Figure 4.41 and Figure 4.42.

Table 4.11 : The compositions of the UV-curing formulations.

Sample	FMI (wt%)	EA (wt%)	UA (wt%)	TPGDA (wt%)	TMP3POTA (wt%)	DPGDA (wt%)	BAc (wt%)	Darocur 1173 (wt%)
EA (Control)	-	50	-	35	10	-	-	5
2.5FMI-EA	2.5	47.5	-	35	10	-	-	5
5FMI-EA	5	45	-	35	10	-	-	5
10FMI-EA	10	40	-	35	10	-	-	5
15FMI-EA	15	35	-	35	10	-	-	5
10BAc-EA	-	40	-	35	10	-	10	5
10FMI-10BAc-EA	10	40	-	30	5	-	10	5
UA (Control)	-	-	55	30	-	10	-	5
5FMI-UA	5	-	50	30	-	10	-	5
10FMI-UA	10	-	45	30	-	10	-	5
15FMI-UA	15	-	40	30	-	10	-	5
10BAc-UA	-	-	45	30	-	10	10	5
10FMI-10BAc-UA	10	-	40	25	-	10	10	5

EA: Epoxy acrylate

UA: Urethane acrylate

TPGDA: Tripropyleneglycol diacrylate

TMP3POTA: Trimethylolpropane [3 PO] triacrylate

DPGDA: Dipropylene glycol diacrylate

BAc: Boron methacrylate

Darocur 1173: Photoinitiator

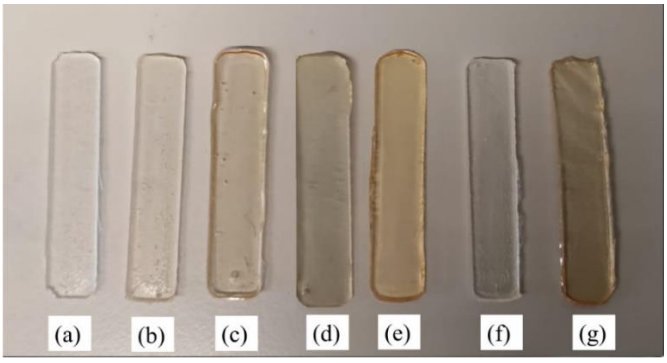

Figure 4.41 : The photos of (a) EA (Control) (b) 2.5FMI-EA (c) 5FMI-EA (d) 10FMI-EA (e) 15FMI-EA (f) 10BAc-EA (g) 10FMI-10BAc-EA films.

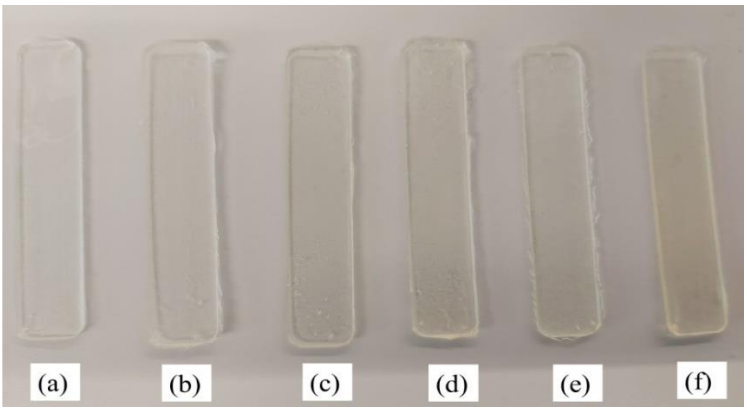

Figure 4.42 : The photos of (a) UA (Control) (b) 5FMI-UA (c) 10FMI-UA (d) 15FMI-UA (e) 10BAc-UA (f) 10FMI-10BAc-UA films.

FT-IR spectroscopy was used to determine the degree of conversion in UV-curable formulations. The decay of the peak area at 1636 cm^{-1} corresponding to the stretching vibration of the acrylate double bond was monitored. The spectra were normalized with the carbonyl peak at 1720 cm^{-1} as an internal standard by integration of the peak area to account for variations in sample thickness and instrument recording. The degree of double bond conversion (X) can be calculated via equation 4.1:

$$(X) = 1 - \frac{(A_{[1636]}/A_{[1720]})_t}{(A_{[1636]}/A_{[1720]})_0}\ x\ 100\% \qquad (4.1)$$

where $(A_{[1636]}/A_{[1720]})_0$ and $(A_{[1636]}/A_{[1720]})_t$ denote the relative absorption of the acrylate double bond before and after a given UV-curing time, respectively. Figure A.1 and Figure A.2 illustrated the FTIR spectra of the UV-curing samples recorded prior to and after UV exposure. The C=C bonds of the epoxy acrylate and urethane acrylate oligomers used in this study react with each other upon prolonged UV exposure and form a tightly cross-linked structure. Therefore, the absorption band at 1636 cm^{-1} was reduced after UV irradiation.

The double bond conversion of the UV-cured films in the presence of different amount of epoxy acrylate oligomer and urethane acrylate oligomer can be seen from Figure 4.43 and Figure 4.44, respectively. As the FMI concentration increased, double bond conversion initially increased slightly. This result is consistent with the property of maleimide monomer to act as a radical-type photoinitiator in acrylate resin. However, maleimide monomer has low efficiency due to its relatively small intrinsic adsorption and rapid consumption through polymerization [64]. Afterwards, double bond conversion decreased as seen in Figure 4.43 and Figure 4.44. There may be two

reasons for this. The first is the decrease in the ratio of epoxy acrylate or urethane acrylate and therefore the decrease in C=C acrylate bonds. The second is that some of the trapped double bonds of maleimide remain unpolymerized due to steric hindrance. Since the acrylate ratio of the epoxy acrylate film containing boron methacrylate is constant, FMI monomer increased the conversion. As the acrylate rate in the urethane acrylate film decreased, the conversion decreased. All double bond conversions were between 80 and 100%. These results proved that UV-curing was highly successful.

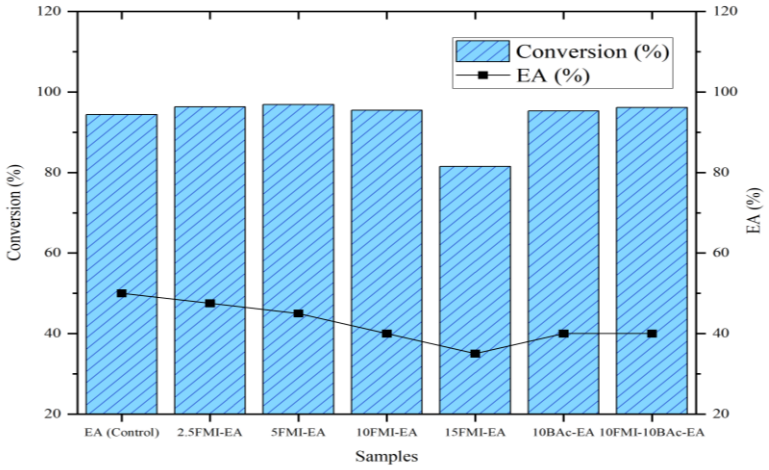

Figure 4.43 : The double bond conversion of the UV-cured films in the presence of different amount of epoxy acrylate oligomer.

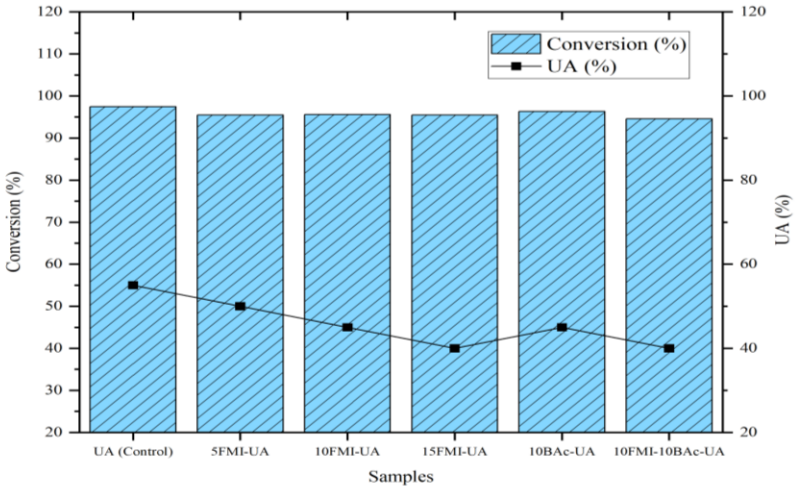

Figure 4.44 : The double bond conversion of the UV-cured films in the presence of different amount of urethane acrylate oligomer.

In order to measure curing and cross-linking degree of curing films, their gel contents were tested. Table 4.12 shows the gel content of films with different FMI content. Gel

content of films were between 90% and 100% which showed high cross-linking degree for the films.

The results of the pencil hardness test of the coatings are given in Table 4.12. The pencil hardness tester is equipped with a set of drawing leads calibrated from HB (softest) to 7H (hardest) and determines the resistance of coatings to the effects of scratching. Pencil that does not scratch the coating is understood as pencil scratch hardness [49]. The increasing FMI monomer content increased the pencil hardness of the cured film from 4H to 6H and 7H. The properties of good hardness would be obtained with poor flexibility. The maleimide ring and phenyl rings in FMI prevented the rotation of the polymer segment, resulting in high hardness.

Table 4.12 : Physical and mechanical properties of UV-cured films.

Sample	Gel Content (%)	Pencil Hardness	Pendulum Hardness (koenig)	Cross-cut Adhesion	Water Absorption
EA (Control)	99	4H	90	1 / 4B	1.5
2.5FMI-EA	100	4H	111	0 / 5B	1.1
5FMI-EA	96	6H	116	0 / 5B	0.7
10FMI-EA	99	6H	122	0 / 5B	0.6
15FMI-EA	96	7H	132	0 / 5B	0.5
10BAc-EA	94	5H	104	0 / 5B	2.2
10FMI-10BAc-EA	97	6H	107	0 / 5B	1.5
UA (Control)	94	4H	69	2 / 3B	0.8
5FMI-UA	93	6H	76	1 / 4B	0.7
10FMI-UA	90	6H	90	0 / 5B	0.6
15FMI-UA	90	6H	94	0 / 5B	0.4
10BAc-UA	91	6H	51	2 / 3B	2.0
10FMI-10BAc-UA	90	6H	54	0 / 5B	1.5

The pendulum hardness is an important test for UV-cured films, and it is related to the chain flexibility, cross-linking network density, chemical structure and the conversion of acrylic groups in the molecular chain. Pendulum hardness test measures the surface hardness in combination with the surface friction. In Table 4.12, the pendulum hardness of coatings as a different content of the FMI was shown. As seen in the Table 4.12, increasing FMI ratio increased the hardness. Since the maleimide in the structure of FMI monomer has a rigid structure, it increased pendulum hardness.

As seen in Table 4.12, the adhesion properties of the coatings were determined by the cross-cut adhesion test. Adhesion increases from 0B or 5 to 5B or 0. The cross-cut adhesion of the coatings was found to increase as the concentration of FMI in the

formulation was increased. This could be attributed to the presence of a polar group (COO-) present in FMI that enables hydrogen bonding with substrates which strengthened interfacial adhesion.

In general, absorbed water has a destructive effect on coating properties, so the water absorption behavior of coatings is an important parameter to determine their final application performance. The water absorption behavior of the UV-cured coatings are shown in Table 4.12. The reason for the regular decrease in water absorption in UV-cured films was that the FMI backbone has fluorine-containing groups with hydrophobic properties. In coatings containing boron methacrylate, the introduction of FMI monomer reduced water absorption due to the hydrophobic fluorine groups in its structure.

The solvent resistance of coatings was examined by immersing film samples in various solvents such as xylene, methanol and chloroform for a 24 time period. The results of solvent resistance are presented in Table 4.13. While the physical appearance of the coatings was good in xylene, they were cracked in methanol and broken in chloroform. Weight changes were generally the same and less than 7%. The uncrosslinked parts dissolved in the solvent might account for the weight loss during the process of the tests.

Table 4.13 : Solvent resistance of UV-cured films.

Sample	Xylene		Methanol		Chloroform	
	Appearance	Weight loss (%)	Appearance	Weight loss (%)	Appearance	Weight loss (%)
EA (Control)	Good	<2	Good	<1	Broken	<1
2.5FMI-EA	Good	<1	Good	<2	Broken	<1
5FMI-EA	Good	<1	Cracked	<3	Broken	<1
10FMI-EA	Good	<1	Cracked	<3	Broken	<1
15FMI-EA	Good	<1	Cracked	<3	Broken	<1
10BAc-EA	Good	<1	Cracked	<5	Broken	<1
10FMI-10BAc-EA	Good	<1	Cracked	<5	Broken	<1
UA (Control)	Good	<2	Cracked	<6	Broken	<1
5FMI-UA	Good	<2	Cracked	<6	Broken	<2
10FMI-UA	Good	<2	Cracked	<7	Broken	<2
15FMI-UA	Good	<2	Cracked	<7	Broken	<2
10BAc-UA	Good	<2	Cracked	<7	Broken	<2
10FMI-10BAc-UA	Good	<2	Cracked	<7	Broken	<2

Chemical resistance of UV-cured coatings were studied in 10% HCl, 10% NaOH solutions as shown in Table 4.14. All films had mass loss <1 in 10% HCl, <4 in 10% NaOH, and most had a yellowish physical appearance. The resistance of coatings to different type of solvents and chemicals were really high. The rigid groups such as the maleimide ring and benzene ring, which can restrict the rotation of polymer segment leading to a strong polymer structure to resist solvents and chemicals.

Table 4.14 : Chemical resistance of UV-cured films.

Sample	HCl (%10)		NaOH (%10)	
	Appearance	Weight loss (%)	Appearance	Weight loss (%)
EA (Control)	Yellowish	<1	Yellowish	<4
2.5FMI-EA	Yellowish	<1	Yellowish	<4
5FMI-EA	Yellowish	<1	Yellowish	<4
10FMI-EA	Yellowish	<1	Cracked	<4
15FMI-EA	Yellowish	<1	Cracked	<4
10BAc-EA	Yellowish	<1	Cracked	<4
10FMI-10BAc-EA	Yellowish	<1	Cracked	<4
UA (Control)	Yellowish	<1	Yellowish	<4
5FMI-UA	Yellowish	<1	Yellowish	<4
10FMI-UA	Yellowish	<1	Yellowish	<4
15FMI-UA	Yellowish	<1	Yellowish	<4
10BAc-UA	Yellowish	<1	Yellowish	<4
10FMI-10BAc-UA	Yellowish	<1	Yellowish	<4

Thermogravimetric analysis (TGA) is a widely used to tool to evaluate the thermal degradation behaviours of polymeric materials. Thermal stability of polymeric materials is an important way to use a flame retardant system, which is mainly related to the release of decomposition products and the formation of char. The TGA results of UV-cured films are listed in Table 4.15. The TGA and DTG curves of the epoxy acrylate cured films under nitrogen atmosphere are shown in Figure 4.45 and 4.46. The TGA and DTG curves of the urethane acrylate cured films under nitrogen atmosphere are shown in Figure 4.47 and 4.48. It was observed that there were two weight loss steps for all coatings. The first step indicated the decomposition of the acrylate, epoxy and urethane bonds from 320 ℃ in epoxy acrylate films and from 290 ℃ in urethane

acrylate films to 410 ℃. The second weight loss occurred at decomposition of the epoxy acrylate, urethane acrylate and maleimide groups at 410-510 ℃.

Table 4.15 : TGA results of UV-cured films.

Sample	%10 weight loss temp. (℃)	%90 weight loss temp. (℃)	Residue at 500 ℃ (%)	Residue at 600 ℃ (%)	Residue at 750 ℃ (%)
EA (Control)	359	500	10.1	7.2	6.4
2.5FMI-EA	351	516	11.2	8.2	7.8
5FMI-EA	345	558	11.7	9.6	7.9
10FMI-EA	329	716	13.2	10.6	9.8
15FMI-EA	313	832	17.6	14.6	12.1
10BAc-EA	336	484	8.8	6.6	6.0
10FMI-10BAc-EA	284	863	19.1	15.1	13.4
UA (Control)	324	455	2.3	1.9	1.1
5FMI-UA	325	460	5.0	4.2	3.1
10FMI-UA	313	463	6.4	5.4	4.9
15FMI-UA	301	501	10.0	8.5	7.3
10BAc-UA	318	457	2.5	2.1	1.5
10FMI-10BAc-UA	290	459	6.3	5.4	3.9

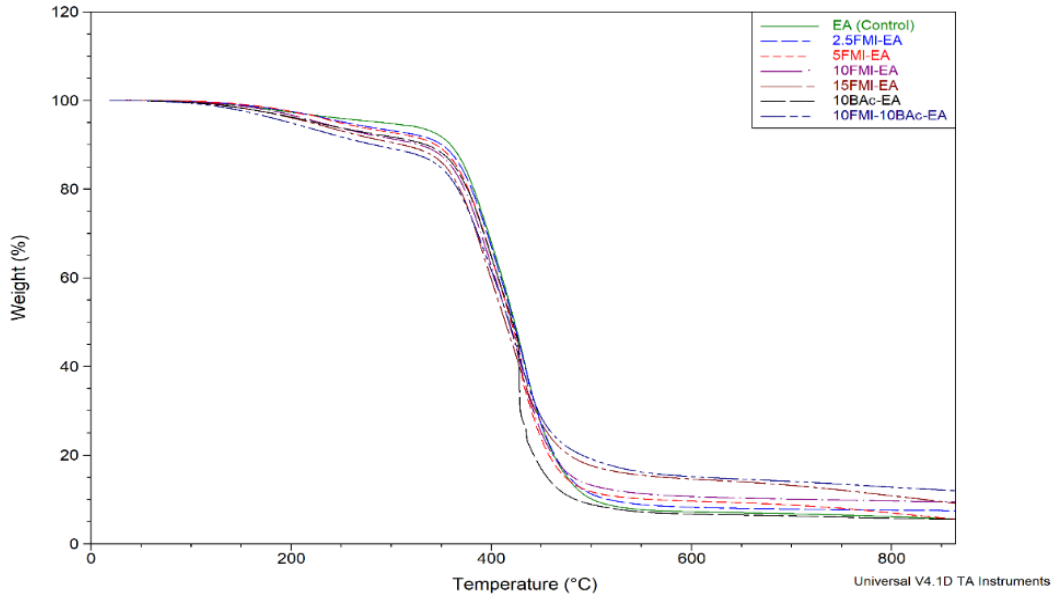

Figure 4.45 : TGA curves of epoxy acrylate UV-cured films.

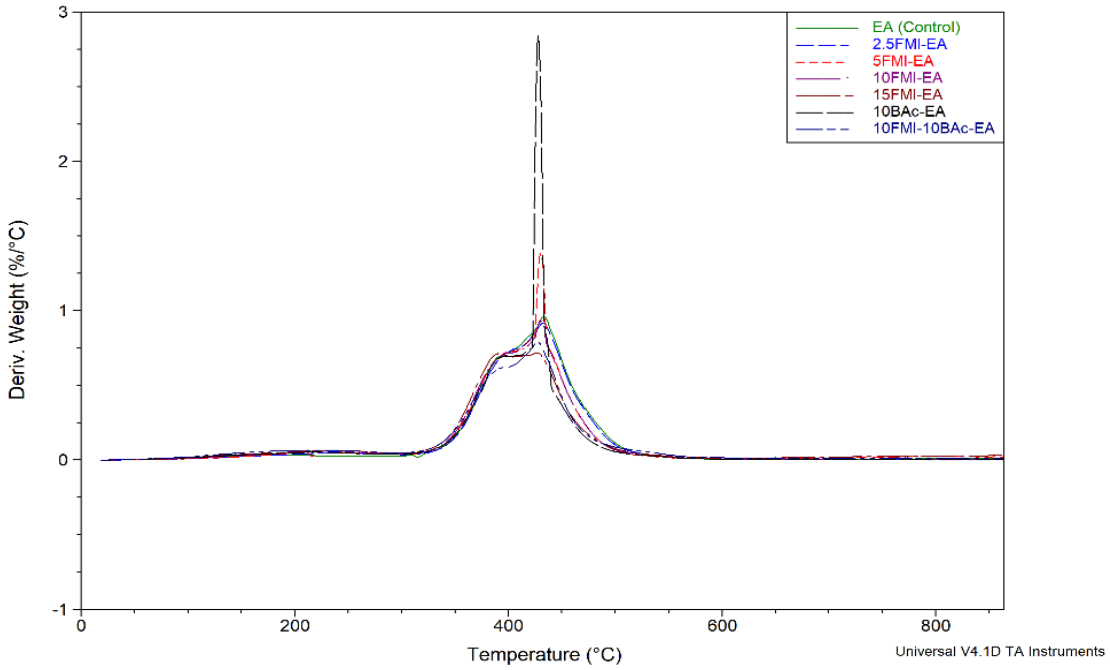

Figure 4.46 : DTG curves of epoxy acrylate UV-cured films.

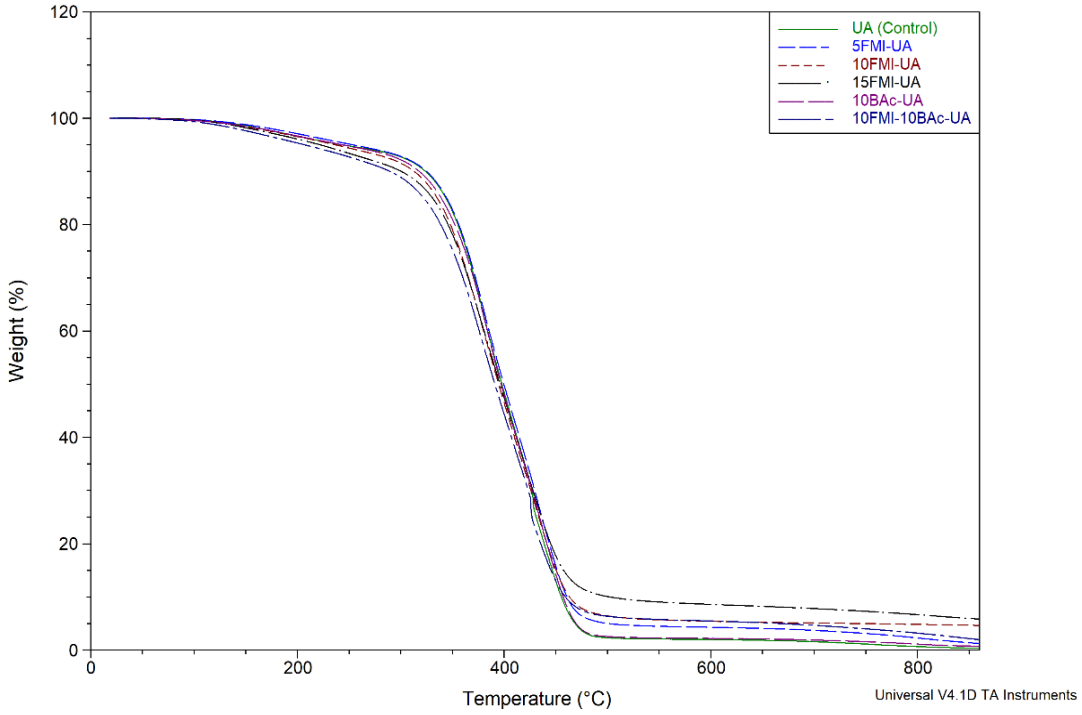

Figure 4.47 : TGA curves of urethane acrylate UV-cured films.

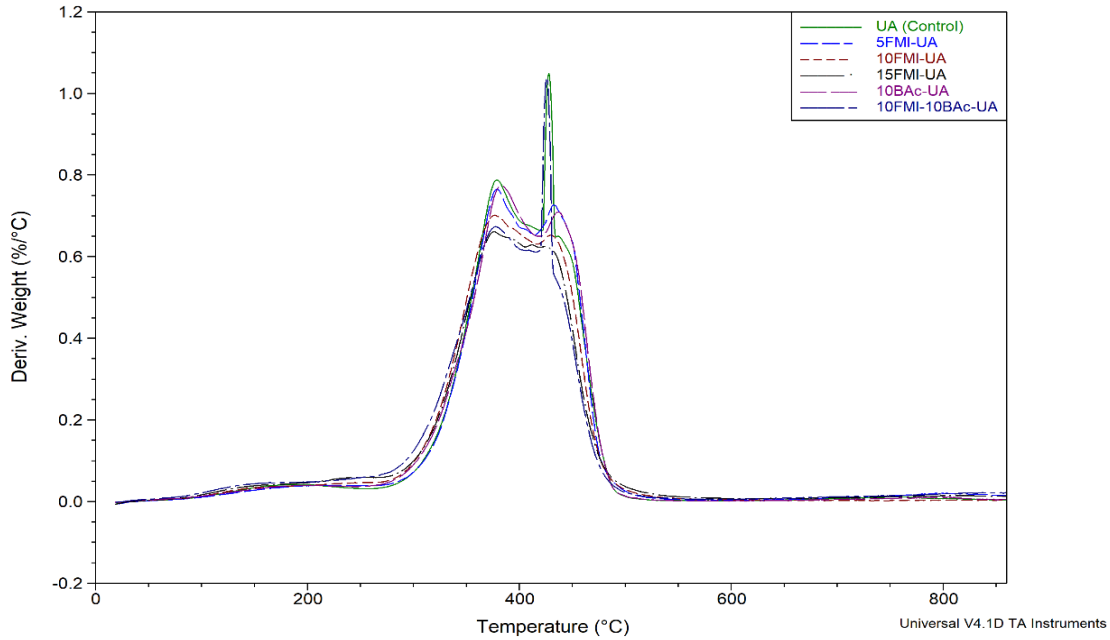

Figure 4.48 : DTG curves of urethane acrylate UV-cured films.

The %90 weight loss temperature shifted from 500 ℃ to 832 ℃ in epoxy acrylate films and shifted from 455 ℃ to 501 ℃ in urethane acrylate films with the incorporation of FMI into the formulations. The increase in %90 weight loss temperature was probably due to the maleimide groups, which are known to be thermally stable. The char yield has been correlated to the flame retardance. There is a significant increase in char residues at 500, 600 and 750 ℃ due to the incorporation of maleimide moieties into polymeric matrix. When borates thermally decompose, they form glassy coatings and caused the thermal conductivity of the surface of the burning material to decrease. There is an increase in char yield and flammability of the material. Therefore, borates are effective flame retardants [65]. Boron-containing films had higher char yield than neat EA and neat UA. The highest char yield in epoxy acrylate films was 10FMI-10BAc-EA, indicating improved thermal stability at high temperatures. The significant increase in char yield was due to the synergistic effect of FMI and boron methacrylate. This effect was observed in 10FMI-10BAc-UA, but not significantly.

LOI is the minimum concentration of oxygen in an oxygen/nitrogen mixture that would just support combustion. The LOI test of the cured films was performed and the results are shown in Table 4.16.

Table 4.16 : LOI values of UV-cured films.

Sample	LOI (%)
EA (Control)	20.8
2.5FMI-EA	21.1
5FMI-EA	21.2
10FMI-EA	21.7
15FMI-EA	21.9
10BAc-EA	21.4
10FMI-10BAc-EA	21.5
UA (Control)	19.0
5FMI-UA	20.2
10FMI-UA	20.3
15FMI-UA	20.6
10BAc-UA	19.9
10FMI-10BAc-UA	20.8

The LOI values of films are shown in Figure 4.49 and Figure 4.50, together with the combustion conditions of films. EA (control) film exhibited a LOI value of 20.8%, and UA (control) film exhibited 19.0%. There was a gradual increase for the LOI values of the coatings flame-retarded by FMI. The increase in LOI values is related with the char yields of the films. The residual char generation increases the decomposition temperature of the resin by avoiding heat exchange from source to the polymer. This result is consistent with char yield data obtained from thermogravimetric analysis [66]. This indicates that increasing the nitrogen and aromatic backbone content in FMI will help improve the flame retardant property of UV-cured films. The LOI value of films increased from 20.8% to 21.4% in EA films, from 19.0% to 19.9% in UA films with incorporation of boron methacrylate.

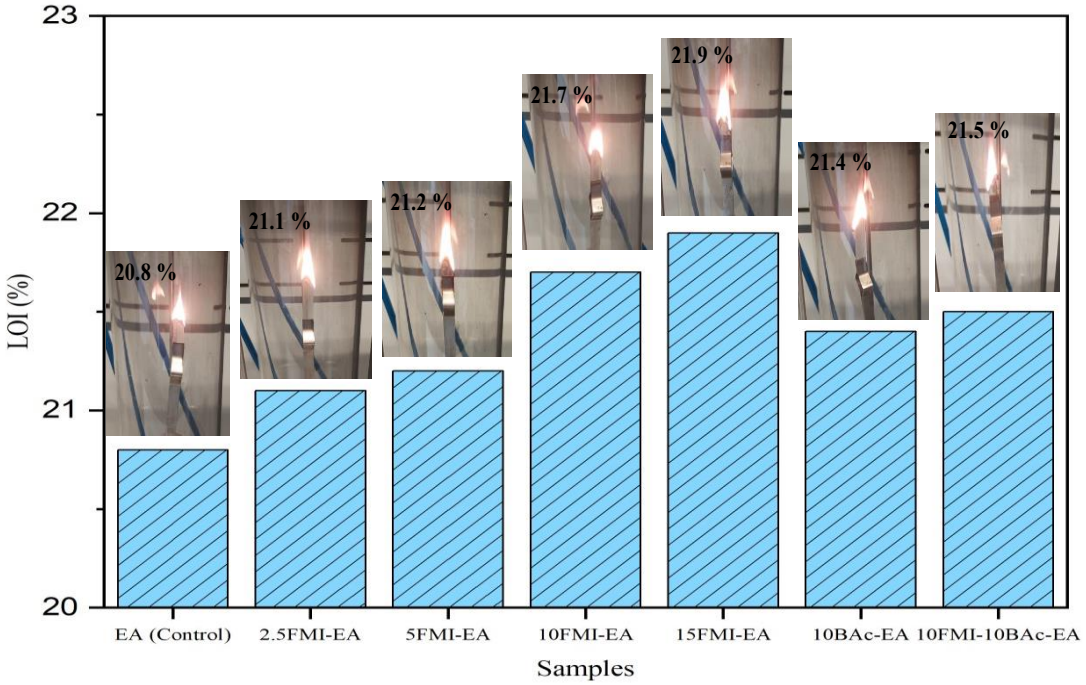

Figure 4.49 : LOI values of EA films (insert: combustion of EA films).

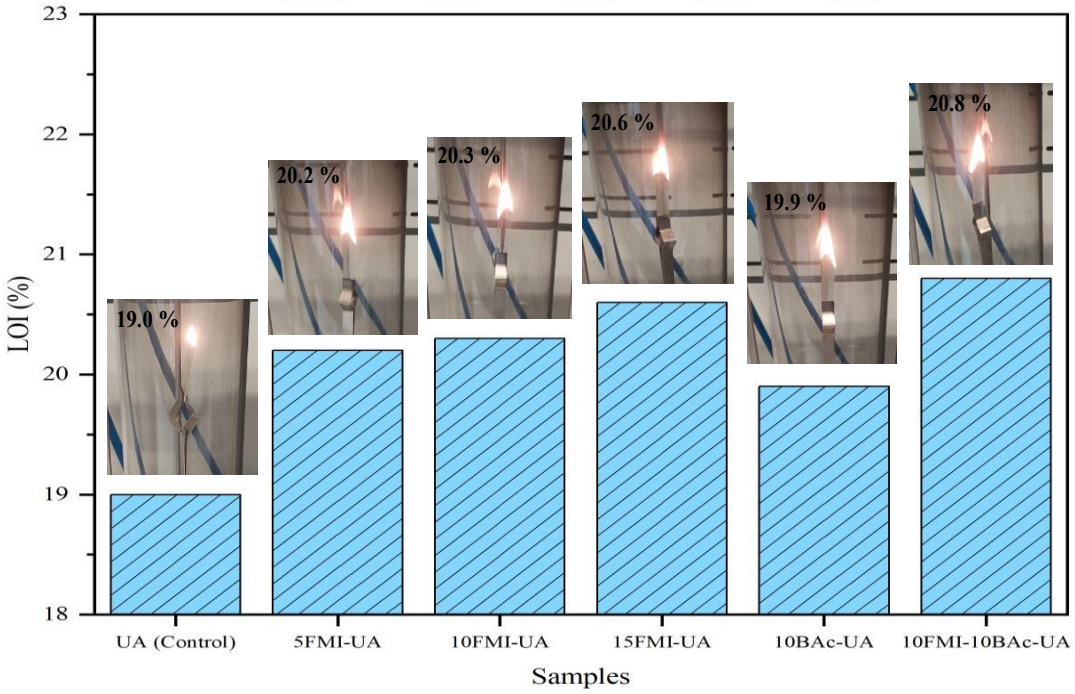

Figure 4.50 : LOI values of UA films (insert: combustion of UA films).

Water vapor released by the endothermic reaction of boron during combustion will dilute oxygen and flammable gases during ignition. Thus, the heat of combustion will be absorbed. This flame inhibition mechanism emphasizes that the inhibition of heat transfer and the slow spread of flames creates a barrier against the flame [67]. In

urethane acrylate films, the highest LOI value of 20.8% was seen in 10FMI-10Bac-UA. The enhanced flame resistance of the 10FMI-10BAc-UA film ascribed to the synergistic effect of FMI and BAc. This effect was not observed significantly in 10FMI-10Bac-EA. Figure 4.51 shows the digital photo of the 10FMI-EA and 10BAc-UA chars from LOI test. Clearly the films gave a good char quality.

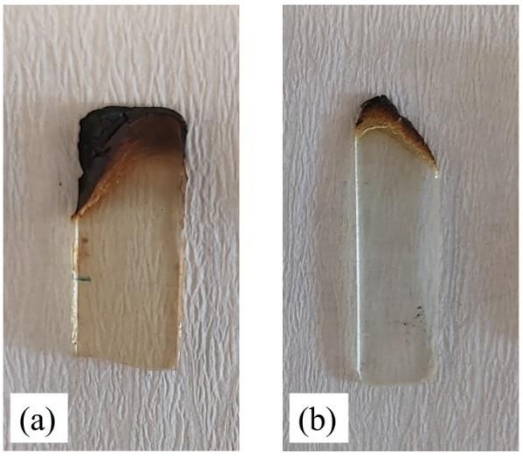

Figure 4.51 : Photographs of char residues from (a) 10FMI-EA (b) 10BAc-UA after LOI test.

The contact angle with distilled water and ethylene glycol of UV-cured films are listed in Table 4.17. Distilled water and ethylene glycol contact angles of UV-cured coatings with different FMI and BAc contents are shown in Figure 4.52 and Figure 4.53. Contact angle measurement was performed to examine the hydrophobicity and oleophobicity of UV-cured coatings. Contact angle measurements of UV-cured films were investigated at room temperature with distilled water and ethylene glycol as the test liquids. The water and ethylene glycol contact angle increased with the increase in FMI content. For measurements 5 μL drop of water and ethylene glycol were tested on the surfaces of coatings. This obviously demonstrates the generation of a more hydrophobic surface as a result of introducing the fluorinated groups. Films containing 10% BAc showed higher contact angle values in distilled water and ethylene glycol than EA (conrol) and UA (control) films. This was expected that because boron methacrylate as the inorganic content made the surface more hydrophobic. The distilled water contact angle value of epoxy acrylate films increased from 79.6° to 98.2° with 10% BAc and 10% FMI, and the contact angle value of urethane acrylate films increased from 73.9° to 88.4°. Boron methacrylate content and FMI monomer significantly increased hydrophobicity property.

Table 4.17 : Contact angle θ (°) with distilled water and ethylene glycol of UV-cured coatings.

Sample	Contact Angle θ (°) with	
	Distilled Water	Ethylene Glycol
EA (Control)	79.6	54.5
2.5FMI-EA	86.3	71.1
5FMI-EA	87.1	72.4
10FMI-EA	90.6	75.1
15FMI-EA	90.7	89.2
10BAc-EA	85.8	69.3
10FMI-10BAc-EA	98.2	73.1
UA (Control)	73.9	54.4
5FMI-UA	80.5	55.0
10FMI-UA	81.3	57.0
15FMI-UA	82.5	65.0
10BAc-UA	84.6	58.3
10FMI-10BAc-UA	88.4	60.7

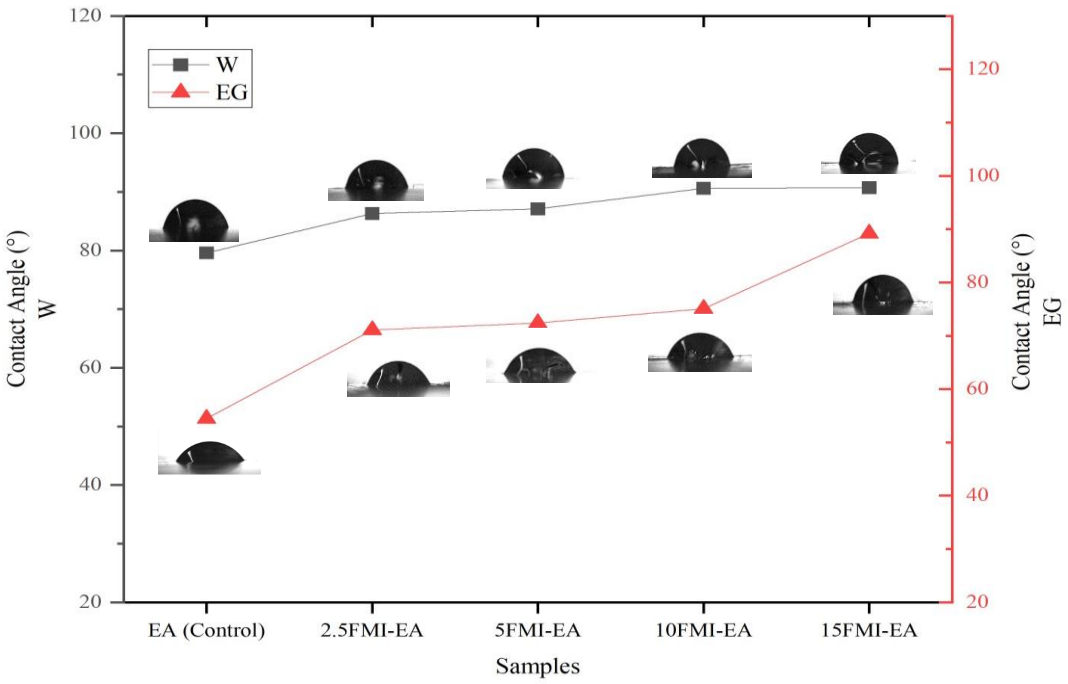

Figure 4.52 : Contact angle of water and ethylene glycol on epoxy acrylate UV-cured coatings.

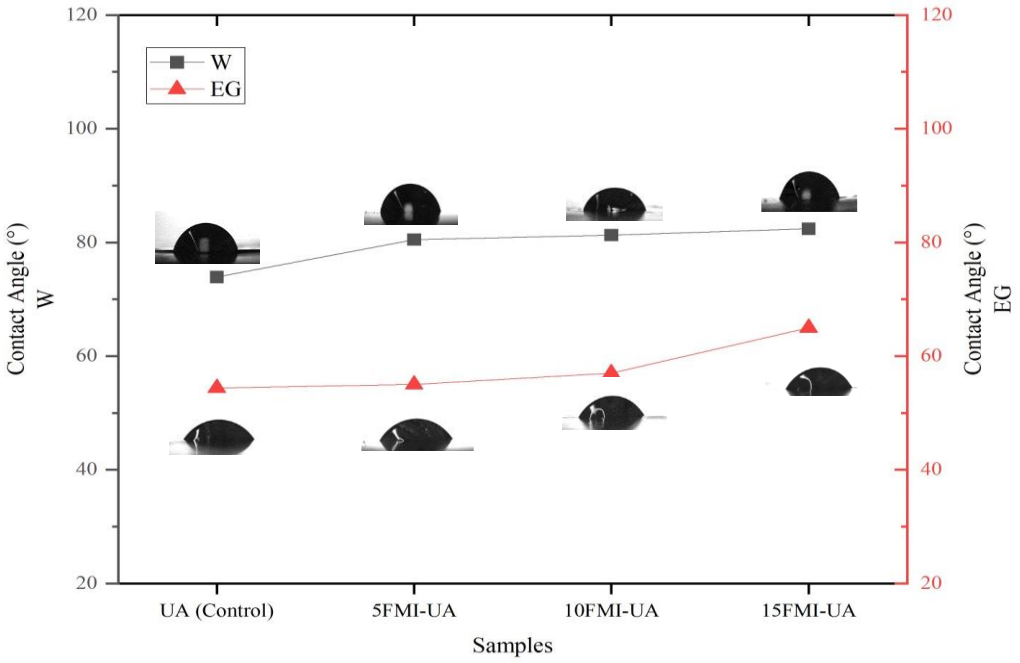

Figure 4.53 : Contact angle of water and ethylene glycol on urethane acrylate UV-cured coatings.

5. CONCLUSION

In this thesis, a new fluorine-containing maleimide monomer, 3,5-bis((perfluorophenyl)methoxy)benzyl-4-(2,5-dioxo-2,5-dihydro-1H-pyrrol-1-yl)benzoate (FMI), was successfully synthesized. The structure of the FMI monomer were thoroughly characterized and confirmed using ^{1}H-NMR, ^{13}C-NMR, ^{19}F-NMR and FT-IR spectroscopy and ESI/MS analysis. The investigated FMI monomer showed good solubility in many organic solvents. The copolymers of AN and St with FMI and homopolymer of FMI were carried out by free radical polymerization using AIBN as an initiator in DMF as a solvent for acrylonitrile copolymer series and in toluene as a solvent for styrene copolymer series at 75 °C. The molecular weights of the polymers were determined by GPC. The characterization of polymers was performed through ^{1}H-NMR spectroscopy. UV-Vis analysis of FMI monomer and p(St-co-FMI) copolymers was performed in 2 mg/100 mL DCM solvent. For the FMI monomer, the first absorption peak with significant absorption in the spectrum was at 270 nm. Additionally, as the FMI ratio decreased in copolymers, the absorbance decreased. Thermal behavior of these polymers was accomplished by DSC and TGA under nitrogen atmosphere. The thermal stability tended to increase as the FMI content was increased in the polymers. The segmental movements of the polymer chains were effectively blocked by the maleimide units, leading to an increase in the Tg value of the copolymers. It was observed in TGA analyzes that as the FMI monomer ratio increased in copolymers, decomposition temperatures and the amount of char residue increased significantly. From the SEM images, it was seen that F atoms affected the texture and covered the surface due to the fluorine orientation towards the surface. Contact angle measurements indicated that wettability decreased significantly as the fluorine-containing maleimide monomer increased in the polymers. Polymer/PAN nanofibers were successfully prepared by the electrospinning techniques. The effects of polymers on the thermal stability of the PAN nanofibers were investigated by TGA. The TGA analyses revealed that the temperature of thermal decompositions and amount of char residues at 500 °C and 600 °C of PAN nanofibers was notably increased in the presence of polymers, contributing to improved thermal stability properties.

From the SEM images, it was observed that the polymers were compatible with PAN to form ultrafine nanofibers, and it was observed that the diameters of the nanofibers decreased as the FMI monomer ratio in the polymers used increased. The contact angle measurements for two test liquids (distilled water and ethylene glycol) revealed that the nanofibers are highly hydrophobic and oleophobic. As the ratio of fluorine-containing monomers increased, the wettability of nanofibers decreased. This synthesized FMI was added to formulations containing epoxy acrylate and urethane acrylate at various different rates. Formulations containing epoxy acrylate and urethane arylate along with FMI were photopolymerized and coated on wooden substrates. As FMI concentration increased, double bond conversion initially increased slightly and then decreased. The reasons for this are that the ratio of epoxy acrylate or urethane acrylate decreases and some of the trapped double bonds of maleimide remain unpolymerized due to steric hindrance. UV curing has proven to be highly successful, with all double bond conversions being between 80 and 100%. All samples exhibited gel content between 90 and 100%, suggesting that all films were highly cross-linked. The maleimide ring and phenyl rings in FMI prevented the rotation of the polymer segment, causing the pencil hardness to increase from 4H to 6H or 7H. Since the maleimide in the structure of the FMI monomer has a rigid structure, the pendulum hardness increased with the increase of the FMI ratio. The presence of a polar group (COO-) present in FMI, which enables hydrogen bonding with substrates enhancing interfacial adhesion, resulted in increased cross-cut adhesion with increasing FMI concentration. Water absorption decreased steadily in UV-cured films. This was because the FMI backbone had fluorine-containing groups with hydrophobic properties. The rigid groups such as maleimide ring and benzene ring gave good results in the resistance of the coatings to different solvents and chemicals. The thermal properties of the coating materials were characterized by TGA. TGA analysis indicated that the increase of FMI content improved the thermal properties and gave higher char yield. The flame retardancy of cured films was investigated by LOI. The LOI results of the cured films showed improved flame retardant properties with increasing FMI content. FMI and BAc increased the flame retardancy by showing a synergistic effect in the urethane acrylate film. The contact angle of water and ethylene glycol increased with increasing FMI content of the cured films.

REFERENCES

[1] **Oswal, S., Chapaneri, N., & Malek, N.** (2007). Radical polymerization of N-(4-butoxycarbonylphenyl) maleimide, its co-polymerization with methyl methacrylate, styrene and acrylonitrile, and the properties of the resulting polymers. *Designed Monomers and Polymers, 10*(6), 487-506.

[2] **Lou, L., Koike, Y., & Okamoto, Y.** (2011). A novel copolymer of methyl methacrylate with N-pentafluorophenyl maleimide: High glass transition temperature and highly transparent polymer. *Polymer, 52*(16), 3560-3564.

[3] **Çılgı, G. K., & Ak, M.** (2020). Thermal degradation kinetics and thermodynamics of maleimide-sytrene based alternating copolymer: A comparative investigation of monomer and polymer structures. *Journal of Molecular Structure, 1221*, 128879.

[4] **Teng, H.** (2012). Overview of the development of the fluoropolymer industry. *Applied Sciences, 2*(2), 496-512.

[5] **Rajkumar, T., & Vijayakumar, C. T.** (2017). Synthesis and characterization of N-[4-(chlorocarbonyl) phenyl] maleimide functionalized graphene oxide and reduced graphene oxide. *Fullerenes, Nanotubes and Carbon Nanostructures, 25*(7), 442-448.

[6] **Ahn, K.-D., Kim, J.-M., Lee, C.-W., Han, D. K., Lee, D.-Y., & Lee, Y.-M.** (2000). Synthesis and radical polymerization of bifunctional maleimides with different functional reactivities. *Journal of Macromolecular Science, Part A: Pure and Applied Chemistry, 37*, 117-131.

[7] **Li , C. Q., Li, H. M., & Liu, P. S.** (2006). Syntheses and thermostability of N-[4-(N'-8-quinolinyl)aminocarbonylphenyl]maleimide/styrene copolymer. *J MATER SCI, 41*, 3811-3813.

[8] **Elias, H.-G.** (2005). Free-Radical Polymerization. In *Macromolecules* (Vol. 1, pp. 309-367).

[9] **Mokhtar, S., Abd-Elaziz, S., & Gomaa, F.** (2010). Synthesis characterizations and properties of a new fluoro-maleimide polymer. *Journal of Fluorine Chemistry, 131*(5), 616-620.

[10] **Peng, L., Ying, Q., Lili, Z., Dahu, Y., Haixiang, S., Yingfei, H., . . . Qi, L.** (2015). Electrospun PS/PAN fibers with improved mechanical property for removal of oil from water. *Marine Pollution Bulletin, 93*(1-2), 75-80.

[11] **Alharbi, A. R., Alarifi, I. M., Khan, W. S., & Asmatulu, R.** (2016). Highly hydrophilic electrospun polyacrylonitrile/polyvinypyrrolidone nanofibers incorporated with gentamicin as filter medium for dam

water and wastewater treatment. *Journal of Membrane and Separation Technology, 5*(2), 38-56.

[12] **Yanılmaz, M.** (2018). Mechanical Properties Of Nylon 6, 6 Nanofiber Membranes. *Journal of Textiles and Engineer, 25*(112), 286-291.

[13] **Yanilmaz, M., Lu, Y., Zhu, J., & Zhang, X.** (2016). Silica/polyacrylonitrile hybrid nanofiber membrane separators via sol-gel and electrospinning techniques for lithium-ion batteries. *Journal of Power Sources, 313*, 205-212.

[14] **Zhang, L., Luo, J., Menkhaus, T. J., Varadaraju, H., Sun, Y., & Fong, H.** (2011). Antimicrobial nano-fibrous membranes developed from electrospun polyacrylonitrile nanofibers. *Journal of Membrane Science, 369*(1-2), 499-505.

[15] **Cox, P. J., & Parker, S. F.** (1996). Maleimide. *Acta Crystallographica Section C: Crystal Structure Communications, 52*(10), 2578-2580.

[16] **Fleš, D., Vuković, R., Kuzmić, A. E., Bogdanić, G., Piližota, V., Karlović, D., . . . Vikić-Topić, D.** (2003). Synthesis and spectroscopic evidences of N-arylmaleimides and N-aryl-2, 3-dimethylmaleimides. *Croatica Chemica Acta, 76*(1), 69-74.

[17] **Li, W., Zhan, Q., & Yang, P.** (2023). Synthesis of poly (maleimide) s with promising performance via Diels–Alder reaction and ring-opening metathesis polymerization. *Journal of Polymer Research, 30*(3), 127.

[18] **Shu, W.-J.** (2006). Studies of novel copolymers for deep-UV photoresists. I. Synthesis and properties of poly (styrene-co-silicon-containing maleimide). *Polymer Journal, 38*(9), 897-904.

[19] **Cakir, T., Serhatli, I. E., & Önen, A.** (2006). Graft copolymerization of methylmethacrylate with N-substituted maleimide-styrene copolymer by ATRP. *Journal of applied polymer science, 99*(5), 1993-2001.

[20] **Kim, J. W., Min, K., Kim, W.-S., Jeon, S. H., & Chang, W. S.** (2009). Liquid crystal photoalignment by a polymaleimide having a photoreactive 2-styrylpyridine derivative as a N-substituent. *Macromolecular Research, 17*, 1043-1046.

[21] **Çakır, T., Onen, A., & Serhatlı, I. E.** (2008). Graft copolymerization of methyl methacrylate with an N-substituted maleimide–liquid-crystalline copolymer by atom transfer radical polymerization. *Journal of applied polymer science, 107*, 2074-2081.

[22] **Pan, W., Liu, H., Wu, S., & Wilén, C. E.** (2006). A novel feed-stock recyclable hyperbranched polymaleimide: Synthesis and characterization. *Journal of applied polymer science, 101*(3), 1848-1852.

[23] **Omayu, A., & Matsumoto, A.** (2008). Thermal properties of N-phenylmaleimide-isobutene alternating copolymers containing polar groups to form intermolecular and intramolecular hydrogen bonding. *Polymer Journal, 40*(8), 736-742.

[24] **Yanagihara, N., & Katoh, T.** (2022). Mineralization of poly(tetrafluoroethylene) and other fluoropolymers using molten sodium hydroxide. *Green Chemistry, 24*(16), 6255-6263.

[25] **Lv, J., & Cheng, Y.** (2021). Fluoropolymers in biomedical applications: state-of-the-art and future perspectives. *Chemical Society Reviews, 50*(9), 5435-5467. doi:10.1039/D0CS00258E

[26] **Ameduri, B.** (2018). Fluoropolymers: the right material for the right applications. *Chemistry–A European Journal, 24*(71), 18830-18841.

[27] **Rudin, A., & Choi, P.** (2013). *The Elements of Polymer Science & Engineering* (3 ed.): Academic Press.

[28] **Guerrero-Santos, R., Saldívar-Guerra, E., & Bonilla-Cruz, J.** (2013). Free radical polymerization. *Handbook of Polymer Synthesis, Characterization, Processing*, 65-83.

[29] **Kusumkar, V. V., Galamboš, M., Viglašová, E., Daňo, M., & Šmelková, J. J. M.** (2021). Ion-imprinted polymers: synthesis, characterization, and adsorption of radionuclides. *14*(5), 1083.

[30] **Dubé, M. A., Saldívar-Guerra, E., & Zapata-González, I.** (2013). Copolymerization. *Handbook of Polymer Synthesis, Characterization, Processing*, 105-125.

[31] **McKeen, L. W.** (2007). *The effect of temperature and other factors on plastics and elastomers*: William Andrew.

[32] **Sada, K., Kokado, K., & Furukawa, Y.** (2014). Polyacrylonitrile (PAN). In *Encyclopedia of Polymeric Nanomaterials* (pp. 1-7). Berlin, Heidelberg.

[33] **El-Aassar, M. R., Masoud, M. S., Elkady, M. F., & Elzain, A. A.** (2018). Synthesis, optimization, and characterization of poly (Styrene-co-Acrylonitrile) copolymer prepared via precipitation polymerization. *Advances in Polymer Technology, 37*(6), 2021-2029.

[34] **Chiang, W.-Y., & Ding, F.-C.** (2000). Copolymerization of n-(4-carboxyphenyl) maleimide with acrylonitrile and the properties of its membrane. *Journal of Polymer Research, 7*, 251-255.

[35] **Abdel-Naby, A. S.** (2012). Ultrasound assisted copolymerization of acrylonitrile with N-amino phenyl maleimides and N-amino phenyl 2, 3 dimethyl maleimides. *Ultrasonics Sonochemistry, 19*(6), 1180-1185.

[36] **Koerner, G. R., Hsuan, G., & Koerner, R.** (2007). The durability of geosynthetics. In *Geosynthetics in Civil Engineering* (pp. 36-65).

[37] **Ke, L., Hu, D., Lu, Y., Feng, S., Xie, Y., Xu, W. J. P. d., & stability.** (2012). Copolymerization of maleimide-based benzoxazine with styrene and the curing kinetics of the resultant copolymer. *Polymer Degradation Stability, 97*(2), 132-138.

[38] **Sastri, V. R.** (2010). Plastics in medical devices. In (pp. 73-119): William Andrew.

[39] **Soykan, C., & Erol, I.** (2004). Radical copolymerization of N-(4-acetyl phenyl)-maleimide and styrene: Monomer reactivity ratios and thermal properties. *Journal of applied polymer science, 91*(2), 964-970.

[40] **McKeen, L. W.** (2018). *The effect of sterilization on plastics and elastomers* (3 ed.): William Andrew.

[41] **Wang, H., & Chu, P. K.** (2013). Surface characterization of biomaterials. In *Characterization of biomaterials* (pp. 105-174): Elsevier.

[42] **Jauhari, J., Aj, S., Nawawi, Z., & Sriyanti, I.** (2021). Synthesis and characteristics of polyacrylonitrile (PAN) nanofiber membrane using electrospinning method. *Journal of Chemical Technology and Metallurgy, 56*(4), 698-703.

[43] **Kobayashi, S., & Müllen, K.** (2015). *Encyclopedia of polymeric nanomaterials*: Springer Berlin Heidelberg Berlin Heidelberg.

[44] **Çakır, M. F.** (2022). An inexpensive contact angle measurement system. *Revista Mexicana de Física, 68*(2), 1-8.

[45] **Wang, K., Lu, Y., Yin, R., Jiang, Y., & Yu, Q.** (2014). Synthesis and photopolymerization kinetics of a single-molecular hydrogen-abstract free radical photoinitiator 1, 3-Benzodioxole-5-yl-Methyl-Maleimide. *Polymer Science Series B, 56*(2), 148-153.

[46] **Ahn, K. D., Kang, J. H., Yoo, K. W., & Choo, D. J.** (2007). Photoinitiator-Free Photopolymerization of Silicon-Containing Maleimides Based on Electron-Donor-Acceptor Systems. *Macromolecular Symposia, 254*(1), 46-53.

[47] **Qiu, J., & Wei, J.** (2014). Thioxanthone photoinitiator containing polymerizable N-aromatic maleimide for photopolymerization. *Journal of Polymer Research, 21*, 1-7.

[48] **Fan, S., Boey, F., & Abadie, M. J. E. P. L.** (2007). UV curing of a liquid based bismaleimide-containing polymer system. *Express Polymer Letters, 1*(6), 397-405.

[49] **Bayramoğlu, G., Ahbab, İ., Kahraman, M. V., & Güngör, A.** (2012). Photocurable cyanate ester containing hybrid coatings by an anhydrous sol–gel technique. *Progress in Organic Coatings, 74*(3), 511-519.

[50] **Wang, X., Wang, B., Xing, W., Tang, G., Zhan, J., Yang, W., . . . Hu, Y.** (2014). Flame retardancy and thermal property of novel UV-curable epoxy acrylate coatings modified by melamine-based hyperbranched polyphosphonate acrylate. *Progress in Organic Coatings, 77*(1), 94-100.

[51] **Cui, J., Yu, G., & Pan, C.** (2014). A novel UV-curable epoxy acrylate resin containing arylene ether sulfone linkages: Preparation, characterization, and properties. *Journal of applied polymer science, 131*(22).

[52] **Park, Y.-J., Lim, D.-H., Kim, H.-J., Park, D.-S., & Sung, I.-K.** (2009). UV- and thermal-curing behaviors of dual-curable adhesives based on epoxy acrylate oligomers. *International Journal of Adhesion & Adhesives, 29*(7), 710-717.

[53] **Ren, Y., Dong, Y., Zhu, Y., Xu, J., & Yao, Y.** (2019). Preparation, characterization, and properties of novel ultraviolet-curable and flame-retardant polyurethane acrylate. *Progress in Organic Coatings, 129*, 309-317.

[54] **Seo, J., Jang, E. S., Song, J. H., Choi, S., Khan, S. B., & Han, H.** (2010). Preparation and properties of poly (urethane acrylate) films for

ultraviolet-curable coatings. *Journal of applied polymer science, 118*(4), 2454-2460.

[55] **Çanak, T. Ç., Hamuryudan, E., & Serhatlı, I. E.** (2013). Synthesis and characterization of perfluorinated acrylate–methyl methacrylate copolymers. *Journal of applied polymer science, 128*(3), 1450-1461.

[56] **Malde, R., Parkes, M. A., Staniforth, M., Woolley, J. M., Stavros, V. G., Chudasama, V., . . . Baker, J. R.** (2022). Intramolecular thiomaleimide [2+ 2] photocycloadditions: stereoselective control for disulfide stapling and observation of excited state intermediates by transient absorption spectroscopy. *Chemical Science, 13*(10), 2909-2918.

[57] **Wu, J., Ren, X., & Soucek, M. D.** (2016). Synthesis and characterization of UV-curable maleimide-terminated imide oligomers. *Progress in Organic Coatings, 100*, 129-140.

[58] **Yoshikawa, M., Yokoi, H., Sanui, K., & Ogata, N.** (1984). Selective separation of water–alcohol binary mixture through poly (maleimide-co-acrylonitrile) membrane. *Journal of Polymer Science: Polymer Chemistry Edition, 22*(9), 2159-2168.

[59] **Çakmakçi, E.** (2019). HDI trimer based fluorine containing urethane methacrylates for hydrophobic photocured coatings. *Polymer-Plastics Technology and Materials, 58*(8), 854-865.

[60] **Park, S. H., Kim, J. H., Moon, S. J., Drioli, E., & Lee, Y. M.** (2018). Enhanced, hydrophobic, fluorine-containing, thermally rearranged (TR) nanofiber membranes for desalination via membrane distillation. *Journal of Membrane Science, 550*, 545-553.

[61] **Yalcinkaya, F., Yalcinkaya, B., Pazourek, A., Mullerova, J., Stuchlik, M., & Maryska, J.** (2016). Surface modification of electrospun PVDF/PAN nanofibrous layers by low vacuum plasma treatment. *International Journal of Polymer Science, 2016*.

[62] **Li, X., Teng, S., Xu, X., Wang, H., Dong, F., Zhuang, X., & Cheng, B.** (2018). Solution blowing of polyacrylonitrile nanofiber mats containing fluoropolymer for protective applications. *Fibers and Polymers, 19*, 775-781.

[63] **Çanak, T. Ç., Akpinar, S., & Serhatli, I. E.** (2017). Homopolymerization and synthesis of a new methacrylate monomer bearing a boron side group: characterization and determination of monomer reactivity ratios with styrene. *Turkish Journal of Chemistry, 41*(2), 209-220.

[64] **Altıntaş, Z., Karataş, S., Kayaman-Apohan, N., & Güngör, A.** (2011). The maleimide modified epoxy resins for the preparation of UV-curable hybrid coatings. *Polymers for Advanced Technologies, 22*(2), 270-278.

[65] **Çanak, T. Ç., Kaya, K., & Serhatlı, I. E.** (2014). Boron containing UV-curable epoxy acrylate coatings. *Progress in Organic Coatings, 77*(11), 1911-1918.

[66] **Chambhare, S. U., Lokhande, G. P., & Jagtap, R.** (2016). UV-curable behavior of phosphorus-and nitrogen-based reactive diluent for epoxy acrylate

oligomer used for flame-retardant wood coating. *Journal of Coatings Technology Research*, *13*, 703-714.

[67] **Patil, D. M., Phalak, G. A., & Mhakse, S. T.** (2018). Boron-containing UV-curable oligomer-based linseed oil as flame-retardant coatings: Synthesis and characterization. *Iranian Polymer Journal*, *27*(10), 795-806.

APPENDICES

APPENDIX A: FT-IR spectra of the films

APPENDIX A

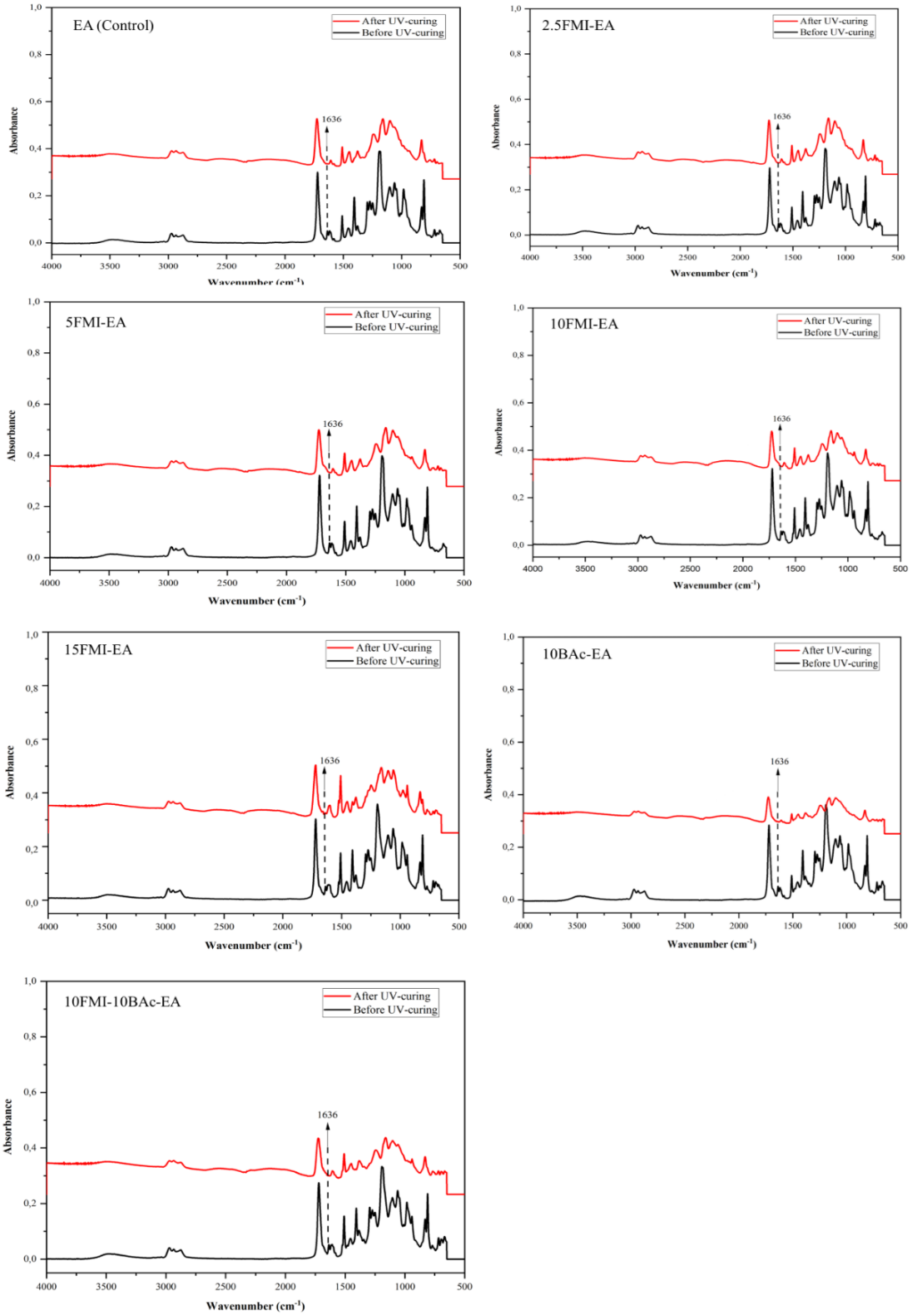

Figure A.1 : FT-IR spectra of the epoxy acrylate films before and after being UV-curing.

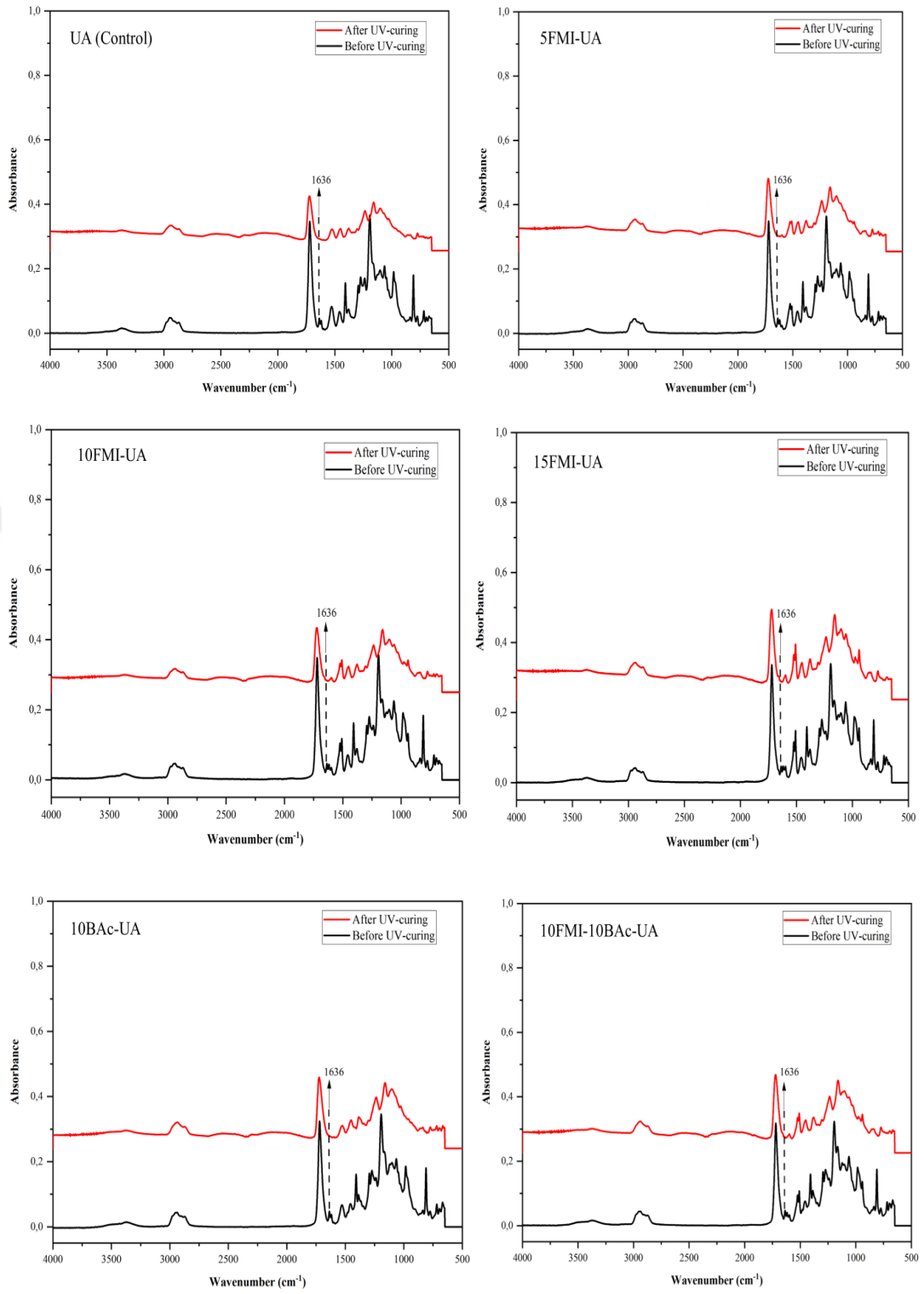

Figure A.2 : FT-IR spectra of the urethane acrylate films before and after being UV-curing.

CURRICULUM VITAE

Name Surname **:** İpek KAYALI

EDUCATION **:**

- **B.Sc.** **:** 2020, Yıldız Technical University, Faculty of Arts and Sciences, Department of Chemistry
- **M.Sc.** **:** 2024, Istanbul Technical University, Graduate School, Chemistry Programme

PUBLICATIONS, PRESENTATIONS AND PATENTS ON THE THESIS:

- **Kayalı İ, Çakır Çanak T.** 2022: Design of maleimide based fluorine containing polymers. 5th International Eurasian Conference on Biological and Chemical Sciences (EurasianBioChem 2022), November 23-25, 2022 Ankara, Turkey.